

From the
Institute for Cardiovascular Prevention
of the Ludwig-Maximilians-Universität München
Director: Univ.-Prof. Dr. med. Christian Weber

Organ-specific ‘ZIP-codes’

Endothelial heterogeneity in steady state and inflammation



Dissertation
zum Erwerb des Doctor of Philosophy (Ph.D.)
an der Medizinischen Fakultät der
Ludwig-Maximilians-Universität zu München

Submitted by
Sanne Lidewij Maas

From
Goes, The Netherlands

2021

Rückseite des Innentitelblattes der Dissertation

Mit Genehmigung der Medizinischen Fakultät der
Ludwig-Maximilians-Universität zu München

First supervisor: Univ.-Prof. Dr. Dr. med. Oliver Söhnlein

Second evaluator: Prof. Dr. Christoph Reichel

Dean: Prof. Dr. med. Thomas Gudermann

Datum of oral defense: 19.05.2022

Abstract

Endothelial cells show a substantial functional heterogeneity depending on the tissue in which they are located. These functional differences were shown to be partly imprinted in the transcriptome. Till date, heterogeneity of the transcriptome has been studied in various organs in a physiological state and acute inflammatory conditions. However, potential fluctuations in endothelial heterogeneity upon changes in the physiological state upon chronic inflammation and the effect of environmental factors on the transcriptomic signature throughout the day are barely studied.

In this thesis we aimed to characterize endothelial heterogeneity by means of a publicly available dataset, *Tabula Muris*, and two new transcriptomic studies. We established a dataset with small bulk RNA sequencing of aorta and lung endothelial cells isolated from mice in steady-state and mice exposed to an acute inflammatory condition. Our second transcriptomic dataset, obtained by single cell sequencing, contained endothelial cells from eight organs (aorta, bladder, bone, colon, kidney, ileum, liver, and lung) which were isolated from mice in steady-state, acute (endotoxemia), and chronic inflammatory (hyperglycemia and hyperlipidemia) conditions. Additionally, circadian rhythmicity was studied by collection the cells at different times of the day (8 am or 8 pm).

Analysis of the *Tabula Muris* provided us with a list of organ-specific genes from mice in a steady state. The effect of an acute inflammatory condition in our small bulk dataset was defined by comparing genetic profiles within and between treatments. Heterogeneity in our single cell dataset was verified by means of differentially expressed, marker, and organ-specific genes detection. Differentially expressed and marker genes seem interesting for possible application strategies while organ-specific genes had often a number of read counts that was too low to be of interest.

This study presents the first data on endothelial heterogeneity under both physiologic and different pathologic conditions at different times of the day. Herewith, adding a new dimension to the field of endothelial heterogeneity and providing a resource for endothelial cell specific gene expression across heterogeneous vascular beds. The cells in this atlas have an enormous yet largely untapped diagnostic and therapeutic potential. As a future perspective, selection of genes encoding for surface proteins might result in the establishment of organ-specific 'ZIP'-codes, allowing to take a first step towards organ-specific drug delivery.

Table of Contents

Abstract	1
Table of Contents	2
Table of Figures	6
Table of Tables	8
Abbreviations	10
1 - Introduction	15
1.1 - The endothelium: a general overview	15
1.1.1 - Angiodiversity	15
1.2 - Heterogeneity	18
1.2.1 - How is endothelium regulated on a local scale?	18
1.2.2 - Heterogeneity of the building blocks.....	18
1.2.2.1 - From genes to translation	18
1.2.2.2 - What about the proteome?.....	21
1.3 - Out of control	23
1.3.1 - Inflammation of the endothelium	24
1.3.2 - Acute inflammation	25
1.3.2.1 - Endotoxemia	25
1.3.3 - Chronic inflammation.....	26
1.3.3.1 - Hyperglycemia and diabetes.....	27
1.3.3.2 - Hyperlipidemia and atherosclerosis	29
1.4 - Circadian rhythmicity	34
1.5 - Aim of the study	37
2 - Materials and Methods	39
2.1 - General buffer preparation	39
2.2 - The <i>Tabula Muris</i> dataset - Endothelial transcriptome in steady state	39
2.2.1 - Dataset	39
2.2.2 - Data processing.....	39
2.3 - Small-bulk RNA-seq - The effect of an inflammatory stimulus on endothelial transcriptome	40
2.3.1 - Mice and tissue collection.....	40

2.3.2 - Genotyping	40
2.3.3 - Harvest	42
2.3.4 - Organ harvest and cell dissociation.....	42
2.3.4.1 - Aorta – Aorta arch and descending aorta	42
2.3.4.2 - Lung	43
2.3.5 - Fluorescence-activated cell sorting	43
2.3.6 - Library preparation	44
2.3.7 - Sequencing.....	45
2.3.8 - Data processing.....	45
2.4 – scRNA-seq - The effect of acute and chronic inflammation together with circadian rhythmicity on endothelial transcriptome	46
2.4.1 - Mice and tissue collection.....	46
2.4.1.1 - Acute inflammatory condition	46
2.4.1.2 - Hyperglycemic condition	46
2.4.1.3 - Hyperlipidemic condition	46
2.4.2 - Organ harvest and cell dissociation.....	47
2.4.2.1 - Aorta - Aortic arch and descending aorta	48
2.4.2.2 - Bladder and kidney.....	48
2.4.2.3 - Bone	48
2.4.2.4 - Colon and ileum	49
2.4.2.5 - Liver.....	49
2.4.2.6 - Lung	49
2.4.3 - Cell counting, antibody and hashtag staining	50
2.4.4 - Fluorescence-activated cell sorting	50
2.4.5 - 10x Genomics.....	51
2.4.6 - Sequencing.....	52
2.4.7 - Data processing.....	52
2.4.7.1 - Demultiplexing and cleaning	52
2.4.7.2 - Hashtag demultiplexing and doublet detection	53
2.4.7.3 - Normalization and clustering.....	53
2.4.7.4 - Cleaning dataset: endothelial cells.....	53
2.4.7.5 - Differently expressed genes.....	54
2.4.7.6 - Creating organ-specific signatures.....	54
2.4.8 - Plasma generation.....	55
2.4.9 - Cholesterol and triglyceride measurement.....	55
2.4.10 - Endotoxin measurement.....	55
3 - Results	57
3.1 - The <i>Tabula Muris</i> dataset - Endothelial transcriptome in steady state	58

3.2 – Small-bulk RNA-seq - The effect of an inflammatory stimulus on endothelial transcriptome of the aorta and lung	59
3.3 – scRNA-seq - The effect of acute and chronic inflammation together with circadian rhythmicity on endothelial transcriptome of eight organs.....	61
3.3.1 - Experimental set-up, quality control, and doublet detection	61
3.3.2 - Cleaning dataset.....	63
3.3.3 - Clustering	66
3.3.4 - Differentially expressed genes	68
3.3.5 - Marker gene detection.....	69
3.3.6 - Organ-specific genes expression	74
4 - Discussion.....	78
4.1 - Endothelial transcriptome in steady state	78
4.1.1 – Studying the endothelial transcriptome in homeostasis by means of a publicly available dataset.....	78
4.1.2 – Original scRNA-seq studies to determine the endothelial transcriptome in homeostasis.....	80
4.1.2.1 Differentially expressed genes	81
4.1.2.2 Marker genes.....	82
4.1.2.3 Organ-specific genes.....	83
4.1.2.4 Combining forces.....	85
4.2 – The endothelial transcriptome of mice exposed to inflammatory stimuli	86
4.2.1 – Acute inflammation	86
4.2.1.1 Sequencing of a small bulk endothelial cells exposed to endotoxin	86
4.2.1.2 10x Genomics and scRNA-seq	89
4.2.2 – Chronic inflammation	90
4.2.2.1 Hyperglycemia and diabetes	90
4.2.2.2 Hyperlipidemia and atherosclerosis	92
4.3 Circadian.....	94
4.4 Limitations and future perspectives	96
References.....	97
Supplement.....	112
Acknowledgments.....	140
Affidavit.....	143

Confirmation of Congruency.....	144
List of scientific publications.....	145

Table of Figures

Figure 1. Overview of the main structures and features of blood vessels.....	17
Figure 2. The characterizes of the diabetic phenotypes.	28
Figure 3. Scheme showing the destruction and reduction of the β cell population by STZ. .	29
Figure 4. Roadmap assisting the choice of an appropriate atherosclerotic mouse model....	31
Figure 5. Mode of action of PCSK9 inducing a hyperlipidemic state.	32
Figure 6. Overview of the ApoE ^{-/-} ,LDR ^{r/-} and PCSK9-AAV mouse models used to study atherosclerosis.....	33
Figure 7. Oscillation of peripheral blood leukocytes and tissue-specific ECs adhesion molecules.....	37
Figure 8. Sorting strategy of endothelial cells from the aorta and lung in homeostasis and inflammatory condition.	44
Figure 9. Construct of the PCSK9 vector.....	47
Figure 10. ECs sorting strategy aorta and lung in homeostasis condition.	51
Figure 11. Visualization of the variation between transcriptomes of ECs isolated from the aorta, brain, kidney, liver, and lung in homeostatic condition.	58
Figure 12. Tissue and acute inflammatory signature in transcriptome of ECs from mice in homeostatic condition compared to acute inflammatory condition.....	60
Figure 13. Experimental workflow of EC sorting, labeling with Feature barcoding technology, 10x Genomics, scRNA-seq, quality control, and doublet detection.	63
Figure 14. <i>In Silico</i> selection of cell types contaminating the endothelial cell dataset.	64
Figure 15. <i>In Silico</i> endothelial cell selection.	65
Figure 16. Clustering of endothelial cells from organs of mice in homeostasis, exposed to an inflammatory stimulus or a chronic inflammatory condition.	67
Figure 17. Differentially expressed genes of the aorta and lung.....	69
Figure 18. Upregulated marker genes of homeostatic mice.	71
Figure 19. Upregulated marker genes of mice exposed to acute inflammation.	72
Figure 20. Upregulated marker genes of mice exposed to hyperglycemia.....	73
Figure 21. Upregulated marker genes of mice exposed to hyperlipidemia.....	74
Figure 22. Organ-specific genes of mice in homeostasis and after being exposed to acute inflammatory stimulus.	76

Figure 23. Organ-specific genes of mice exposed to chronic inflammatory conditions.	77
Supplementary Figure 1. Doublet detection of endothelial cells of homeostatic mice and mice experiencing acute inflammation.	112
Supplementary Figure 2. Doublet detection of endothelial cells mice experiencing chronic inflammation.....	113
Supplementary Figure 3. Differentially expressed genes of mice in homeostasis sacrificed in the morning.	114
Supplementary Figure 4. Differentially expressed genes of mice in homeostasis, organs were harvested in the evening.	115
Supplementary Figure 5. Differentially expressed genes of mice exposed to an acute inflammatory stimulus sacrificed in the morning.	116
Supplementary Figure 6. Differentially expressed genes of mice exposed to an acute inflammatory stimulus, organs were collected in the evening.	117
Supplementary Figure 7. Differentially expressed genes of mice exposed to hyperglycemia sacrificed in the morning.	118
Supplementary Figure 8. Differentially expressed genes of mice exposed to hyperglycemia sacrificed in the evening.	119
Supplementary Figure 9. Differentially expressed genes of mice exposed to hyperlipidemia sacrificed in the morning.	120
Supplementary Figure 10. Differentially expressed genes of mice exposed to hyperlipidemia, organs were collected in the evening.....	121

Table of Tables

Table 1. Overview of the organs included in studies focusing on endothelial heterogeneity.	23
Table 2. General buffers.	39
Table 3. Genotyping PCR master mix.	41
Table 4. Genotyping primers.....	41
Table 5. Genotyping cycler protocols.....	42
Table 6. Hashtaged organs with TotalSeq™-B Feature Barcodes.	50
Table 7. Number of organ-specific gene transcripts and transcripts encoding for endothelial surface protein.	59
Table 8. Upregulated and organ-specific genes within a condition.....	61
Table 9. Upregulated and organ-specific genes between conditions.	61
Table 10. Overview of the number of endothelial cells per organ, treatment, and moment of organ collection.....	66
Table 11. Overview of the number of organ-specific genes.....	75
Supplementary Table 1. Organ-specific genes and organ-specific genes encoding for surface proteins.	122
Supplementary Table 2. Top 10 upregulated and organ-specific genes of endothelial cells isolated from the aorta and lung from mice in homeostasis.....	123
Supplementary Table 3. Aorta and lung top 10 upregulated and organ-specific genes of endothelial cells isolated from mice exposed to acute inflammation.	124
Supplementary Table 4. Top 10 upregulated and organ-specific genes of endothelial cells of the homeostatic condition.	125
Supplementary Table 5. Top 10 upregulated and organ-specific genes of endothelial cells isolated from mice exposed to acute inflammation.	126
Supplementary Table 6. Top-10 DE genes in homeostatic condition.	127
Supplementary Table 7. Top-10 marker genes in homeostatic condition.....	128
Supplementary Table 8. Top-10 Organ-specific genes in homeostatic condition.....	129
Supplementary Table 9. Top-10 DE genes in acute inflammatory condition.	130
Supplementary Table 10. Top-10 marker genes in acute inflammatory condition.....	131
Supplementary Table 11. Top-10 Organ-specific genes in acute inflammatory condition..	132
Supplementary Table 12. Top-10 DE genes in hyperglycemic condition.	133
Supplementary Table 13. Top-10 marker genes in hyperglycemic condition.	134

Supplementary Table 14. Top-10 organ-specific genes in hyperglycemic condition.	135
Supplementary Table 15. Top-10 DE genes in hyperlipidemic condition.	136
Supplementary Table 16. Top-10 marker genes in hyperlipidemic condition.	137
Supplementary Table 17. Top-10 organ-specific genes in hyperlipidemic condition.	138
Supplementary Table 18. Number of marker genes of mice in homeostasis and exposed to acute and chronic inflammation.	139

Abbreviations

2D-LC-MS/MS	2D-Liquid Chromatography-Tandem Mass Spectrometry
3110099E03Rik	RIKEN cDNA 3110099E03 gene
A2m	Alpha-2-macroglobulin
Aard	Alanine and arginine rich domain containing protein
Aass	Amino adipate-semialdehyde synthase
AAV	Adeno associated virus
AAV-PSCK9	Adeno associated virus carrying proprotein convertase subtilisin/kexin type 9
Acta2	actin alpha 2
Adgrl3	Adhesion G protein-coupled receptor L3
ADHD	Attention-deficit/hyperactivity disorder
Adrb1	Adrenoceptor beta 1
Ajap1	Adherens junctions associated protein 1
Amp	Ampicillin
ANS	Autonomic nervous system
Apod	Apolipoprotein D
Apoe	Apolipoprotein E
Aqp7	Aquaporin 7
BGHpA	Bovine Growth Hormone Polyadenylation Signal
BMAL1	Brain and Muscle Aryl Hydrocarbon Receptor Nuclear Translocator-like Protein 1
Bmp2	Bone morphogenetic protein 2
bp	base pairs
BSA	Bovine serum albumin
CASP	Colon Ascendens Stent Peritonitis
CD	Cluster of differentiation
Cdh5	Cadherin 5
cDNA	complementary DNA
CETP	Cholesteryl ester transfer protein
Cldn	Claudin
Clec4g	C-Type lectin domain family 4 member G
CLOCK	Circadian Locomotor Output Cycles Kaput
CLP	Caecal Ligation and Puncture
Col1a1	Collagen Type I Alpha 1 Chain
Counts	Sequence fragment assigned
CPM	Counts per million mapped reads
Cry	Cryptochrome
Ctrl	Control
Cxcl	Chemokine (C-X-C motif) ligand

Cyt11	Cytokine like 1
DAMPs	Damage-Associated Molecular Patterns
DAPI	4',6-Diamidino-2-phenylindol
DE	Differential Expressed
Dkk	Dickkopf WNT signaling pathway inhibitor
dl	Deciliter
DIk1	Delta like non-canonical notch ligand 1
DNA	Deoxyribonucleic acid
Dnase1b3	Deoxyribonuclease 1 like 3
dNTP	Deoxynucleoside triphosphate
DTT	Dithiothreitol
e.g.	exempli gratia
Ear1	Eosinophil-associated ribonuclease 1
EC	Endothelial Cell
EDL	Extensor digitorum longus
EDTA	Ethylenediaminetetraacetic acid
Emcn	Endomucin
ERCC	External RNA Controls Consortium
Fabp4	Fatty acid-binding protein 4
FACS	Fluorescence-activated cell sorting
Fbn1C1039G	Mutant fibrillin-1 allele
FBS	Fetal Bovine Serum
FC	Fold change
Fcgr2b	Fc fragment of IgG receptor IIb
FDR	False discovery rate
Fgf1	Fibroblast growth factor
Foxf1a	Forkhead box F1a
FSC	Forward scattered light
Gata4	GATA binding protein 4
GEM	Gel Bead-in-Emulsion
GLM	Generalized linear model
Glp1r	Glucagon like peptide 1 receptor
GPCR	G-protein-coupled receptors
Gpr182	G protein-coupled receptors 182
Grtp1	Growth hormone regulated TBC protein 1
hAAT	Human Alpha-1 Antitrypsin
Hand2	Heart and neural crest derivatives expressed 2
Hba-a1	Hemoglobin A
Hbb-bs	Hemoglobin B

HBSS	Hanks balanced salt solution
HCR	Human Apolipoprotein E/C-I Gene Locus Control Region
HDL	High-density lipoprotein
HFD	High-fat diet
hIAPP	Human islet amyloid polypeptide
HPA	Hypothalamic-pituitary-adrenal
Hpgd	15-Hydroxyprostaglandin dehydrogenase
i.e.	id est
i.p.	intraperitoneal
i.v.	intravenous
ICAM	Intercellular Adhesion Molecule
Igfbp5	Insulin-like growth factor-binding protein
Il13ra2	Interleukin 13 receptor subunit alpha 2
Il6	Interleukin 6
Isl1	ISL LIM homeobox 1
Itgbl1	Integrin subunit beta like 1
ITR	Inverted Terminal Repeat,
kg	Kilogram
LCN2	Lipocalin 2
LDL	Low-density lipoprotein
LDL-C	LDL cholesterol
Ldlr	Low-density lipoprotein receptor
logFC	Log fold change
Lphn3	Latrophilin 3
LPS	Lipopolysaccharide
Lypd6	Ly6/PLAUR domain-containing protein 6 precursor
Lyve1	Lymphatic vessel endothelial hyaluronan receptor 1
M	Molar
MAD	Median absolute deviations
Maf	MAF BZIP transcription factor
MAPK	Mitogen-Activated Protein Kinase
MD-2	Myeloid Differentiation factor 2
Meis2	Meis homeobox 2
Mfsd2a	Major facilitator superfamily domain 2A
mg	Milligram
min	minutes
mM	Millimolar
Mrc 1	Mannose receptor C-type 1
mRNA	messenger RNA

MRSA	Methicillin-Resistant Staphylococcus aureus
ND	Normal diet
ng	nanogram
Nkx2-3	NK2 homeobox 3
NPAS2	Neuronal PAS Domain Protein
Oit3	Oncoprotein induced transcript3
PAMPS	Pathogen-Associated Molecular Patterns
PBS	Phosphate-Buffered Saline
PCA	Principal component analysis
PCR	Polymerase chain reaction
PCSK9	Proprotein convertase subtilisin/kexin type 9
Pdgfrb	Platelet derived growth factor receptor beta
Pdprn	Podoplanin
Pecam1	Platelet and endothelial cell adhesion molecule 1
Per	Period
Pf4	Platelet factor 4
pg	picogram
Pglyrp1	Peptidoglycan recognition protein 1
Plat	Plasminogen activator, tissue type
Plscr2	Phospholipid scramblase 2
Plxnc1	Plexin c1
Ppbp	Pro-platelet basic protein
Procr	Protein C receptor
Prox1	Prospero homeobox 1
Prx	Periaxin
Ptpnc1	Protein tyrosine phosphatase receptor type c
QL	Quasi-likelihood
Rasgef	RasGEF domain family member
Raver2	Ribonucleoprotein, PTB binding 2
Rbp7	Retinol Binding Protein 7
RFP	Red Fluorescent Protein
RNA	Ribonucleic Acid
RNA-seq	RNA-sequencing
RPMI	Roswell park memorial Institute
Rspo3	R-Spondin 3
RT	Reverse transcription
Scgb3a1	Secretoglobin Family 3A Member 1
SCN	Suprachiasmatic nucleus
Scn7a	Sodium voltage-gated channel alpha subunit 7

scRNA-seq	Single-cell RNA seq
sec	secondes
Sele	E-Selectin
Selp	P-Selectin
Sema3c	Semaphorin 3C
SI	Small Intestine
Slc	Solute carrier family member
Slco	Solute carrier organic anion transporter family member
Sprr2b	Small proline rich protein 2B
SSC	Side scattered light
Stab2	Stabilin 2
STZ	Streptozotocin
T1D	type 1 diabetes
T2D	type 2 diabetes
Tbx5	T-box transcription factor 5
Tfpi	Tissue factor pathway inhibitor
TLR4	Toll-Like Receptor 4
TMEM	Transmembrane protein
TMM	Trimmed Mean of the M-values
TRAP	Translating Ribosome Affinity Purification
tSNE	t-Distributed Stochastic Neighbor Embedding
TSO	Template-switching oligos
Tspan7	Tetraspanin 7
U	Units
VCAM	Vascular cell adhesion protein
VE-cad	Vascular endothelial cadherin
VEGF	Vascular endothelial growth factor
VLDL	Very-low-density lipoproteins
WBC	White blood cell
WD	Western-type diet
Wnt	Wnt Family Member
Zfp36	Zinc finger protein 36
ZT	Zeitgeber
μl	Microliter
μM	Micrometer

1 - Introduction

1.1 - The endothelium: a general overview

The body contains 1.2 trillion endothelial cells (ECs), which together cover an area of 400 square meters¹. They line the entire cardiovascular system and serve as the interface between the circulating blood and tissues. This single layer of squamous ECs is also known as the endothelium. The ECs are sophisticated processing centers, and their versatility is fascinating. They function as sensory and signaling cells and contribute to virtually every cardiovascular function. In contrast to other sensory and signaling cells, ECs can sense multiple types of input and generate different types of output. This versatility permits the endothelium to regulate a variety of processes, such as blood pressure, blood flow rate, and blood distribution by modifying cell proliferation, vascular tone, and cell migration into the vessel wall². Further they control the exchange of cells as well as molecules between the tissue and the blood, which is achieved by regulating vascular permeability through coordinating the gap size between the ECs, resulting in a size-selective sieving process². The endothelium encompasses the whole body and is specialized to the needs of distinct organs. It is therefore not surprising that the branches of the vascular tree come in different flavors.

1.1.1 - Angiodiversity

There are two major components that define the flavors of the vascular tree. The angiodiversity can be divided into the different vessel types (arteries, arterioles, capillaries, venules, and veins) and the organ-specific diversity in a distinct microvascular bed (continuous, fenestrated, discontinuous/sinusoidal capillaries). Which both will be touched upon below.

Arteries, arterioles, capillaries, venules, and veins are exposed to organ- and situation-specific varying biochemical and physical milieus, which affect the molecular properties of the cellular building blocks. The endothelial monolayer in arteries and veins shows both an uninterrupted (continuous) endothelial layer, whereby ECs interact with their neighbor via tight junctions. However, these vessel types differ upon the physical milieu, since most arteries carry oxygenated blood away from the heart, while most veins carry unoxygenated blood towards the heart. The ECs, the building blocks of the endothelium, have a different morphology, as venous ECs are generally thinner and shorter than arterial ECs, which are longer and more narrow or ellipsoidal^{3, 4}. Arterioles represent the primary site of vascular resistance⁵ and they distribute the blood flow into the capillary bed, which is the most versatile vascular bed.

Capillaries have organ-specific structural differences, which was first observed in the 1960s, using electron microscopy⁶. They got classified into three groups: continuous, fenestrated, or

sinusoidal. Most organs have capillaries with a continuous, barrier-forming endothelium (lungs, brain, skin, and heart), which are characterized by tightly connected ECs that are surrounded by a continuous basement membrane. Another type of capillary bed is found in the organs involved in secretion (e.g. macromolecules from endocrine organs) or filtration (e.g. excess fluid and waste products in the kidneys) as their capillaries have a fenestrated endothelium (renal glomeruli, endocrine and exocrine glands, and gastric and intestinal mucosa). The fenestrated and sinusoidal endothelium share multiple similarities. Nevertheless, the diameter of the fenestrae in sinusoidal capillaries are bigger compared to the ones in fenestrated capillaries (200 nm to 70 nm, respectively). Furthermore, sinusoidal capillaries lack diaphragms, their basement membrane is less dense, and are therefore also called discontinuous endothelium^{3, 5, 7}. Discontinuous endothelium can be found in liver, spleen, and bone marrow and provides the highest permeability for circulating cells and large molecules through gaps in the ECs and basement membrane⁷ (**Figure 1**).

Additionally, differences are shown between the permeability of capillaries and post-capillary vessels. Lipid-soluble materials, small solutes, and water can freely cross the endothelium of capillaries, however, rates may differ among the vascular beds. On the contrary, post-capillary venules are generally non-permeable, and permeability only occurs upon damage or through active transportation. Specific transporters as caveolae and vesiculo–vacuolar organelles facilitate transcytosis, a process of larger molecules passing the barrier. Lack of post-capillary venules permeability is supported by the high density of vesiculo-vacuolar organelles and the absence of tight junctions⁸.

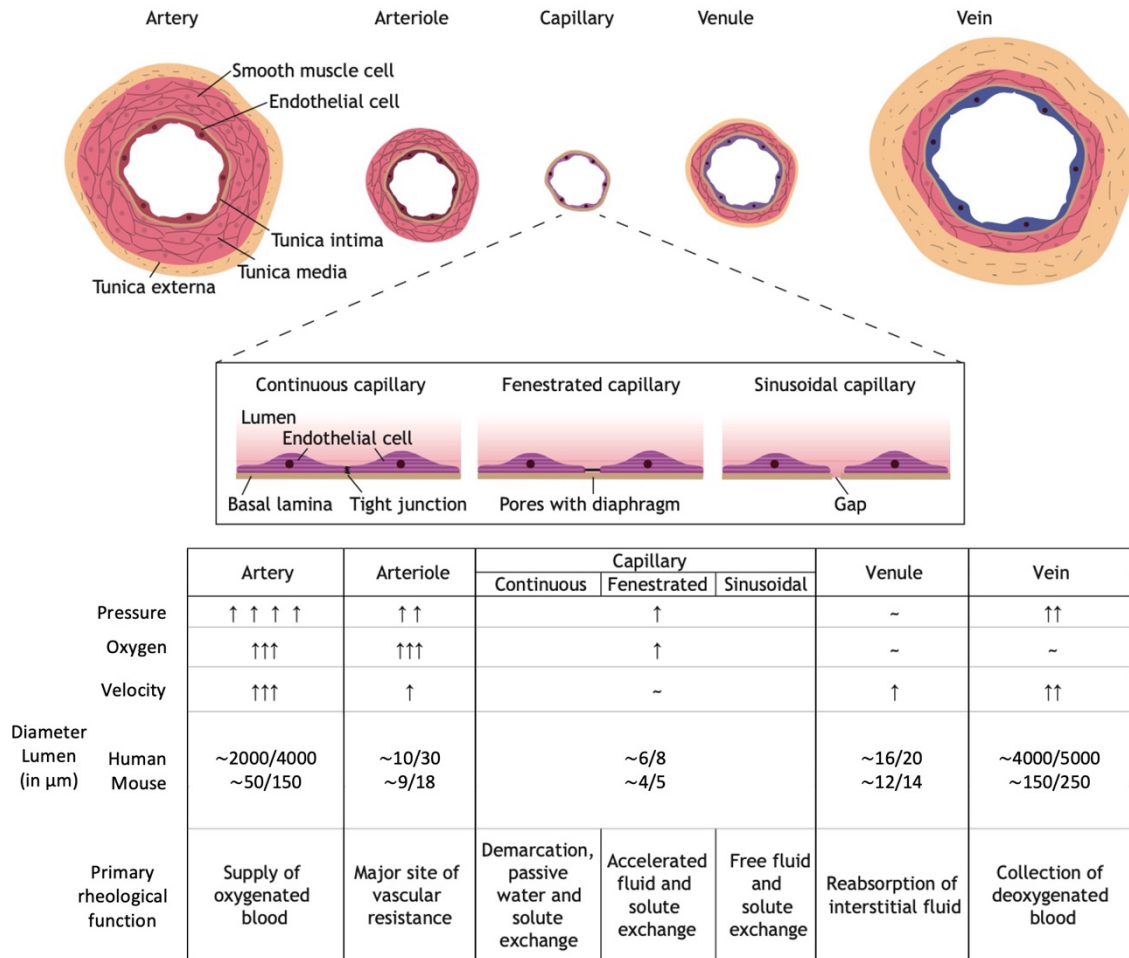


Figure 1. Overview of the main structures and features of blood vessels.

The diversity of structural and rheological features of the different vessel types are depicted. A specific function of arteries is their ability to carry oxygenated blood, except for pulmonary and umbilical arteries, away from the heart. While arterioles are known to be the primary site of vascular resistance and have only an intima and tunica media. The capillaries have the smallest diameter of all vessels in the vascular system and can be divided into three major types, namely continuous, fenestrated, and sinusoidal capillaries. Continuous capillaries perform distinct barrier functions and permit the diffusion of lipid-soluble material, small solutes, and water. Fenestrated and sinusoidal capillaries have both a discontinued EC lining, which are called fenestrae. The fenestrae in the fenestrated capillaries are spanned by a diaphragm, whereas sinusoidal endothelium lacks these diaphragms and have a devided basement membrane. Fenestrated ECs are filtration and absorption functions. Sinusoidal ECs line the vessels in the haematopoietic organs as the bone marrow, spleen and liver. Blood flows from the capillaries into the venules, where after it is drained into veins. Venules have media and tunica externa opposed to the arterioles. However, their tunica media is poorly developed resulting in thinner walls and larger lumen compared with arterioles. Veins have, in contrast to arteries, a thick tunica externa, but generally a much thinner media. Furthermore, they mainly carry oxygen-poor blood. Reprinted from Jakab and Augustin, 2020⁵.

The building blocks of the endothelium are the ECs. Recently, multiple studies focused on profiling the heterogeneity of thousands of (single) ECs, allowing for the molecular dissection of the angiodiversity and looking into the organ-specific heterogeneity of the endothelium and its ECs.

1.2 - Heterogeneity

1.2.1 - How is endothelium regulated on a local scale?

The endothelium regulates many general processes, however it also embraces organ-specific functions, such as regulating pulmonary alveolar repair⁹, glomeruli filtration and maintenance of vascular normalcy in the kidney^{10, 11}, myocardial hypertrophy in the heart¹², and hepatic regeneration in the liver¹³. The local characteristics of the endothelium are continuously optimized and defined by stimuli from the microenvironment, but also by epigenetic changes. Microenvironmental cues, such as hypoxia, shear stress, specific growth factors, cytokines, and hormones can affect the genomic, transcriptomic, and proteomic profile of the ECs¹⁴. These modifications are non-heritable and occur due to changes in transcriptional and posttranslational alterations of proteins. However, epigenetic modifications, like histone acetylation, DNA and/or histone methylation, are heritable and alter gene expression directly. Extracellular signals trigger these epigenetic modifications, and changes may persist even after removing these external cues¹⁵. The importance of both the microenvironment and the epigenetics was demonstrated when ECs were cultured for several passages and tissue-specific epigenetic modifications were preserved and transmitted during mitosis¹⁴, while 50% of the microenvironment-related gene expression patterns disappeared together with major architectural characteristic^{16, 17}.

1.2.2 - Heterogeneity of the building blocks

The variety in organ-specific functions of ECs makes it not surprising that transcriptomic studies show remarkable heterogeneity of ECs from different organs^{18, 19}. Translatomics and proteomic studies confirmed the heterogeneity of ECs on translome and proteome levels. Interestingly, heterogeneity was also shown to be affected by inflammation^{20, 21}. Additionally circadian rhythmicity has been shown to influence the heterogeneity of ECs²² and the expression of some surface markers varied between vessel types²³⁻²⁵. The findings regarding gene and antigen EC heterogeneity will be reviewed below.

1.2.2.1 - From genes to translation

Genes in the endothelium can be characterized in different groups, namely constitutively or inducible and endothelial-specific or -unspecific. Furthermore, genes can be expressed throughout the endothelium or only in specific EC subsets²⁶. Strikingly, only a few endothelial-specific genes are expressed across the vascular tree. Two of these genes are *Cdh5* (Cadherin 5, also known as vascular endothelial (VE)-cadherin) and *Robo4* (Roundabout Guidance Receptor 4)^{17, 27-29}. A wider variety of endothelial-specific genes, constitutive and/or inducible, can be allocated to a specific EC subset.

Microarray and bulk Ribonucleic Acid-sequencing (RNA-seq) of organ-specific ECs has revealed distinct gene expression patterns, both in mice and humans. Nolan *et al.* focused on determining EC diversity and performed microarray with ECs collected from mice in steady state from nine different organs. They found that the microvascular bed of each organ is composed of organ-specialized ECs, presenting unique modules of genes coding for adhesion molecules (e.g. Lung CD36, Liver CD44). Furthermore, ECs of each organ expressed unique combinations of genes coding for angiocrine factors, chemokines, transcription factors, and metabolic profiles³⁰. Differences were also observed in human ECs. Marcu *et al.* isolated ECs from four different organs three months after gestation and observed distinct expression patterns supporting organ-specific development. Additionally, the expression patterns could be linked to organ-specific functions as angiogenic potentials, barrier properties, and metabolic rates. Also, organ-specific genes were identified, namely 74 genes in the heart, 29 in the kidney, 13 in the lung, however none in the liver. Some genes were not organ specific but were significantly more expressed in one organ when compared to another organ. For example, *Gata4* (GATA binding protein 4), *Hand2* (Heart and neural crest derivatives expressed 2), *Tbx5* (T-box transcription factor 5), and *Tbx20* were 200-fold higher expressed in the heart, compared to the kidney. These genes were identified to be of importance for the development of the heart and valve formation³¹. These findings show the presence of organ-specific surface markers as well as diversity in gene expression related to the functions of an organ. It must be considered that Marcu *et al.* passaged the cells three times before RNA was isolated for sequencing, which might have led to a loss of gene expression patterns and may have reduced the amount of identified organ-specific genes³¹. Further research could focus on whether and to which extent ECs are phenotypically different. At a single-cell level EC heterogeneity could be studied within a single tissue to define if ECs in a particular vascular bed are heterogeneous. Furthermore, phenotypical profiles of a variety of organs could be compared to identify distinct organ-specific characteristics.

Single-cell RNA seq (scRNA-seq) studies profiled the transcriptome of ECs in a variety of tissues in health and pathological conditions, among them the aortic endothelium³², bone marrow³³, brain^{34, 35}, brain and lung^{36, 37}, heart³⁸, heart (myocardial infarction)³⁹, kidney⁴⁰⁻⁴², liver (fibrosis⁴³, cirrhosis⁴⁴), lung⁴⁵, and lung (tumor)⁴⁶. Of interest, most of the studies made their dataset publicly available and created an interactive online database, which can be helpful to facilitate the assessment of the heterogeneity of ECs of a variety of tissues. For example, an endothelial database was launched, named EndoDB⁴⁷, which is continuously updated and aims to collect transcriptomic datasets obtained by bulk RNA-seq and single-cell RNA-seq of ECs. Additionally, two single-cell atlases were published focusing on various cells

isolated from multiple tissues, which gave an interesting glimpse into the heterogeneity of all cells. However, EC heterogeneity was underrepresented in these studies since this was not their primary objective^{48, 49}.

Recently, transcriptome atlases were created that focused on EC heterogeneity within as well as between organs. Kalucka *et al.* performed single-cell RNA-seq of ECs from 11 tissues and identified enriched EC marker genes for each tissue, revealing distinct signatures of ECs from each tissue (except for the soleus, extensor digitorum longus (EDL) and skeletal muscles). Interestingly, some EC markers were only expressed by only one single tissue (brain: *Pglyrp1* (Peptidoglycan recognition protein 1), testis: *Lcn2* (Lipocalin 2), and lung: *Tmem100* (Transmembrane protein 100)), whereas other EC markers (*Fabp4* (Fatty acid-binding protein 4), *Aqp7* (Aquaporin 7), *Nkx2-3* (NK2 homeobox 3)) were conserved across more tissue. Additionally, they found transcriptomic signatures of arterial, venous, capillary, and lymphatic ECs¹⁸. Surprisingly, lymphatic ECs clustered together, suggesting that lymphatic ECs do not have a tissue-specific molecular signature. Arterial and venous ECs from one specific tissue clustered together, indicating that vascular EC heterogeneity is mainly determined by tissue specificity rather than arterial, capillary, or venous identity¹⁸. Another study that focused on endothelial heterogeneity used a publicly available dataset. Paik *et al.* used the *Tabula Muris* murine dataset⁴⁹ and analyzed the endothelial single-cell transcriptional signature from 12 organs. ECs from some organs presented tissue-specific differentially expressed (DE) genes (e.g. brain, kidney, liver and lung), whereas other tissues (e.g. adipose tissue, heart, aorta) showed considerable overlap in gene expression. The organ-specific DE genes were used to determine organ-specific unique pathways by performing gene set enrichment analysis. Thereby, organ-specific as well as unique pathways could be identified, such as unique pathways included axon guidance in cardiac ECs and ErbB signaling in brain ECs, whereas pathways like *MAPK* (Mitogen-Activated Protein Kinase) and *Wnt2* (Wnt Family Member 2) were shared among multiple organs. Further tissue-specialization of ECs was demonstrated by ligand-receptor interaction analysis, finding unique crosstalk in each organ between ECs and parenchymal cells¹⁹.

The studies mentioned above focused on the total cellular messenger RNA (mRNA) profile of ECs. However, the question arises if the transcriptome resembles the proteome. Cleuren *et al.* studied the EC translome of five organs via Translating Ribosome Affinity Purification (TRAP). They were able to identify organ-specific genes in the brain (18 genes, e.g. *Cldn13* (Claudin 13), *Slc19a3* (Solute carrier family 19 member 3)), heart (5 genes, e.g. *A2m* (Alpha-2-macroglobulin), *Itgbl1* (Integrin subunit beta like 1)), kidney (8 genes, e.g. *Calca* (Calcitonin Related Polypeptide Alpha), *Gata5*), liver (10 genes, e.g. *Gm13994*, *Il13ra2* (Interleukin 13

receptor subunit alpha 2)) and lung (27 genes, e.g. *Aard* (Alanine and arginine rich domain containing protein), *Ear1* (Eosinophil-associated ribonuclease 1)). Furthermore, they compared the transcriptome with the translome by TRAP which specifically captures the actively translated mRNAs. Interestingly, comparison of samples of total cellular mRNA and actively translated mRNA showed only minor changes within a given tissue when depicted in a principal component analysis. These data demonstrate that the transcriptome signatures can serve as a template for the corresponding tissue translome¹⁷. The question remains if the transcriptome and translome are a proxy for the proteome.

1.2.2.2 - What about the proteome?

The proteome of ECs has been studied before using different approaches, such as phage display, proteomics and stainings. Rajotte *et al.* used phages already in 1998 to identify organ-specific molecular diversity of ECs. The phage libraries were injected intravenously into mice, followed by recovering the phage from seven organs. Three organs were selected for detailed phage homing analysis based on their difference in embryological derivation, function, location, and size (lung, skin, and pancreas). Selective phage homing to the vasculature revealed unique peptide sequences, suggesting a widespread system of endothelial specificities among tissues. Evidence of organ-specific endothelial heterogeneity was provided by immunohistochemistry and visualization of the phage in the blood vessels of the specific organ⁵⁰. Furthermore, Cleuren *et al.* also identified a kidney- and liver-specific EC marker (kidney: *3110099E03Rik* (RIKEN cDNA 3110099E03 gene) and liver: *Wnt9b*) and visualized the proteins by immunofluorescent stainings¹⁷.

Another study studied the vascular cells surface proteome in steady-state and in a mouse model of sepsis. Toledo *et al.* created a vascular cell surface proteomic atlas of five organs. The vasculature of the mice was flushed with biotin, and biotin-labeled cells were selected by running the single-cell suspension of the organs through microchromatography cartridges, which were labeled with streptavidin. The samples were digested and analyzed through 2D-Liquid Chromatography-Tandem Mass Spectrometry (2D-LC-MS/MS). The liver and kidney, isolated from mice in a steady-state, showed 138 common proteins and 409 and 533 organ-specific proteins, respectively. The proteome profile changed on a global as well as organ-specific level in septic mice, as 75 organs-specific genes were found in the kidney, 275 in the heart, 85 in the brain, 18 in white adipose tissue, 88 in the liver, and 57 proteins were expressed in all organs. This showed organ-specific heterogeneity of the vascular cell surface proteome, and additionally the proteome remodeling on a general as well as an organ-specific manner triggered by sepsis²¹. The results regarding the acute inflammatory condition will be further discussed in chapter 1.3.1 'Inflammation of the endothelium'.

Apart from Toledo *et al.*, most of the studies focused on ECs in a homeostatic state. Only limited research is conducted examining gene and protein expression changes occurring when the body is in a diseased state, such as inflammation. The influence of different physiological states of the body on ECs heterogeneity will be further discussed in the chapter 1.3 'Out of control'.

It is important to consider that, in general, organ-specific genes found by Nolan *et al.* (Microarray³⁰), Kalucka *et al.* (scRNA-seq¹⁸), and Toledo *et al.* (TRAP transcriptome²¹) do not always overlap. Some overlap is found when (only) two studies were compared, such as *Slc19a3* in the brain^{17, 18} and *Fgf1* (fibroblast growth factor) in the lung^{18, 30}. One side note, the studies sometimes use different aliases for the genes, therefore it can be difficult to compare the datasets. Another difficulty to compare the datasets is the variety of organs that are chosen to study (**Table 1**). When comparing different organs to each other it can make a big difference which organs are included, e.g. including the colon and ileum (SI, Small Intestine) will give different results than when the ileum (SI) is exchanged with ECs from the heart. Furthermore, the preparation of the samples varies drastically, not only between studies, but even within a study the method to digest the organs and obtain individual cells differs. Additionally, the concern was raised that isolation procedures required to prepare a single cell suspension for sequencing analysis may perturb the abundance of mRNA^{51, 52}. Interestingly, Cleuren *et al.* compared two digestion methods, namely enzymatic digestion vs. TRAP, and indeed identified drastic differences between the results. When comparing the two methods, they observed a 48.2% difference in the genes expressed in brain ECs and 21.6% difference in liver ECs. The variation found in the kidney ECs was less, as only a difference of 7.4% was observed. Furthermore, hierarchical clustering of the EC transcriptomes showed that the brain and liver ECs show more similarities based on the method of sample preparation than by tissue of origin¹⁷. Therefore, at least within one study the protocol used to digest the tissues should be consistent for all organs to obtain reliable and comparable results.

Table 1. Overview of the organs included in studies focusing on endothelial heterogeneity.

Green = organ is included in the study, white = organ is not included in the study. EDL – Extensor digitorum longus, RNA – Ribonucleic acid, RNA-seq – RNA sequencing, scRNA-seq – single cell RNA sequencing, TRAP – Translating Ribosome Affinity Purification.

	Nolan	Cleuren	Jambusaria	Kalucka	Paik	Rajotte	Toledo
	Microarray	RNA-seq (TRAP)	RNA-seq (RiboTag)	scRNA-seq	scRNA-seq	Phage display	Proteomics
Adipose tissue							
Adrenal gland							
Aorta							
Brain							
Bone marrow							
Colon							
Diaphragm							
EDL							
Heart							
Kidney							
Liver							
Lung							
Mammary gland							
Pancreas							
Retina							
Skeletal muscle							
Skin							
Small intestine							
Soleus							
Spleen							
Testis							
Trachea							
Uterus							

1.3 - Out of control

In homeostasis, the endothelium functions as an anti-inflammatory and anticoagulatory surface. However, an insult to the ECs can result into a dysfunction endothelium. These insults can be a consequence of underlying vascular diseases such as atherosclerosis and hypertension but also due to disturbed blood flow problems associated with diabetes⁵³⁻⁵⁵. The activation of ECs leads to a change in function and presentation of adhesion molecules on the endothelial surface, and the heterogeneity of the endothelium will be altered compared to homeostasis. Most of the studies discussed in the previous chapter describe endothelial heterogeneity in steady state, although recent studies also examine the effect of diseases on

endothelial heterogeneity, for example by analysing the transcriptomic and proteomic endothelial profile in models of liver fibrosis⁵⁶, liver cirrhosis⁴⁴, lung tumor⁴⁶, myocardial infarction³⁹, and sepsis^{17, 20, 21}. Nevertheless, most studies only examine the endothelial heterogeneity in one organ. Only the studies focusing on the effect of sepsis report on endothelial heterogeneity of a variety of organs. The results observed in this study will be discussed in chapter 1.3.1 'Inflammation of the endothelium'.

It would be of interest to expand our knowledge on endothelial heterogeneity by studying various inflammatory conditions and organs. This is of importance, because elderly people suffer often from inflammatory diseases, such as diabetes and/or CVDs. Therapeutic interventions are often performed in rather late life stages, in which patients often also cope with additional comorbidities, such as bladder issues, lung inflammation or other acute inflammatory conditions. Targeted therapeutic approaches to treat diabetes or CVDs should take these comorbidities into consideration and not hamper the host immune defense in a general manner. A better understanding of the organ-specific EC heterogeneity in homeostasis and upon inflammatory diseases could therefore contribute to the generation of disease and tissue-specific therapeutic strategies. With this knowledge, it would be, among others, possible to implement organ-specific drug delivery targeting one organ when the body is in a specific non-physiological state, such as an inflammatory one.

1.3.1 - Inflammation of the endothelium

Inflammation is a tightly regulated process that can be of sterile or a pathogenic origin. The innate immune system, the first line of host defense, mediates the inflammatory process and aims at restoring homeostasis. However, an insult might damage and activate the ECs and unleashing a coordinated cascade of events to remove the damaged tissue or eliminate pathogenic insults⁵⁷. Upon tissue injury, Damage-Associated Molecular Patterns (DAMPs) or, in non-sterile inflammation, Pathogen-Associated Molecular Patterns (PAMPs) will be released⁵⁸. The DAMPs and PAMPs, stimulate sentinel cells, like macrophages, dendritic and mast cells, leading to the recruitment of leukocytes, primarily neutrophils, to the site of inflammation. The neutrophils pass into the inflamed tissue by interacting with the adhesion molecules and chemokines present on the ECs. Eventually, leukocytes will migrate through or in-between the ECs to reach the side of inflammation. The acute inflammatory process must be controlled and shut down actively to successfully achieve tissue regeneration and healing, a process known as the resolution of inflammation. Unsuccessful resolution can lead to excessive tissue damage and progress towards an uncontrolled chronic, self-promoting inflammation⁵⁹. In the chapters below acute inflammation and chronic inflammation and what

is known about the influence of these two types of inflammatory conditions EC heterogeneity will be discussed.

1.3.2 - Acute inflammation

A variety of animal studies are available focusing on acute inflammation. A common model to study acute systemic inflammation is a model of sepsis induced by endotoxins. The pathogenesis of sepsis involves a dysregulation of pro- and anti-inflammatory mediators, and interestingly, this animal model has been used to assess the efficacy of potential therapeutic agents. The available animal models of sepsis can be divided into three main classes, namely endotoxemia models (e.g. Lipopolysaccharide (LPS) administration), bacterial infection models (e.g. *Escherichia coli* infusion), and host-barrier disruption models (e.g. Colon Ascendens Stent Peritonitis (CASP) and Caecal Ligation and Puncture (CLP)). The endotoxemia models are widely used while they are simple to perform⁶⁰.

1.3.2.1 - Endotoxemia

Circulating bacterial endotoxin are key mediator of injury and acute tissue inflammation^{61, 62}. Endotoxins are small bacteria-derived molecules, which can be found in the outer membrane of cyanobacteria and gram-negative bacteria. For example, in the membrane of an *Escherichia coli*, approximately two million LPS molecules can be found, and bacteria excrete large amounts of LPS upon cell division, cell death, and growth^{63, 64}. LPS interacts with macrophages and monocytes, via binding of the toxic lipophilic lipid component with macrophage scavenger receptor and CD11b/CD18 or via glycoprotein CD14 interacting with the Toll-Like Receptor 4 (TLR4)/Myeloid Differentiation factor 2 (MD-2) complex, resulting in the production of pro-inflammatory cytokines⁶⁵.

Several reports already focused on identifying organ-specific EC transcriptome, translome, and proteome responses to systemic (acute) inflammatory injury. For example, Jambusaria *et al.* exposed mice to LPS and studied EC heterogeneity changes in the brain, heart, and lung by RNA-seq. Interestingly, upon exposure to LPS, the endothelium maintained its distinct organ-specific molecular identity. In the heart and brain ECs expressed *Sele* (coding for E-Selectin) and *Selp* (coding for P-Selectin) were identified as marker genes for the LPS-induced acute (heart) and late (brain) inflammatory model²⁰. These proteins are classical inflammatory adhesion molecules. Thereby, both organs are vulnerable to thrombotic events, as P-Selectin is a critical mediator in platelet aggregation and thrombosis⁶⁶. On the contrary, the lung ECs isolated from the LPS-induced acute inflammatory model upregulated the chemokines *Cxcl1* (chemokine (C-X-C motif) ligand 1) and *Cxcl9*²⁰. The change in expression profile in the lung could be explained by severe loss of lung endothelium due to the endotoxin

exposure⁶⁶. After prolonged exposure to endotoxins (24 hours), all tissues showed an upregulation in genes associated with leukocyte recruitment and chemotaxis pathways, suggesting that all organs share a broad program of inflammatory signaling upon exposure to systemic endotoxemia²⁰.

Another study, namely Cleuren *et al.*, also found that ECs preserved their distinct organ-specific molecular identity upon LPS exposure. Gene ontology analysis resulted in the yield of terms associated with immune response and host defense, as expected. Interestingly, ECs shifted to a procoagulant state as they expressed less profibrinolytic and anticoagulant genes upon LPS challenge. The organ-specific EC transcriptome contained more down-regulated genes than up-regulated genes. *Procr* (Protein C receptor) was identified within the limited set of up-regulated genes as an organ-specific variation. *Procr* was mainly up-regulated in the lung and liver, though down-regulated in the brain, heart, and kidney¹⁷. It is important to note that this study implemented whole tissue RNA-seq, which is a limitation since changes in more abundant cellular subsets can mask cell-type specific response.

Another study used a systemic inflammatory response to sepsis induced by Methicillin-Resistant *Staphylococcus aureus* (MRSA) to identify the endothelial changes. MRSA does not contain endotoxins and is derived from gram-positive bacteria. Systemic and local changes of the vascular proteome triggered by sepsis were unraveled in five organs. Collectively, the data indicate that MRSA-sepsis triggers extensive proteome remodeling of the vascular cell surfaces in a tissue-specific manner. The five organs shared a group of 57 proteins that changed in all examined organs, whereas other proteins altered in a tissue-specific manner. The changes in the liver (88), kidney (75), and heart (85) stood, while in the white adipose tissue (18) and brain (8) only a few proteins significantly changed between infected and non-infected ECs²¹.

These studies give an exciting insight into the effect of LPS exposure resulting in changes of the endothelial heterogeneity. However, as most studies only considered a few organs, a general overview of the LPS-mediated heterogeneity is still lacking.

1.3.3 - Chronic inflammation

Acute inflammation can progress into chronic inflammation when the inflammation is not resolved, and tissue homeostasis is not reached. During inflammation, circulating neutrophils are alarmed by tissue-resident cells of the innate immune system. The triggered neutrophils migrate to the inflamed area and promote the recruitment of inflammatory monocytes,

enhancing a pro-inflammatory environment⁶⁷. Under normal conditions, neutrophils undergo apoptosis after fulfilling their task⁶⁸, and the apoptotic bodies get cleared by macrophages. Upon clearance of the apoptotic neutrophils, macrophages undergo an inflammatory phenotypical switch, namely from a pro- to an anti-inflammatory phenotype^{69, 70}. This anti-inflammatory phenotype secretes pro-resolving signals which decrease the inflammatory cascade. Failure of clearance of inflammatory cells leads to their accumulation, which may result in excessive tissue damage and ultimately in chronic inflammation^{57, 59} as seen in for example cardiovascular diseases, diabetes, chronic obstructive pulmonary disease, chronic kidney disease, and cirrhosis. The chapters below will focus on diabetes and CVDs, and its main underlying cause, atherosclerosis.

1.3.3.1 - Hyperglycemia and diabetes

The main clinical and diagnostic features of diabetes is hyperglycemia and impaired glucose tolerance. In this multifaceted metabolic disorder, the glucose status of the human body is affected due to an insulin deficiency or resistance to its function. Eventually, chronic hyperglycemia can lead to organ dysfunction and failure of the retina, kidneys, nerves, heart, and blood vessels⁷¹. There is a well-established clinical relationship between diabetes and CVD, as diabetes patients have a significantly increased risk of also suffering from CVDs⁷².

Diabetes can be divided into two broad pathogenetic categories: type 1 (T1D) and type 2 diabetes (T2D). Some patients cannot be classified in one of the two groups due to the complexity of the pathogenesis involving immunological, genetic and neuroendocrinological pathways. In T1D, there is an absolute lack of insulin caused by immune-mediated destruction of pancreatic β cells, which is the main hallmark of this disorder. However, the exact mechanism causing the absence of insulin is still vaguely understood since hyperglycemia only emerges when more than 90% of the β cells are absent⁷³. There is evidence for genetic predisposition as well as environmental triggers of the disease⁷⁴. T1D is one of the most common chronic autoimmune diseases in children, as 90% of diabetic children have diabetes type 1^{75, 76}. On the other hand, T2D, previously referred to as “adult-onset diabetes” or “noninsulin-dependent diabetes”, accounts for 90–95% of all diabetic cases and is therefore, the most common form of diabetes. T2D develops due to a defect in insulin resistance and T1D due to insulin deficiency⁷⁷. Known risk factors for T2D are genetic factors, obesity, low energy expenditure, a sedentary lifestyle, and unhealthy dietary habits⁷⁸. The causes and characteristics of both types of diabetes are summarized in **Figure 2**.

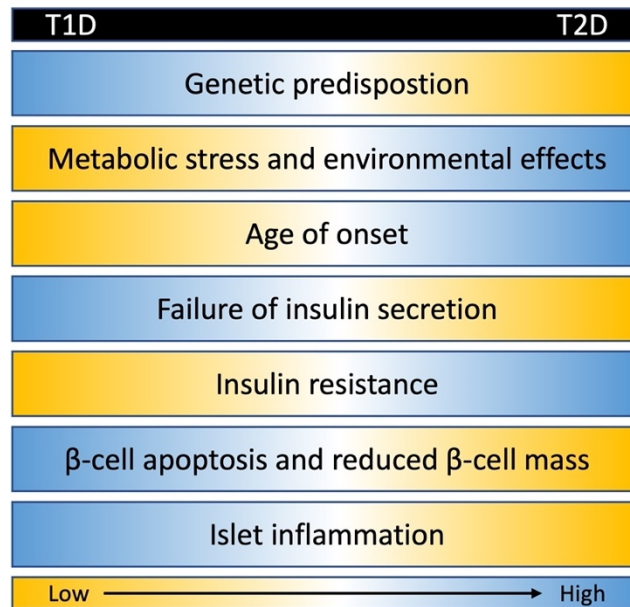


Figure 2. The characterizes of the diabetic phenotypes.

T1D and T2D are the same disorder, however the phenotype of diabetes are distinguishable by variety of factors, which can be intrinsic as well as acquired. The cause of T1D is not clearly defined yet, but there is evidence for strong genetic predisposition. Islet inflammation leads to β cell apoptosis, reducing the B cell mass, leading to complete dependence on pump or daily insulin injections and specialized care. T2D caused by metabolic stress and environmental determinants, as diet and physical activity. Furthermore, it is characterised by increased blood sugar levels which are a result of insulin resistance. T1D – Type 1 Diabetes, T2D – Type 2 Diabetes. Adapted from Khawandanah, 2019⁷⁸.

There are different mouse models available to study hyperglycemia, which can be T1D (insulin- deficient) or T2D (insulin- resistant) models. T1D can be induced chemically (e.g. Streptozotocin (STZ)), genetically (e.g. AKITA mice), or virally (e.g. Coxsackie B virus). Furthermore, a spontaneous autoimmune model is available (non-obese diabetic mice). T2D is more difficult to provoke, as specific mouse strains have to be used, such as monogenic models (e.g. leptin^{ob/ob} mice), polygenic models (e.g. KK mice) or β cell dysfunction models (e.g. Human islet amyloid polypeptide (hIAPP) mice)⁷⁹.

Especially STZ administration is a quick way to induce hyperglycemia, and subsequently diabetes. STZ is a toxic glucose analog, which is derived from Streptomyces achromogenes. In the clinic, it is used as a chemotherapeutic agent to treat pancreatic β cell carcinoma. STZ induces hyperinsulinemia and hyperglycemia by damaging pancreatic β cells⁸⁰ (**Figure 3**). STZ preferably accumulates in pancreatic β -cells by binding to the glucose transporter 2, due to its similarity with the chemical structure of glucose. Depending on the dose of STZ, a diabetic state can be induced in two ways. A single high dose of STZ targets β cells by its alkylating property. It kills insulin-producing β -cells selectively, which corresponds to the mode of action of cytotoxic nitrosourea compounds⁸¹. On the other hand, a low dose of STZ is

administered for consecutive days and elicits an inflammatory reaction, which is probably related to the release of glutamic acid decarboxylase autoantigens. The inflammatory processes, including infiltration of lymphocytes in the pancreatic islets, lead to the destruction of β cells, resulting in the induction of a hyperglycemic state⁸².

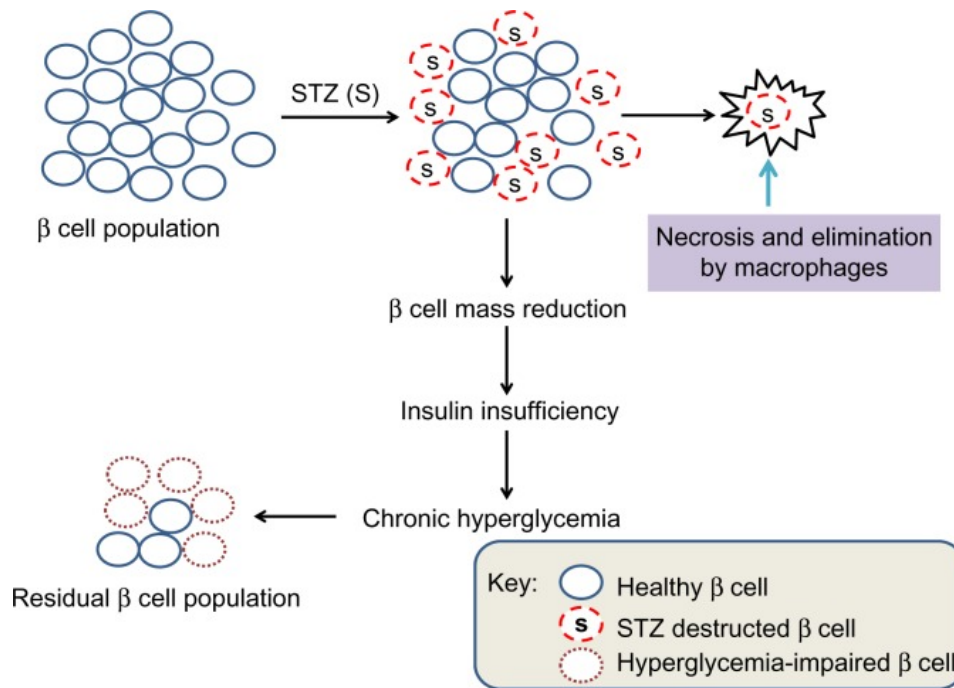


Figure 3. Scheme showing the destruction and reduction of the β cell population by STZ.

STZ toxicity to β cells is short-lived. However, affected β cells undergo necrosis and are eliminated by macrophages. The loss of β cells mass leads to insulin insufficiency and eventually chronic hyperglycemia. Residual β cells are exposed to this persistent hyperglycemic environment, which can lead to the impairment of mitochondrial function resulting in the further impairment of the β cell population. STZ – Streptozotocin. Reprinted from Wu and Yan, 2015⁸³.

Some changes have been observed in ECs from diabetic rats and human. For example, in diabetic rats and patients with T1D, vascular endothelial growth factor (VEGF) expression was increased in ECs^{84, 85}. Furthermore, diabetes was also associated with the upregulation of other molecules, such as calcineurin-A- α ⁸⁶, fractalkine⁸⁷, adrenomedullin and its receptor receptor-activity-modifying protein 2⁸⁸ in glomerular ECs of rats. The studies above highlight some changes in ECs upon diabetes, although the effect of diabetes on organ-specific endothelial heterogeneity has not yet been studied.

1.3.3.2 - Hyperlipidemia and atherosclerosis

Another factor involved in the manifestation of a chronic inflammatory condition is hyperlipidemia. Hyperlipidemia is a term that refers to genetic or acquired disorders that are characterized by high levels of circulating lipids, such as cholesterol, fats, or triglycerides in

the blood. These blood lipid levels can be controlled by ongoing medication. Millions of people worldwide display mildly elevated plasma lipids levels due to their poor lifestyle and diet. Notably, hyperlipidemia is a known risk factor for CVD⁸⁹.

CVDs were responsible for 17.3 million deaths per year and remain the number one contributor to mortality worldwide⁹⁰. The main underlying cause of CVDs is atherosclerosis. Atherosclerosis is a complex chronic inflammatory condition in which the arterial wall of large and medium-sized arteries is affected. The disease is characterized by a maladaptive inflammatory response and dysregulated lipid metabolism, resulting in lesion formation in the arterial wall^{58, 91, 92}. Silent progression of the disease constitutes a significant concern worldwide⁹³, since lesion progression can result in plaque rupture, thrombus formation and eventually the occlusion of arteries. Plaque rupture can lead to life-threatening clinical manifestations, such as ischemic stroke or myocardial infarction^{59, 94, 95}. A better understanding of the pathology of atherosclerosis, and CVDs, is needed to determine ways to reduce or avoid the incidence of coronary events and thereby decrease the number of cardiovascular-related deaths worldwide.

Atherosclerosis is a complex disease since its pathophysiology is triggered by various risk factors, including aging, diabetes, hyperlipidemia, and hypertension⁹⁶. To study the immunometabolic processes of this disease, it is needed to explore the underlying molecular mechanisms. Therefore, animal models are required that recapitulate the pathophysiology of the disease. Notably, atherosclerosis is a highly complex human disease and has no perfect animal model that mimics all features. An evident example is the dissimilarity of the lipoprotein metabolism. Mice transport cholesterol in high-density lipoprotein (HDL) particles, while cholesterol in humans is transferred in low-density lipoprotein (LDL) particles. Additionally, mice are normally protected against atherosclerosis due to this improved reverse cholesterol transport pathway⁹⁷. This phenomenon in mice can be explained by the lack of the cholesteryl ester transfer protein (CETP). CETP promotes the transfer of triglycerides from very-low-density lipoproteins (VLDL) to HDL and cholesterol esters from HDL to VLDL. High expression of CETP in humans leads to increased levels of VLDL- and LDL-cholesterol (LDL-C) levels. Another critical difference is that mice produce additional mouse-specific bile acids, namely α - and β -muricholic acids. These more hydrophilic bile acids reduce the absorption of lipids in the intestine⁹⁸. Moreover, mice have a different composition of secondary and tertiary bile acids and an increased synthesis of bile acids compared to humans, facilitating a better reverse cholesterol transport and excretion of cholesterol via the feces in mice⁹⁹. Several animal models are available to study atherosclerosis, however based on the focus of the research an appropriate model should be selected (**Figure 4**). In this thesis the focus is on

hyperlipidemia and diabetes. Therefore, mice models of suggested to study diabetes, lipoprotein metabolism or immune & inflammation seemed suitable models for this thesis.

To provide an appropriate model to study the pathophysiology of atherosclerosis, genetic and dietary manipulations are used. The various genetic models all alter the lipoprotein profile to mimic a more human-like lipid profile, characterized by increased amounts of VLDL- and LDL-particles which thereby triggers an atherosclerosis-prone setting¹⁰⁰⁻¹⁰⁴.

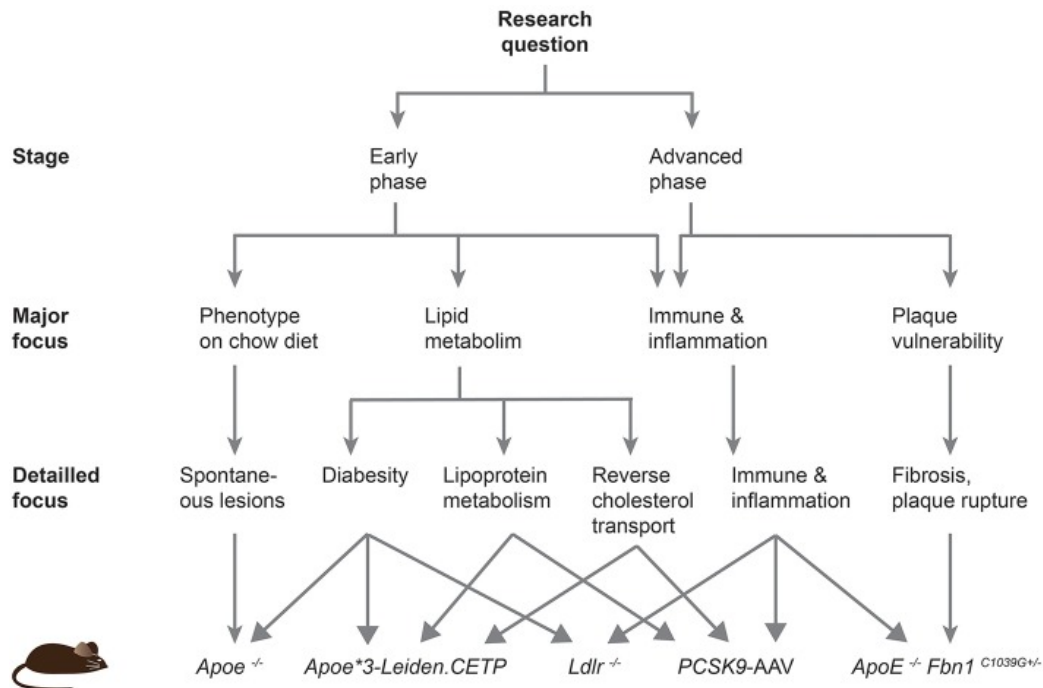


Figure 4. Roadmap assisting the choice of an appropriate atherosclerotic mouse model.

This scheme could assist current and future research to select an appropriate atherosclerotic mouse model based on the specific research question. AAV – adeno associated virus, PCSK9 – Proprotein convertase subtilisin/kexin type 9, ApoE – Apolipoprotein E, CETP – cholesteryl ester transfer protein, Fbn1^{C1039G} – mutant fibrillin-1 allele, Ldlr – Low density lipoprotein receptor. Reprint from Oppi *et al.*, 2019¹⁰⁵.

Two independent research groups described the model using a so-called adeno associated virus (AAV) carrying proprotein convertase subtilisin/kexin type 9 (PCSK9)^{103, 104}. This model is attractive since time and cost-intensive germline genetic engineering is not required. The human subtilize, PCSK9, is a serine protease and is highly expressed in the liver^{106, 107}. In brief, in normal circumstances, the LDL receptor (LDLR) is responsible for clearing most of the LDL cholesterol (LDL-C) from the plasma by carrying the lipoprotein particles into cells. The LDLR is eventually recycled and will be relocated to the cells surface. However, the presence of circulating PCSK9 disturbs the recycling process. PCSK9 binds to the LDLR followed by co-internalized and lysosomal degradation of the receptor, resulting in the reduction of hepatic uptake of LDL^{106, 108}. The decrease of LDL uptake leads to an increase of

circulating plasma LDL, generating a hyperlipidemic state and causing athero-prone mice (Figure 5).

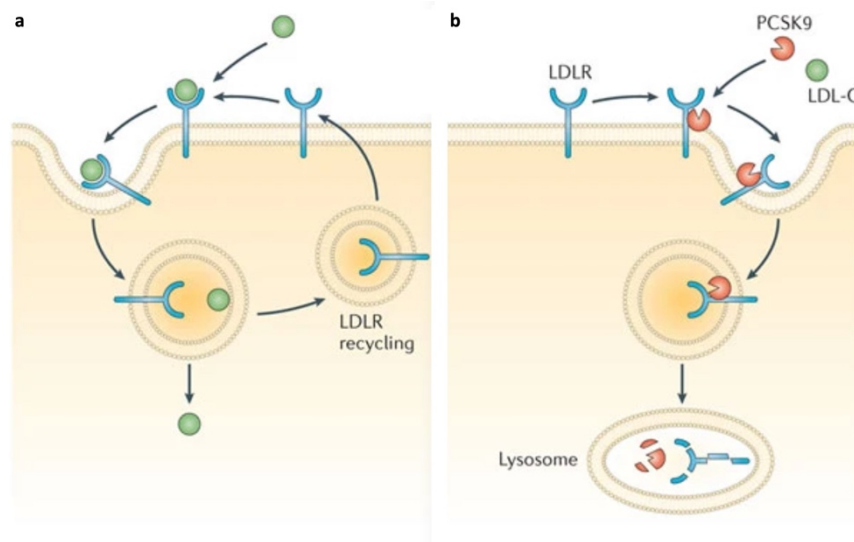


Figure 5. Mode of action of PCSK9 inducing a hyperlipidemic state.

(a) LDL-C is removed from the blood stream by binding to the LDLR. The LDLR incorporates the LDL-C into the cells, after which the LDLR is recycled and reappears on the cells surface. (b) Extracellular PCSK9 binds the LDLR, driving internalization and lysosomal degradation of the receptor. LDL-C continues to circulate resulting in hyperlipidemia. LDL – Low-density lipoprotein, LDL-C – LDL cholesterol, LDLR – LDL receptor, PCSK9 – Proprotein Convertase Subtilisin Kexin. Adapted from Mullard, 2012¹⁰⁹.

AAV vectors can ensure long-term transgene expression¹¹⁰⁻¹¹². Roche-Molina *et al.* and Bjørklund *et al.* showed that mice expressed stable amounts of PCSK9 mRNA in the liver 1-year post single intravenous injection with a gain-of-function mutant of *Pcsk9* (human D374Y or murine D377Y, respectively)^{103, 104}, confirming the chronic effect of one AAV injection. No adverse effects, such as signs of immunologic response or liver damage, were observed. Of interest, total serum cholesterol levels were doubled compared to control mice. Furthermore, feeding the mice a high-fat diet intensified hyperlipidemia by a four-fold increase in plasma cholesterol levels while keeping an equal distribution between VLDL and LDL particles¹⁰⁴. Interestingly, in other mouse models of atherosclerosis, an equal distribution of cholesterol particles is not observed. The ApoE^{-/-} model shows a non-human-like lipid profile, with a very high increase of VLDL, increased LDL, and decreased HDL levels, which makes this model not the ideal model to study atherosclerosis, since translation from mouse to human will be difficult. Furthermore, ApoE plays a role in inflammation and its deficiency will influence plaque development. The LDL^{-/-} model is more appropriate model to study atherosclerosis since it mimics a more human-like lipid profile. However, plaques will not develop spontaneously and a high-fat diet (HFD) or western-type diet (WTD) is needed to induce plaque formation. On the other hand, PCSK9-AAV model has a big advantage, since no genetic modification are needed to establish this model. The LDL^{-/-} model and PCSK9-AAV model seem more similar

in respect to the lipid profile, compared to the ApoE^{-/-} model. However, the distribution of the lesions and their composition are rather similar between models after a WTD of 20 weeks¹¹³(Figure 6).







	Model	Lipid profile	Plaque distribution and characteristics (20 weeks WD)	Advantages & limitations
ApoE ^{-/-}	Disruption of the ApoE gene 	Plasma cholesterol: 400-600 mg/dl on ND >1000 mg/dl on WD Lipoproteins: ↑↑ VLDL ↑ LDL ↓ HDL	 Fibrous plaques: Smooth muscle cells Extracellular matrix Inflammatory cells Necrotic core	<ul style="list-style-type: none"> ➢ Develops atherosclerosis on ND ➖ No human-like lipid profile ➖ ApoE plays a role in inflammation → influence plaque development ➖ No spontaneous plaque rupture, thrombosis and complications
LDLr ^{-/-}	Disruption of the LDL receptor gene 	Plasma cholesterol: 200-300 mg/dl on ND >1000 mg/dl on WD Lipoproteins: ↓ VLDL ↑↑ LDL = HDL	 Fibrous plaques: Smooth muscle cells Extracellular matrix Inflammatory cells Necrotic core	<ul style="list-style-type: none"> ➢ Human-like lipid profile (LDL) ➢ Functional ApoE → no impact on inflammation ➖ Complex lesion development requires a WD ➖ No spontaneous plaque rupture, thrombosis and complications
PCSK9-AAV	Single Adeno-Associated Virus-mediated gene transfer of mutant PCSK9 	Plasma cholesterol: 300 mg/dl on ND >1000 mg/dl on WD Lipoproteins: ↓ VLDL (only on WD) ↓ LDL = HDL	 Fibrous plaques: Smooth muscle cells Extracellular matrix Inflammatory cells Necrotic core	<ul style="list-style-type: none"> ➢ No genetic modification needed ➖ Lesion development requires a WD ➖ No spontaneous plaque rupture, thrombosis and complications

Figure 6. Overview of the ApoE^{-/-},LDLr^{-/-} and PCSK9-AAV mouse models used to study atherosclerosis.

This figure describes the three different models of atherosclerosis and their total plasma cholesterol levels on a ND or WD, lipoprotein profile, plaque distribution and characteristics, and advantages and limitations. The plaque distribution in the aortic artery is shown for mice fed a WD for 20 weeks. The composition of most lesions in the aortic root or brachiocephalic artery at that time point is displayed. AAV – Adeno associated virus, ApoE – Apolipoprotein E, HDL – High-density lipoprotein, LDL - Low-density lipoprotein, LDLr - Low-density lipoprotein receptor, ND – Normal diet, PCSK9 - Proprotein convertase subtilisin/kexin type 9, VLDL - Very-low-density lipoproteins, WD – Western-type diet, Adapted from Veseli et al., 2017¹¹³.

Atherosclerotic lesions form in the regions of disturbed blood flow. The disturbed flow influences gene expression in ECs, although not much is known regarding the effect of disturbed blood flow and atherosclerosis on endothelial heterogeneity. Nevertheless, the transcriptome and chromatin accessibility showed to be highly heterogeneous and plastic when ECs enriched from the left- and right carotid artery exposed to disturbed flow and stable flow, respectively, were compared. The disturbed flow induced a dramatic transition of ECs from an athero-protective phenotype to an athero-prone phenotype. This phenotypical switch resulted in endothelial inflammation and dysfunction, permeability, and endothelial-to-mesenchymal transition, and thrombosis¹¹⁴. Additionally, previous studies showed that leukocyte adhesion oscillated, and recruitment to atherosclerotic lesions peaks during the transition from the activity to the resting phase. In contrast, recruitment to the microvascular

beds peaked during the early activity phase²⁵. This shows that recruitment oscillates and does not occur heterogeneously in different vessel types, indicating that vessel heterogeneity seems to influence leukocyte recruitment.

1.4 - Circadian rhythmicity

The behavior of the majority of organisms is coordinated by daily environmental changes generated by the earth's rotation. Examples of such environmental changes include light/darkness, temperature, and seasonal cycles. Furthermore, food availability and uptake are essential factors that influence behavior. Continuous exposure to environmental changes drives the development and evolution of organisms. As a response, organisms adapt their immune system and metabolism to environmental changes by establishing 24-hour rhythms of their physiological processes¹¹⁵. Hence, analyzing a certain cell type, or a tissue, at different times of the day may result in differences in the assessed parameters. Therefore, to rule out variability due to circadian rhythmicity, throughout the experiment, the evaluation should be performed at the same time of the day.

This daily rhythm, also known as circadian rhythm (Circa Diem - 'for about a day'), was described for the first time in 1729. The French geophysicist Jean Jacques d'Ortous de Mairan observed that the leaves of the *Mimosa pudica* folded and unfolded in a circadian manner¹¹⁶. The circadian rhythm affects oscillations in cells across many species, including birds, cyanobacteria, flies, fungi, plants, and humans. This rhythm controls about 10-20% of the mammalian genome directly and more than 20% in an indirect way^{115, 117, 118} and 40% of all protein-coding genes show circadian rhythmicity, a phenomenon that seems mostly organ specific¹¹⁹.

The circadian pacemaker is regulating the circadian expression of genes and proteins and is also known as the central clock. The clock consists of 20.000 nerves and resides in the suprachiasmatic nucleus (SCN) in the hypothalamus¹²⁰. This intrinsic biological clock is preserved across many species¹¹⁵, with the sleep-wake cycle as its most distinct output. However, it also regulates the locomotor activity, body temperature, the cardiovascular and digestive system, and the endocrine and immune system¹²¹⁻¹²³. The SCN major entrainment factor or Zeitgeber (ZT, from the German 'time giver') is light^{124, 125}. Mammals experience the light signal via the eye, which is forwarded via the retinohypothalamic tract to the SCN. Here the signal can be translated by hypothalamic-pituitary-adrenal (HPA) axis or via the autonomic nervous system (ANS). In turn, the peripheral clocks (e.g. immune cells and vessels) are coordinated by internal ZT as temperature and glucocorticoids^{122, 125, 126}. More recently, it has

been observed that feeding-related metabolic cues and humoral entrainment were also crucial to regulate circadian rhythms. For example, the circadian rhythm in the liver is heavily influenced by food uptake^{127, 128}.

The central clock synchronizes all processes in the body via entraining the peripheral clocks via systemic and endocrine clues^{120, 124, 125, 129}. Virtually all cells contain clock machinery components¹²⁵. The peripheral clocks share the same clock machinery as the central clock; however, they regulate tissue-specific genes and functions^{118, 130-132}. The basic machinery of the clocks is based on a transcription-translation feedback loop. The genes *Per* (Period) and *Cry* (Cryptochrome) are rhythmically transcribed and negatively regulate their transcriptional activators CLOCK (Circadian Locomotor Output Cycles Kaput), BMAL1 (Brain and Muscle Aryl Hydrocarbon Receptor Nuclear Translocator-like Protein 1) and NPAS2 (Neuronal PAS Domain Protein)¹³³. The peripheral, as well as the central clocks, are cell-autonomously. The clocks need to interact with each other to maintain synchrony between cells. Synchrony is vital while loss of synchrony leads to desynchronization of the peripheral clocks get, and their oscillatory patterns flatten out over time¹²⁵.

Circadian rhythmicity has been study in different pathological conditions and the relationship between circadian rhythm and infections was studied already 60 years ago. It was observed that mice died in a circadian manner after administering a high dose of endotoxins¹³⁴. Additionally, the susceptibility to pneumococcal infection depends on rhythmic adrenocortical secretions or light¹³⁵. More recently, it has been shown that systemic cues led to differential circadian oscillations in chemokines and endothelial adhesion molecule expression in a tissue-specific manner^{25, 122}. At the same time, the number of ECs do not seem to oscillate in vessel of the lung¹³⁶. Moreover, research has identified that molecular clocks influence leukocyte immune cell trafficking, host-pathogen interactions, and the activation of innate and adaptive immunity^{123, 124}.

Scientists try to identify how environmental and genetic disruptions of the circadian clock can cause exacerbated pathologies in animals or humans¹³⁷⁻¹⁴¹. It is widely known that humans suffering from diseases as asthma, acute coronary syndrome, acute myocardial infarction, rheumatoid arthritis, or ventricular arrhythmias show a circadian variation in the occurrence of disease markers and symptoms¹⁴²⁻¹⁴⁶. Arising from this, many studies investigate whether drugs are more efficient when given at specific times of the day, also known as chrono-immunotherapy. Notably, most of the top-selling drugs control circadian targets¹¹⁹. In chronobiology, researchers study different aspects of the oscillations, such as amplitude, the difference between mean and peak values, the acrophase, the highest (peak) and the lowest

value (trough). The term ZT is used to indicate the timing of the entrainment stimulus. Under the external cue of light/darkness, the term ZT is used to describe the timing of the light turning on or off (e.g. in a 12h:12h light/darkness scheduling in an animal facility: ZT0 = onset of light, ZT12 = end of light).

The light/darkness cues have revealed to control ECs regulatory functions in a circadian way. The functions controlled by circadian rhythms varies from cytokine production, leukocyte mobilization from the bone marrow to leukocyte recruitment to tissues under homeostatic as well as an acute inflammatory condition^{122, 147-150}. Furthermore, the peripheral blood leukocyte counts oscillate throughout the day and a peak can be observed during the behavioral resting phase (total white blood cells (WBC), ZT5)^{22, 122, 151} (**Figure 7a**). Interestingly, leukocytes were observed to predominantly immigrate into peripheral tissues, during the organism's active phase. This recruitment has been linked to the oscillatory change in the expression profile of adhesion molecules on leukocytes as well as ECs²² (**Figure 7b**). Additionally, as mentioned above, Zhang *et al.* also showed circadian rhythmicity of 40% of the protein-coding genes, a phenomenon which was mainly organ specific¹¹⁹. Interestingly, many prescribed drugs target oscillating genes, and most of these drugs have short half-lives. Therefore, timed-optimized delivery, chrono-pharmacology, may harbor an immense benefit and may permit enhanced therapeutic efficacy while reducing side effects¹⁵². Consequently, a better understanding of the role of this rhythmicity on organ-specific heterogeneity would be of great interest to optimize chronotherapeutic targeting approaches. Ideally treatments could become specific by directing drugs at a specific time of the day to one specific organ. To achieve this our knowledge on organ-specific EC heterogeneity in homeostasis and upon different inflammatory conditions should be improved.

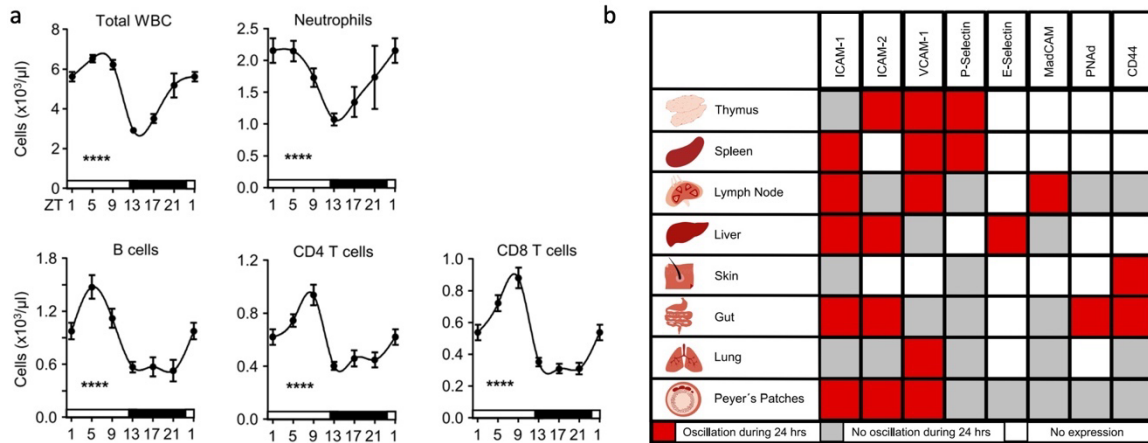


Figure 7. Oscillation of peripheral blood leukocytes and tissue-specific ECs adhesion molecules.

(a) Total leukocyte and leukocyte subset counts over 24 hr. **(b)** Map of rhythmic protein expression of endothelial cell-adhesion molecules of various organs (n = 3–6 mice with 6 time points measured each). ECs – Endothelial cells, WBC – White blood cell, ZT - Zeitgeber time²².

1.5 - Aim of the study

Within this thesis, I aim to characterize the endothelial transcriptome of mice in steady-state and different inflammatory conditions (acute inflammation – endotoxemia, and chronic inflammation – hyperglycemia (diabetes) and hyperlipidemia (atherosclerosis)) of eight organs (aorta, bladder, bone, colon, ileum, kidney, liver, and lung), while cells were harvested in the morning (ZT1, 8 am) or evening (ZT13, 8 pm). The eight organs were selected based on their angiodiversity, namely the vessels in the aorta, bladder, bone, and lung are covered by continuous endothelium, while the vessels in the colon, ileum, and kidney are lined with fenestrated and the liver with sinusoidal endothelium. Different conditions were studied to facilitate the identification of condition specific targets, which might be beneficial for patients coping with a chronic inflammatory disease, and additionally coping with other inflammatory co-morbidities. In such situations, compromising host defenses might jeopardize the patient and organ- and disease-specific targets, 'ZIP'-codes, might protect the patient. ECs will be isolated in the morning and evening to incorporate the circadian aspect, facilitating identification of more suitable markers of drug delivery. Consequently, possibly enhancing therapeutic efficacy by chrono-pharmacology while drug targets might oscillate during the day. To study EC heterogeneity ZT1 and ZT13 were selected since the number of circulating leukocytes vary the most between these two time-points, which might correlate with molecule expression on the endothelium. Eventually, DE, marker, and organ-specific genes will be identified, which will pave the way to the establishment of an atlas of endothelial heterogeneity. This thesis incorporated the difference between ECs in steady- and different inflammatory

states and includes the effect of circadian rhythmicity on endothelial heterogeneity, contributing to the establishment of an atlas of EC heterogeneity.

2 - Materials and Methods

2.1 - General buffer preparation

The protocols for red blood cell lysis buffer and HANKs buffer preparation can be found below (Table 2).

Table 2. General buffers.

Buffer and solution	Recipe
Antibody staining solution	1X PBS (GIBCO) supplemented with 20 µl/ml mouse serum (Sigma Aldrich), 20 µl/ml rabbit serum (Sigma Aldrich), 20 µl/ml human serum (Sigma Aldrich) + 50 µl HANKs buffer
Na-Citrate buffer	0.1 M Na-Citrate (Sigma Aldrich), 0.1 M Citric acid (Sigma Aldrich), pH 4.5
Digestion medium	RPMI1640 (GIBCO), 10% FBS (Thermo Fisher Scientific)
HANKs	10X HANKs buffered salt solution (HBSS, Sigma Aldrich), 0,06% BSA (Serva), 0.5 mM diNaEDTA (Sigma Aldrich)
Red blood cell lysis	150 mM NH ₄ Cl (Sigma Aldrich), 10 mM KHCO ₃ (Sigma Aldrich), 0.1 mM diNaEDTA (Sigma Aldrich), pH 7.4
Segregation buffer	1X HBSS (Sigma Aldrich), 2.5 mM Hepes (Sigma Aldrich), 5 mM EDTA, 5% FBS (Thermo Fisher Scientific)

2.2 - The *Tabula Muris* dataset - Endothelial transcriptome in steady state

2.2.1 - Dataset

The *Tabula Muris* consortium published the single-cell transcriptomics of 20 mouse organs (four male and three female adult C57BL/6 mice). They created a *Tabula Muris*, an online open-access database containing a compendium of single cell transcriptome data from mice under homeostatic conditions⁴⁹. In short, two methods were used to separate single-cells for scRNA-seq, namely fluorescence-activated cell sorting (FACS) and microfluidic droplet-based sorting. The *Tabula Muris* Consortium reported a high variability in the number of genes detected per cell between organs and methods. Therefore, only the data acquired from the FACS was used. The consortium identified clusters within a given tissue and annotated cell types based on known markers. Five organs were selected to study the ECs transcriptome.

2.2.2 - Data processing

Data processing was done by Markus Joppich (Ph.D. student from Prof. Zimmer, Teaching and Research Unit Bioinformatics Institut für Informatik, LMU). Cells were excluded from

downstream analysis when they had less than 500 detected genes and less than 50,000 confidentially mapped reads. Log-normalization was performed to convert raw counts to log counts per million and counts were subsequently scaled. The effects of confounding factors, such as total number of reads, ribosomal RNA, and percentage of External RNA Controls Consortium (ERCC) an RNA spike-in Mix control, were removed from the dataset by linear regression. Upregulated genes with a false discovery rate (FDR) of ≤ 0.05 and a Log Fold Change (logFC) of ≥ 0.8 were selected for downstream analysis. Surface expression was predicted based on text mining of PubMed articles and with the use of databases predicting the subcellular location of the protein (databases: UniProt, Pfam, and InterPro annotation).

2.3 - Small-bulk RNA-seq - The effect of an inflammatory stimulus on endothelial transcriptome

2.3.1 - Mice and tissue collection

Experiments were performed using five months old female VE-cadherin-cre-rfp^{flx/flx} mice derived from in-house breeding. Two experimental conditions were studied, a homeostatic and acute inflammatory condition. The mouse experiencing acute inflammation was injected intraperitoneally (*i.p*) with a dose of 20 mg/kg LPS from Escherichia coli O111:B4 (Thermo Fisher Scientific), diluted in 1X Phosphate-Buffered Saline (PBS)(GIBCO). The mouse was sacrificed four hours after the injection at ZT3 (10 am). All animal procedures were performed according to national guidelines for animal welfare and were approved by the Government of Upper Bavaria (Regierung von Oberbayern, TierSchG AZ ROB- 55.2-1-54-2532-233-2015).

2.3.2 - Genotyping

Tail biopsies and genotypic analysis was performed by Ms. Schengel (Medical technical assistant, Prof. Söhnlein, LMU). The tissues were incubated in 250 μ l of tissue lysis buffer with proteinase k solution (0,2 mg/ml, Qiagen) and digested at 56°C overnight. DNA was isolated with a QIAextractor (Qiagen) according to the manufacturer's instructions. Polymerase chain reaction (PCR) reagent mixes were prepared (**Table 3**) and contained either wildtype- and/or mutant allele-detecting primer pairs (**Table 4**). The PCR reaction programs were set to verify the expression of VE-cad and ROSA26 flox STOP flox RFP (Red Fluorescent Protein) construct (**Table 5**). The PCR products were analyzed with a QIAxcel Advanced System (Qiagen), according to the manufacturer's instructions. For VE-cad transgenic mice a band was observed at 345 base pairs (bp), while for wild type mice no bands were observed. The bands for ROSA26 flox STOP flox RFP could be observed at 500 bp for wild type, 300 bp for transgenic and at 500 and 300 bp for heterozygote animals. A positive and negative (water) control was included in every analysis.

Table 3. Genotyping PCR master mix.

Reaction component	Final concentration
5X Green Gotaq Flexi buffer (Promega)	1X
25 mM MgCl ₂ (Sigma Aldrich)	1,5 mM
dNTPs (Sigma Aldrich)	0,2 mM
Forward Primer (Sigma Aldrich)	0,5 μM
Reverse Primer (Sigma Aldrich)	0,5 μM
GoTaq DNA polymerase (Promega)	0,05 U/μl
Genomic DNA (Promega)	200 ng

Table 4. Genotyping primers.

VE-cad	5'-3'-sequence
VE-cadherin forward	CCA GGC TGA CCA AGC TGA G
VE-cadherin reverse	CCT GGC GAT CCC TGA ACA
Internal positive control forward	CTA GGC CAC AGA ATT GAA AGA TCT
Internal positive control reverse	GTA GGT GGA AAT TCT AGC ATC ATC C

ROSA26 flox STOP flox RFP	5'-3'-sequence
ROSA26 wild type reverse	GGA GCG GGA GAA ATG GAT ATG
ROSA26 mutant reverse	GCG AAG AGT TTG TCC TCA ACC
ROSA26 common forward	AAA GTC GCT CTG AGT TGT TAT

Table 5. Genotyping cyclor protocols.

PCR cycle protocols for VE-cad and ROSA26 flox STOP flox RFP. min – minutes, PCR - Polymerase chain reaction, RFP – Red Fluorescent Protein, sec – seconds, VE-cad – VE-cadherin.

VE-cad			ROSA26 flox STOP flox RFP		
Step	Temperature (°C)	Time	Step	Temperature (°C)	Time
1	94	2 min	1	94	5 min
2	94	20 sec	2	94	1 min
3	65	15 sec	3	67	1 min
4	68	10 sec	4	72	1 min
Repeat steps 2-4 for 10 cycles			Repeat steps 2-4 for 4 cycles		
5	94	15 sec	5	94	1 min
6	60	15 sec	6	62	1 min
7	72	10 sec	7	72	1 min
Repeat steps 5-7 for 28 cycles			Repeat step 5-7 30 cycles		
8	72	2 min	8	72	5 min
9	21	5 min	9	4	hold

2.3.3 - Harvest

The mice were anesthetized by intraperitoneal injection of a Ketamine/Xylazine overdose (100 mg/kg Ketamine (Medistar) and 7 mg/kg Xylazine (Rompun, Bayer vital GmbH), diluted in saline solution 0.9% (Braun). After 4 min the mice were injected intravenously (*i.v.*) with antibodies to stain the glycocalyx, ECs, and leukocytes, using AlexaFluor647-conjugated Isolectin (50 µg, GS-IB₄ *Griffonia simplicifolia*, I32450, Thermo Fisher Scientific), PE/Cyanine7-conjugated CD31 (10 µg, clone MEC13.3, 102524, BioLegend), and Super Bright 600-conjugated CD45 (3 µg, clone 30-F11, 63-0451-82, eBioscience) respectively. The heart was punctured, and the blood was collected in tubes containing ethylenediaminetetraacetic acid (EDTA, Sarstedt) to avoid coagulation by chelating calcium ions. The vascular system was perfused with 10 ml of 1X PBS (GIBCO) with 0.5 mM EDTA (Karl Roth), after which the lung, aortic arch, and descending aorta were isolated. A single-cell suspension was prepared to perform FACS.

2.3.4 - Organ harvest and cell dissociation

2.3.4.1 - Aorta – Aorta arch and descending aorta

After the harvest, the aortic arch and descending aorta were placed in ice-cold 1X PBS (GIBCO). Digestion took place in digestion medium (RPMI1640 (GIBCO), 10% Fetal Bovine Serum Fetal Bovine Serum (FBS)(Thermo Fisher Scientific)) containing Liberase (1,25 mg/ml, Roche) and Actinomycin-D (final concentration 45 µM, Merck). The organ was chopped into

small fragments and incubated at 37°C for 1 hour. Afterwards, 1 ml of HANKs buffer was added, and the lysate was filtered through a 35 µM cell strainer cap (Falcon).

2.3.4.2 - Lung

The right superior lobe was taken, added to 1X PBS (GIBCO) containing Liberase (1,25 mg/ml, Roche) and Actinomycin-D (final concentration 45 µM, Merck). The lobe was chopped into small fragments and incubated at 37°C, 300g for 30 min. HANKs buffer was added to stop the digestion and the cells were filtered through a 50 µM cell strainer (Sysmex). The cells were pelleted, resuspended in red blood cell lysis buffer, to lyse red blood cells, and incubated for 1 min on ice. HANKs buffer was added to stop the lysis reaction.

2.3.5 - Fluorescence-activated cell sorting

FACS is a laser-based method used to identify the expression of intracellular and extracellular molecules and sort cells of interest. Fluorescently labeled antibodies, which interact with these molecules, are used to stain the cell. Cells in a single cell suspension are pass through a laser beam and several detectors pick up the forward and sideward scattered light as well as fluorescent signals. The forward scattered light (FSC) provides information regarding the size of the cell, whereas the side scattered light (SSC) allows to discriminate cell granularity. A fluorescent signal and intensity underline the presence of the molecule on or in the cell that is targeted by the antibody labeled with the fluorescent probe.

Right before FACS, 4',6-Diamidino-2-phenylindol (DAPI, 1:5000, Thermo Fischer Scientific) was added to the single-cell suspension of the aorta and lung sample. This dye only passes through the cell membrane of dead cells and is therefore used to visualize cell viability. FACS was performed with a BD FACSAria III Cell Sorter (BD Bioscience), and the following strategy was used to sort ECs: DAPI-CD45-VE-cad+CD31+Isolectin+ (**Figure 8**). Single cell sorting of 50 cells per organ per well, resulting in a small-bulk, took place in a 96 well plate, containing 4 µL lysis buffer with ERCC (1:24,000,000, Ambion, Life Technologies), 2.5 mM Deoxynucleoside triphosphate (dNTP), 2.5 µM oligo-dT, 0.05% Triton X-100 (Sigma), and 2 U/µL recombinant RNase inhibitor (Clontech). The plates were centrifuged and stored at -80°C.

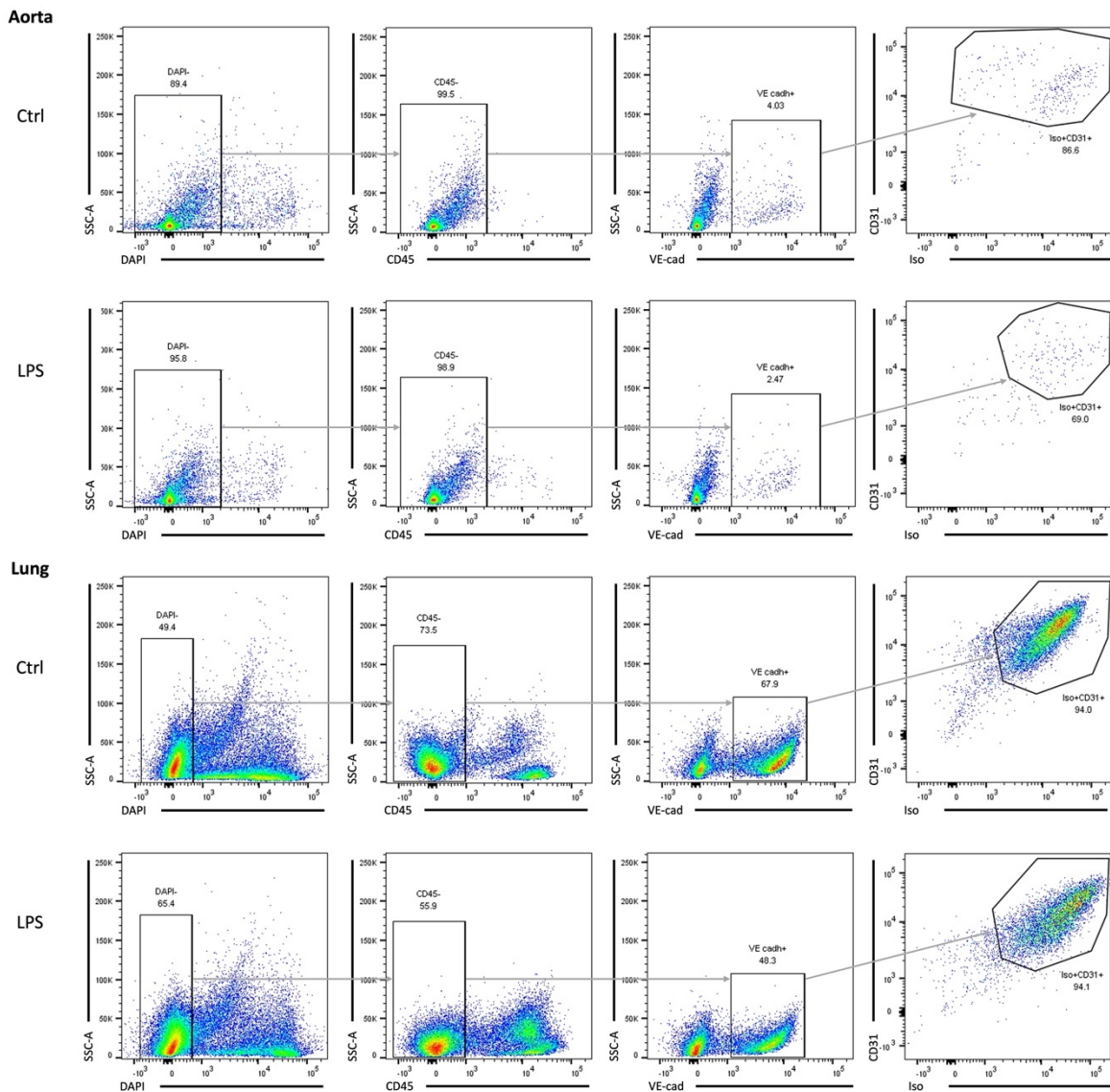


Figure 8. Sorting strategy of endothelial cells from the aorta and lung in homeostasis and inflammatory condition.

VE-cadherin-cre-rfp^{flox/flox} mice were injected with antibodies against Isolectin, CD31 and CD45. ECs from the aorta and lung from a mouse in homeostatic condition (n=1) and acute inflammatory condition (i.p. LPS injection 4 hours prior harvest, n=1) were sorted (DAPI⁻CD45⁻VE-cad⁺CD31⁺Isolectin⁺) and send for RNA sequencing to characterize the transcriptome of the ECs. DAPI – 4',6-Diamidino-2-phenylindol, ECs – Endothelial cells, Ctrl – Ctrl, Iso – Isolectin, LPS – Lipopolysaccharide, SSC – Side scattered light, VE-cad - Vascular Endothelial Cadherin.

2.3.6 - Library preparation

Library was prepared by Simon Besson-Girard (Ph.D. student from Dr. Özgün Gokce, Institute for Stroke and Dementia Research, LMU). The 96-well plates were thawed, incubated for 3 min at 72°C, and afterwards kept on ice. To perform reverse transcription (RT), a mix of 0.59 µL H₂O, 0.5 µL SMARTscribe™ Reverse Transcriptase (Clontech), 2 µL 5x First Strand buffer, 0.25 µL Recombinant RNase Inhibitor (Clontech), 2 µL Betaine (5 M Sigma), 0.5 µL Dithiothreitol (DTT, 100 mM), 0.06 µL MgCl₂ (1 M Sigma), 0.1 µL Template-switching oligos

(TSO; 100 μ M AAGCAGTGGTATCAACGCAGAGTACrGrG+G) was added to each well. The RT reaction mixes were incubated for 90 min at 42°C followed by 5 min at 70°C, 10 cycles of 2 min at 50°C, 2 min at 42°C, and finally for enzyme inactivation, 5 min at 70°C. Pre-amplification of cDNA was achieved by adding 12.5 μ L KAPA HiFi Hotstart 2x (KAPA Biosystems), 2.138 μ L H₂O, 0.25 μ L ISPCR primers (10 μ M, 5' AAGCAGTGGTATCAACGCAGAGT-3), and 0.1125 μ L Lambda Exonuclease, followed by incubation of samples for 30 min at 37°C, 3 min at 95°C, and 18 cycles of 20 sec at 98°C, 15 sec at 67°C, and 4 min at 72°C, and a final extension for 5 min at 72°C. Libraries were cleaned using AMPure bead (Beckman-Coulter) cleanup (0.7:1 ratio of beads to PCR product). The quality and quantity of the libraries was assessed by a Bio-analyzer (Agilent 2100), and Qubit 4.0 Fluorometer (Invitrogen, LifeTechnologies) using for both the DNA high sensitivity assay kits. All samples were normalized to 160 pg/ μ L. Sequencing libraries were constructed using an in-house produced Tn5 transposase¹⁵³ and barcoded with the Illumina Nextera XT (FC-131-1096, Illumina). The libraries were pooled and cleaned by three rounds of AMPure bead (Beckman-Coulter) cleanup (0.8:1 ratio of beads to library).

2.3.7 - Sequencing

Sequencing was performed by the Munich Sequencing Alliance. Libraries were sequenced 2x150 reads bp paired-end on an Illumina HiSeq4000.

2.3.8 - Data processing

After sequencing, data processing was performed by Simon Besson-Girard (Ph.D. student from Dr. Özgun Gokce, Institute for Stroke and Dementia Research, LMU). Samples were demultiplexed with the bcl2fastq software from Illumina. Followed by trimming and quality control by Trim Galore and Cutadapt, respectively. The samples were aligned onto the mouse genome using rnaSTAR¹⁵⁴ version GRCm38. Read counts were collected using the parameter "quantMode GeneCounts" of rnaSTAR and using the unstranded values. Further processing was done with the Seurat package in R v.2.3.4¹⁵⁵. Low-quality samples were removed from the dataset based on the number of genes detected (min 1,000 unique genes/pool), percentage of mitochondrial genes (max 0.5%), percentage of ERCCs (5% max) and number of reads on a log₁₀ scale (between 5 to 6.5), resulting in 20 pools passing the quality-control. Gene expression was normalized to log(CPM+1 (Counts per million mapped reads+1)) using the NormalizeData function of Seurat (scale factor of 1,000,000). Dataset was corrected for sequencing depth by regression against the total number of reads and for eventual amplification bias using the ScalteData function and the percentage of ERCCs. The top 1,000

most variable genes were considered for the principal component analysis (PCA). PC1 explained 51.3% of the variance, while PC2 explained 20.7%.

2.4 – scRNA-seq - The effect of acute and chronic inflammation together with circadian rhythmicity on endothelial transcriptome

2.4.1 - Mice and tissue collection

Tissues were collected from 12 weeks old male VE-cadherin-cre-rfp^{flox/flox} mice derived from in-house breeding. The mice were kept under four experimental conditions, namely homeostasis, acute inflammation, hyperglycemia, and hyperlipidemia. Mice were harvested at either ZT1 (8 am) or ZT13 (8 pm). The aortic arch, descending aorta, bladder, kidney, bone, colon, ileum, liver, and, lung were harvested. All animal experiments are approved by the local ethical committee for animal experimentation (TierSchG AZ ROB- 55.2-1-54-2532-233-2015). Genotyping was executed as described in chapter 2.3.2.

2.4.1.1 - Acute inflammatory condition

Mice of 12 weeks old were injected *i.p.* with LPS from Escherichia coli O111:B4 (Thermo Fisher Scientific). This cell wall protein of gram-negative bacteria was administered at a dose of 20 mg/kg diluted in 1X PBS (GIBCO). The mice were sacrificed four hours after the injection.

2.4.1.2 - Hyperglycemic condition

Eight weeks old mice were injected *i.p.* with STZ (50 mg/kg dissolved in 0.1M Natrium-Citrate buffer (pH 4.5), Santa Cruz Biotechnology) for five consecutive days¹⁵⁶. Streptozotocin destroys the insulin-producing β -cells of the pancreas, leading to persistent hyperglycemia. One week before the harvest, the level of hyperglycemia was assessed with the use of a glucose tolerance test. The mice were fasted for six hours, followed by measuring the basal plasma glucose level. Followed by administration of a dose of glucose (1 mg/kg glucose in NaCl₂, B. Braun Melsungen AG) intraperitoneally. The blood glucose level was measured at 15, 30, 45, 75, and 120 min after administration. Blood was drawn through puncturing the lateral tail vein with a cone-free 22-23G cannula and blood glucose was measured with an Accu-Chek Performa (Roche). Mice were sacrificed four weeks after the last STZ injection.

2.4.1.3 - Hyperlipidemic condition

The hyperlipidemic condition is established by transduction with a AAV8 carrying a gain-of-function mutation of *Pcsk9*, namely D377Y. These transgenic mice start overexpressing *Pcsk9* with the D377Y mutation in the liver. The secreted protein binds to the LDLR, leading to an increased endosomal and lysosomal degradation of LDLR¹⁰⁸. The decreased amount of liver

LDLR leads to a reduced hepatic uptake of LDL and therefore increased plasma cholesterol levels resulting in a state of hyperlipidemia¹⁵⁷. In this experimental group, the AAV (**Figure 9**, Vector Biolabs) was administrated intravenously (titer: 1×10^{11} vector genomes/mouse in 100 μ l NaCl₂, B. Braun Melsungen AG) to eight weeks old mice. This method was used without having to intercross the VE-cadherin-cre-rfp^{flox/flox} mice with *ApoE*^{-/-} or *Ldlr*^{-/-} mice, as a single injection with the AAV8 carrying PCSK9-D377Y is sufficient to induce hyperlipidemia when combined with HFD feeding¹⁰³. Mice were fed an HFD, containing 21% fat and 0.15% cholesterol (ssniff), for four weeks to induce a hyperlipidemic condition.

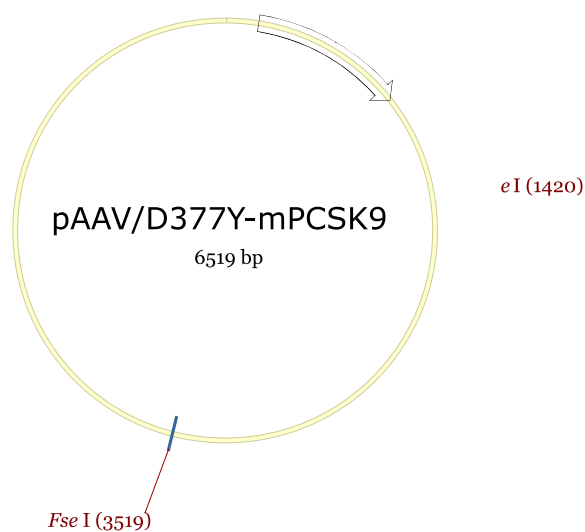


Figure 9. Construct of the PCSK9 vector.

Vector carrying murine PCSK9 with the gain of function mutation D377Y, under the hAAT promotor. Amp – Ampicillin, apoE – Apolipoprotein E, BGHpA – Bovine Growth Hormone Polyadenylation Signal, hAAT – Human Alpha-1 Antitrypsin, HCR – Human Apolipoprotein E/C-I Gene Locus Control Region, ITR – Inverted Terminal Repeat,

2.4.2 - Organ harvest and cell dissociation

To optimally standardize EC isolations, we isolated ECs from all eight tissues on the same day. Unfortunately, different conditions and time-points could not be harvested on the same day, due to experimental restrictions. A high cell viability is required, therefore samples cannot be kept on ice for long periods and must be processed swiftly, due to the large amount of samples it would not be possible to maintain a high cell viability.

A drop of blood was collected by puncturing the lateral tail vein with a cone-free 22-23G cannula and blood glucose was measured with an Accu-Chek Performa (Roche). The mice were anesthetized by intraperitoneal injection of a Ketamine/Xylazine overdose (100 mg/kg Ketamine (Medistar) and 7 mg/kg Xylazine (Rompun, Bayer vital GmbH), diluted in saline

solution 0.9% (Braun). The blood was collected by heart puncture and added to EDTA tubes (Sarstedt). The vascular system was perfused with 10 ml of 1X PBS (GIBCO) with 0.5 mM Ethylenediaminetetraacetic acid (EDTA, Karl Roth). The aortic arch and descending aorta, bladder, bone, colon, kidney, ileum, liver, and lung were harvested from three mice and pooled before the preparation of single cell suspensions.

2.4.2.1 - Aorta - Aortic arch and descending aorta

After the harvest of the aorta was placed in ice-cold 1X PBS (GIBCO). Digestion took place in RPMI1640 (GIBCO) + 10% FBS (Thermo Fisher Scientific) containing Liberase (1,25 mg/ml, Roche) and Deoxyribonuclease (DNase) (10 mg/ml, Sigma Aldrich). The organ was chopped into small fragments and incubated at 37°C for 30 min. Afterward, HANKs buffer was added, and the lysate was filtered through a 35 µM cell strainer cap. The cells were pelleted at 300g for 5 min, resuspended in red blood cell lysis buffer, and incubated for 1 min on ice. HANKs buffer was added to stop the lysis reaction. The single-cell suspensions from the three aortas were pooled.

2.4.2.2 - Bladder and kidney

The bladder and left kidney were extracted, and the urine was removed from the bladders. The organs were pooled (three bladders or three kidneys) and placed in ice-cold 1X HBSS (Sigma Aldrich). The two samples were placed in ice-cold 1X HBSS (Sigma Aldrich) containing calcium and magnesium with Liberase (1,25 mg/ml, Roche) and DNase (10 mg/ml, Sigma Aldrich). The organs were cut into small fragments and incubated at 37°C for 30 min. The digestion was stopped by adding HANKs buffer and the cells were filtered through a 50 µM cell strainer (Sysmex). After centrifugation, at 300g for 5 min, the cells were resuspended in red blood cell lysis buffer and incubated for 1 min on ice. The reaction was stopped by HANKs buffer.

2.4.2.3 - Bone

The left femur was extracted and placed in ice-cold 1X PBS (GIBCO). The femurs were flushed with 1 ml of 1X PBS (GIBCO), to remove the bone marrow cells, pooled, and placed in 1X PBS (GIBCO) containing Liberase (1,25 mg/ml, Roche) and DNase (10 mg/ml, Sigma Aldrich). After 20 min of incubation at 37°C, the bones were minced with the use of scissors and incubated for another 10 min at 37°C. To stop the digestion, HANKs buffer was added, and the cells were filtered through a 50 µM cell strainer (Sysmex). The cells were pelleted (300g for 5 min) and lysed for 1 min with red blood cell lysis buffer on ice. The lysis reaction was stopped by adding HANKs buffer.

2.4.2.4 - Colon and ileum

The colon, 3 cm after the cecum, and ileum, 3 cm before the cecum, were excised and washed with ice-cold 1X HBSS (Sigma Aldrich) without calcium and magnesium. The Peyer patches and excrement were removed. The colon and ileum's replicates were merged, and the two tissues were incubated in a pre-warmed segregation buffer at 37°C for 30 min under agitation, to remove the epithelial cells and intraepithelial lymphocytes. The tissues were further washed on a 50 µM cell strainer (Sysmex) with 1X HBSS (Sigma Aldrich) without calcium and magnesium and digested in 1X HBSS (Sigma Aldrich) containing calcium and magnesium with Liberase (1,25 mg/ml, Roche) and DNase (10 mg/ml, Sigma Aldrich). Digestion took place under constant agitation (300g) at 37°C for 30 min. The digestion stopped after adding HANKs buffer and the cells were filtered through a 70 µM cell strainer (Sysmex). After pelleting the cells, at 300g for 5 min, they were resuspended in red blood cell lysis buffer and incubated for 1 min on ice. Lysis was stopped after HANKs buffer was added.

2.4.2.5 - Liver

The left lobe of the liver was collected and placed in 1X PBS (GIBCO) at room temperature (RT). Equal pieces of the liver replicates were merged, and digestion took place in RPMI1640 (GIBCO) containing Liberase (1,25 mg/ml, Roche) and DNase (10 mg/ml, Sigma Aldrich). The livers were minced into small fragments and incubated at 37°C for 30 min. Afterwards, HANKs buffer was added and the lysate was passed through a 100 µM filter followed by a 40 µM cell strainer cap. RPMI1640 (GIBCO) was added and the cells were pelleted at 100g for 3 min, with rotor deceleration set to 6 (scale 1-9) to prevent dislodging of the cell pellet. The supernatant was collected, which contains the ECs, Kupffer and dead hepatocytes, and centrifuged at 163g for 10 min. The supernatant was discarded, and the pellet was resuspended in 25 ml RPMI1640 (GIBCO), followed by two centrifugation steps at 25g for 3 min. Both times ECs were found in the top 20 ml of the supernatant, which was collected with a 10 ml pipette (Costar) in a 50 ml falcon tube (Sarstedt). The collected 40 ml of RPMI1640 (GIBCO) containing the ECs was spun down at 163g for 10 min to pellet the cells, and the supernatant was removed. The pellet containing the ECs was resuspended in red blood cell lysis buffer and incubated for 1 min on ice. HANKs buffer was added to stop the lysis reaction.

2.4.2.6 - Lung

The right superior lobe was taken, and all three-lobe replicates were placed into 1X PBS (GIBCO) containing Liberase (1,25 mg/ml, Roche) and DNase (10 mg/ml, Sigma Aldrich). The lobes were chopped into small fragments and incubated at 37°C, 300g for 30 min. HANKs buffer was added to stop the digestion and the cells were filtered through a 50 µM cell strainer

(Sysmex). The cells were pelleted at 300g for 5 min, resuspended in red blood cell lysis buffer, and incubated for 1 min on ice. HANKs buffer was added to stop the lysis reaction.

2.4.3 - Cell counting, antibody and hashtag staining

Single-cell suspensions were kept on ice and the number of cells was counted. Per organ, an aliquot of 5 million cells was taken for antibody and hashtag staining. The aliquots were pelleted, and each aliquot was labeled with 45 µl of antibody staining solution supplemented with CD31 (0.8 µg, APC, clone: MEC13.3, BioLegend) and CD45 (1.6 µg, Brilliant Violet 605, clone: 30-F11, BioLegend). Furthermore, 5 µl of hashtag, from TotalSeq™-B Feature Barcode technology (0.25 µg, clone MHC1 M1/42; CD45 30-F11, BioLegend) for 10x Genomics 3' Single Cell Gene expression kit, was added to the cells suspension (**Table 6**).

Table 6. Hashtaged organs with TotalSeq™-B Feature Barcodes.

SI – Small intestine (Ileum)

Organ	Hashtags	Order nr.	Lot nr.	Sequence
Aorta	TotalSeq™-B 0301 anti-mouse Hashtag 1	155831	B289040	ACCCACCAGTAAGAC
Bone	TotalSeq™-B 0302 anti-mouse Hashtag 2	155833	B289033	GGTCGAGAGCATTCA
Bladder	TotalSeq™-B 0303 anti-mouse Hashtag 3	155835	B289046	CTTGCCGCATGTCAT
Colon	TotalSeq™-B 0304 anti-mouse Hashtag 4	155837	B289035	AAAGCATTCTTCACG
Kidney	TotalSeq™-B 0305 anti-mouse Hashtag 5	155839	B289037	CTTTGTCTTTGTGAG
Lung	TotalSeq™-B 0306 anti-mouse Hashtag 6	155841	B289041	TATGCTGCCACGGTA
SI	TotalSeq™-B 0307 anti-mouse Hashtag 7	155843	B289034	GAGTCTGCCAGTATC
Liver	TotalSeq™-B 0308 anti-mouse Hashtag 8	155845	B289036	TATAGAACGCCAGGC

The antibodies and hashtags were incubated with the single-cell suspension for 30 min on ice. HANKs buffer was added, and cells were pelleted, at 300g for 5 min. This pellet washing was repeated three times. After the third wash, HANKs buffer was added containing DAPI (1:10,000, Thermo Fischer Scientific).

2.4.4 - Fluorescence-activated cell sorting

Cells were sorted by FACS with the following sorting strategy: DAPI⁻CD45⁻ and either VE-cad⁺CD31⁺, VE-cad⁺CD31⁺ and VE-cad⁺CD31⁻ (**Figure 10**). Of each organ, 20.000 cells were sorted as bulk and collected in one Protein LoBind tube (Eppendorf) that contained 1X PBS

(GIBCO) with 1% Bovine serum albumin (BSA)(Serva). Thereby, the tube eventually contained 160.000 ECs of eight different organs. Upon analysis, organs can be discriminated by the hashtags. Two aliquots were taken to determine the viability of the cells. In the first aliquot, the viability was verified in a counting chamber with the use of Trypan blue (GIBCO) and additionally the number of cells was verified. The second aliquot was used to review the cell viability by flow cytometry, by re-staining the aliquot with DAPI (1:5,000, Thermo Fischer Scientific). Only the samples with a viability of 85% and higher were used for 10x Genomics experiments.

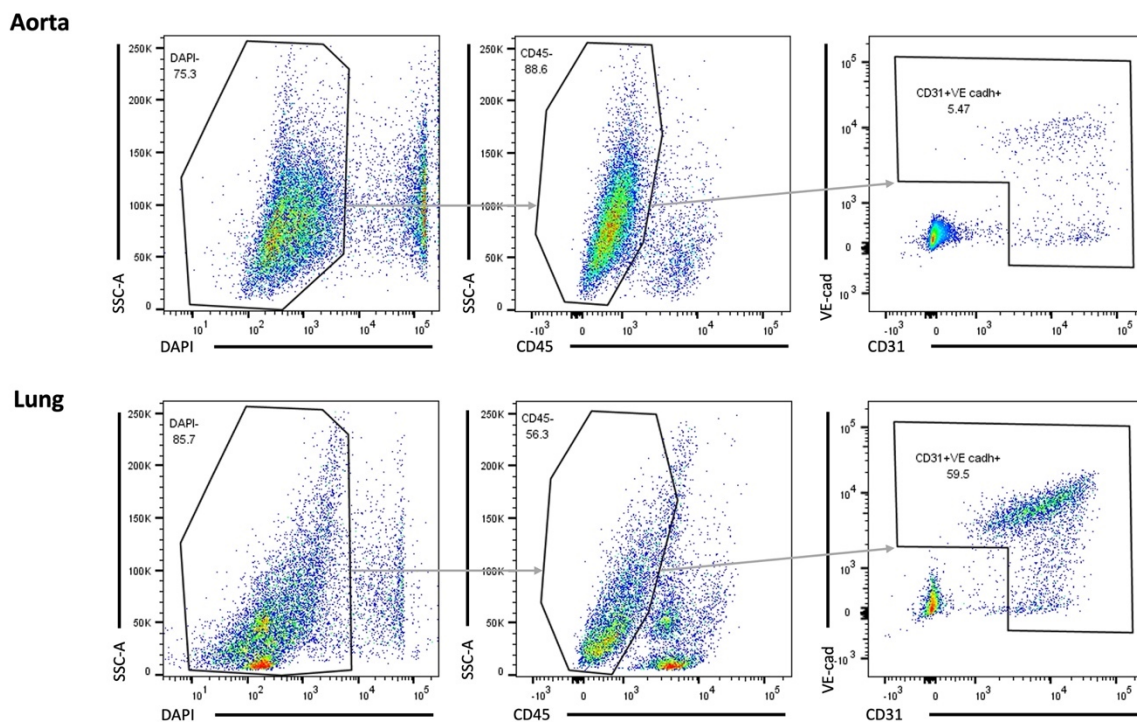


Figure 10. ECs sorting strategy aorta and lung in homeostasis condition.

Single cells suspension of VE-cadherin-cre-rfp^{flox/flox} were stained with antibodies against CD31 and CD45. ECs from the aorta and lung were sorted (DAPI⁺CD45⁺VE-cad⁺CD31⁺). ECs – Endothelial cells, DAPI – 4',6-Diamidino-2-phenylindol, SSC – Side scattered light, VE-cad - Vascular Endothelial Cadherin.

2.4.5 - 10x Genomics

Cells were mixed with a single-cell master mix, and the resulting cell suspensions were loaded on a 10x Chromium Next Gel Bead-in-Emulsion (GEM) Chip G with a target cell recovery for each library of 10,000 cells. The single-cell libraries were produced using the Chromium Next GEM Single Cell 3' Reagent Kits v3.1 with Feature Barcoding technology for Cell Surface Protein, according to the manufacturer's instructions (user guide CG000206 Rev D, 10x genomics). Each cell receives a barcode, resulting in the ability to treat the cells that were sorted in bulk as a single cells dataset. In short, in the chip the cells react with barcoded Single

Cell 3' V3.1 Gel Beads resulting in the generation of GEMs. GEM generation is directly followed by dissolving of the Gel Bead, release of the primers, and lysing any co-partitioning of the cell. Incubation with the primers leads to the generation of barcoded full-length cDNA from poly-adenylated mRNA and barcoded DNA from the cell surface protein Feature Barcode.

The cell barcoded products were purified, and the cell barcoded complementary DNA (cDNA) molecules were amplified via PCR to generate sufficient mass for library constructions. The number of PCR cycles was determined by measuring the quantity of cDNA using the BioAnalyzer High Sensitivity DNA Chip (Agilent Technologies). Size selection was used to separate the two types of libraries. Amplified full-length cDNA from poly-adenylated mRNA was used to generate 3' Gene Expression libraries and amplified DNA from cell surface protein Feature Barcodes to construct the Cell Surface Protein libraries. To optimize cDNA amplicon size, enzymatic fragmentation and size selection was performed.

2.4.6 - Sequencing

Before sequencing the libraries will be pooled, hence libraries were assigned a sample index to appoint treatment and timepoint upon analysis. The following steps were executed by Novogene. The insert size and quantity of the 3' Gene Expression and Cell Surface Protein libraries were determined using an Agilent Bioanalyzer with a high sensitivity chip (Agilent), and a KAPA DNA quantification kit for Illumina platforms (KAPA Biosystems). The libraries were pooled according to the target cell number loaded in a 4:1 ratio (3' Gene Expression : Cell Surface Protein libraries). Novogene sequenced the generated libraries on an Illumina HiSeq4000 read type PE150.

2.4.7 - Data processing

2.4.7.1 - Demultiplexing and cleaning

Gene expression matrices were generated using the CellRanger software (10x Genomics, version 3.1.0). The samples were demultiplexed with CellRanger `mkfastq` and aggregated and normalized for sequencing depth among multiple gene expression libraries using CellRanger's `aggr normalize`. The samples were aligned onto the mouse genome using `rnaSTAR`¹⁵⁴, version GRCm38. Further processing was done with the Bioconductor package¹⁵⁸ in R v.3.3.4. The following quality control steps were performed and cells and genes not fitting the recruitments were removed from the dataset: (i) genes expressed by less than five cells; (ii) cells that had a library size or expressed some genes that were three median absolute deviations (MAD) from the median; (iii) and genes from the mitochondrial genome using the functions `perCellQCmetrics` and `isOutlier`, both from the `scater` package¹⁵⁹. Furthermore,

genes that were expressed by less than five cell and low-abundance genes (ave.counts >= 0.00001) were removed.

2.4.7.2 - Hashtag demultiplexing and doublet detection

Hashtags and doublets were identified with the help of the CiteFuse package. The data was normalized (Trimmed Mean of the M-values (TMM)) and log-transformed by the `normalizeExprs` function. Dimension reduction on the Hashtags counts was executed by the `scater` package¹⁵⁹ using `runTSNE` or `runUMAP`, and the `visualiseDim` function from the CiteFuse package was used to visualize the reduced dimension plots. The dataset contained data from eight samples (subsets) which were pooled before 10x Genomics. The samples were demultiplexed and the eight clusters observed on t-Distributed Stochastic Neighbor Embedding (tSNE) plots equate to the eight different organs. Hereafter, doublets were identified. These doublets were a result of co-encapsulation of two or more cells within one droplet, resulting in a hybrid transcriptome of multiple cells. The CiteFuse package was used to implement a stepwise approach to detect and remove doublet. First, the cross-sample doublets were detected via the `crossSampleDoublets` function. Second, within-sample doublets were identified with help of the `withinSampleDoublets` function and finally, the doublet cells, both within and between organs, were removed from the dataset for the downstream analysis¹⁶⁰.

2.4.7.3 - Normalization and clustering

Data was normalized with `logNormCounts` function of the `scran` package¹⁶¹. The library size was converted into size factors to ensure that the normalized expression values were still on the same scale as the raw data, which was achieved with the use of the `librarySizeFactors` function. The data was pre-clustered with `quickCluster`, which led to the normalization of the cells in each cluster separately. Furthermore, the size factors were also rescaled to be comparable across clusters. This was done to avoid the assumption that most genes were non-DE across the entire population. Now only a non-DE majority between pairs of clusters is required, which is a weaker assumption for the dataset containing highly heterogeneous populations of only ECs. Both `librarySizeFactors` and `quickCluster` are from the `scater` package¹⁵⁹.

2.4.7.4 - Cleaning dataset: endothelial cells

The purity of the endothelial dataset was verified by examining the presence of non-EC markers. The dataset was checked and cleaned with the help of the `perCellQC` function from the `scater` package¹⁵⁹. Potential problematic cells were identified by classifying the number of known non-EC and EC genes. ECs were annotated based on the expression

of non-EC marker genes, namely lymphatic ECs: *Prox1* (Prospero homeobox 1) and *Pdpr* (Podoplanin), fibroblasts: *Col1a1* (Collagen type I alpha 1 chain), erythrocytes: *Hba-a1* (Hemoglobin A), *Hba-a2* and *Hbb-bs* (Hemoglobin B), smooth muscle cells *Acta2* (actin alpha 2), pericytes: *Pdgfrb* (Platelet derived growth factor receptor beta), leukocytes *Ptpnc* (Protein tyrosine phosphatase receptor type c), platelets: *Pf4* (Platelet factor 4), *Ppbb* (Pro-platelet basic protein) and the vascular EC marker genes *Pecam1* (Platelet and endothelial cell adhesion molecule 1), *Cdh5* and *Lyve1* (Lymphatic vessel endothelial hyaluronan receptor 1). Contaminating cells, which expressed non-ECs gene markers, were removed and downstream analysis was performed with ECs only.

2.4.7.5 - Differently expressed genes

The DE analysis was performed on “pseudo-bulk” expression profiles, where each single cell was seen as a replicate, using quasi-likelihood (QL) methods from the *edgeR* package^{162, 163}. Bulk normalization was applied with the function *calcNormFactors*, followed by setting up the design matrix for statistical modelling. With the help of *model.matrix* the groups were assigned as follows, the gene expression of one organ was compared against the remaining seven organs (rest). The negative binomial dispersions were estimated with the *estimateDisp* function. The QL dispersion was also estimated with the *glmQLFit* function, it fits a generalized linear model (GLM) to the counts for each gene, followed by estimating the QL dispersion from the GLM deviance. The two dispersion types eventually complemented each other in the downstream analysis. The difference in gene expression between the selected organ and the rest organs was tested using *glmQLFTest*. The DE genes were defined as non-zero logFC with an FDR of less than 5%. The DE genes were eventually depicted in Volcano plots with the help of the *EnhancedVolcano* package¹⁶⁴. All datapoint were depicted but cut off in the Volcano plots were set at a logFC of 2 and a p-value of 0.05.

2.4.7.6 - Creating organ-specific signatures

Marker genes were identified and were defined as DE genes that represent one organ specifically. These organ-specific signatures were identified with the help of the *findMarkers* function from the *scran* package¹⁶¹. This function ranked the genes that were DE in any pairwise comparison, by adjusting the p-values using a bonferroni correction considering the total number of genes in the dataset. Cut-off point of a logFC of 0, 0.5, 1, and 2 were selected and an FDR of less than 0.05. The top-5 marker genes were depicted with the *plotHeatmap* function and the top-1 markers with *plotExpression* (both logFC > 0 and FDR < 0.05). These two plots contained DE genes, which were markers of the specific organ. On the other hand, organ-specific genes were identified, by selecting genes that were only expressed (logcounts)

in the ECs of one organ. These genes were also depicted with the `plotExpression` function. The `plotHeatmap` and `plotExpression` function are both from the `scater` package¹⁵⁹.

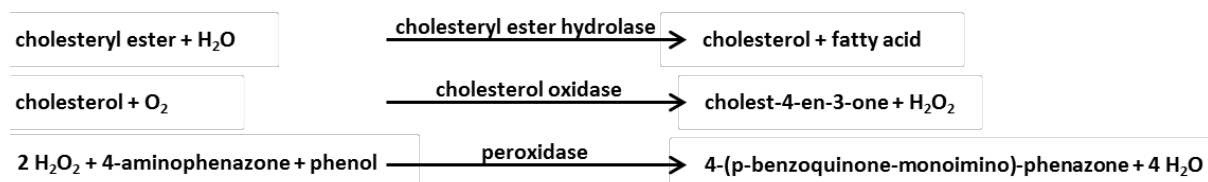
2.4.8 - Plasma generation

Blood samples were collected in EDTA tubes (Sarstedt) and spun down at 3,000g for 15 min at 4°C to generate the plasma from total blood. Plasma was collected and stored at -80°C for further analysis, such as cholesterol, triglyceride, and endotoxin measurement

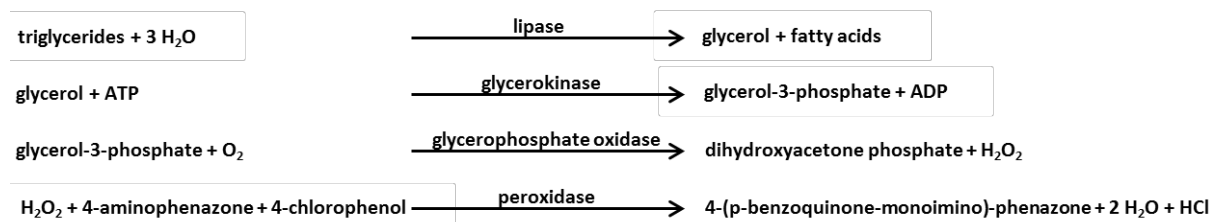
2.4.9 - Cholesterol and triglyceride measurement

Cholesterol and triglyceride levels were quantified in the plasma samples utilizing an enzymatic reaction (CHOD-PAP and GOP-PAP kit, Roche). Plasma was thawed on ice, triglyceride levels were measured in undiluted samples, while cholesterol levels were measured in the sample that was diluted 1:5. A standard series of cholesterol (0.05 µg/µl – 1.56 µg/µl) and triglycerides (0.04 µg/µl – 1.35 µg/µl) was created according to the manufacturer’s protocol. A 96-well plate (Falcon Corning) was prepared, by adding a duplicate of 5 µl of all samples and standard solutions, followed by the addition of 200 µl of the reaction solution (including all substrates necessary for the enzymatic reaction described below). The plate was incubated for 30 min in the dark at RT. Absorbance was thereafter measured at 510 nm with a Tecan Infinite F200 Pro Plate Reader (Tecan Life Sciences Home).

The enzymatic reaction that took place to determine the cholesterol levels:



The enzymatic reaction that took place to determine the triglyceride levels:



2.4.10 - Endotoxin measurement

LPS levels in the plasma were assessed with the Pierce Chromogenic Endotoxin Quant kit (Thermo Fisher Scientific), according to the manufacturer’s instructions. In short, the plasma samples were diluted in endotoxin free water (1:50). The blood was collected in tubes

containing EDTA (Sarstedt), therefore the diluted samples had to be heat inactivated (15 min at 70°C) to remove EDTA traces since EDTA can interfere with the assay. A 96-well plate (Falcon Corning) was prepared by adding 50 µl of samples in duplicates to the plate. Amebocyte lysate reagent was added to all wells, and the plate was incubated for 30 min at 37°C, followed by the addition of the chromogenic substrate solution and incubation of the plate at 37°C for another 6 min. The stop solution was added, and absorption was measured with a Tecan Infinite F200 Pro Plate Reader (Tecan Life Sciences Home) (wavelength 405 nm).

3 - Results

As described before, the aim of this study is to identify endothelial organ-specific and upregulated genes in mice in steady-state and mice exposed to different inflammatory conditions. Additionally, the effect of circadian rhythmicity on the endothelial transcriptome will be addressed. The chapters of the result section will be introduced below. Knowledge on organ-specific endothelial heterogeneity contributes the field of drug delivery. A promising agonist that could be interesting to use in organs-specific drug deliver will be tested and the ability of this antagonist to interfere with leukocyte recruitment will be addressed. The final goal of this thesis is to make a start in the establishment of an atlas regarding endothelial heterogeneity.

In line with this general aim, the obtained experimental results presented in this thesis will be divided into different sub-chapters.

Chapter 3.1 entitled 'The *Tabula Muris* dataset - Endothelial transcriptome in steady state' will describe data that was acquired with the use of the *Tabula Muris* dataset. This publicly available dataset was used to study whether ECs of five organs differ in such extent that organ-specific genes can be identified.

Chapter 3.2 'Small-bulk RNA-seq - The effect of an inflammatory stimulus on endothelial transcriptome of the aorta and lung' portrays the results of a small-bulk RNA-seq experiment using ECs isolated from homeostatic mice and mice which were challenged with an inflammatory stimulus. In this chapter, it will be established whether the aortic and lung endothelial genotype changes upon exposure to this inflammatory stimulus.

In chapter 3.3 'scRNA-seq - The effect of acute and chronic inflammation together with circadian rhythmicity on endothelial transcriptome of eight organs' will be studied. The role of acute inflammation (endotoxemia) as well as chronic inflammatory (hyperglycemia and hyperlipidemia) together with circadian rhythmicity on the endothelial transcriptome changes will be addressed. A scRNA-seq experiment of eight organs resulted in an overview with upregulated as well as several organ-specific genes, paving the way to the assembly of an atlas of endothelial heterogeneity.

3.1 - The *Tabula Muris* dataset - Endothelial transcriptome in steady state

The publicly available *Tabula Muris* dataset was used to characterize the endothelial transcriptome of five organs. The whole dataset contained out of 53760 cells, which were not only ECs. No preselection or sorting was performed before sequencing, and the dataset contains therefore all cells of the organs. After quality control 44949 cells remained, which were in total expressing 23341 genes. The number of total cells sorted of the five organs varied drastically, namely 408 of the aorta, 3401 of the brain non-myeloid, 519 of the kidney, 714 of the liver, to 1716 cells of the lung. The cells were clustered and cell types (e.g. hematopoietic progenitors, myeloid, lymphoid, mesenchymal, epithelial cells) were assigned by the means of known marker genes of the different cell type. Eventually, for this thesis the ECs were selected, resulting in the presence of 188 aortic, 715 brain, 126 kidney, 182 liver and 693 lung ECs available for further analysis. The gene transcript seems to be partly organ-specific, whereas significantly upregulated organ-specific gene were found in all organs, 6 genes in the aortic ECs, 77 genes in the brain ECs, 4 in the kidney ECs, 84 in the liver ECs, and 48 genes in the ECs of the lung (**Figure 11** and **Table 7**).

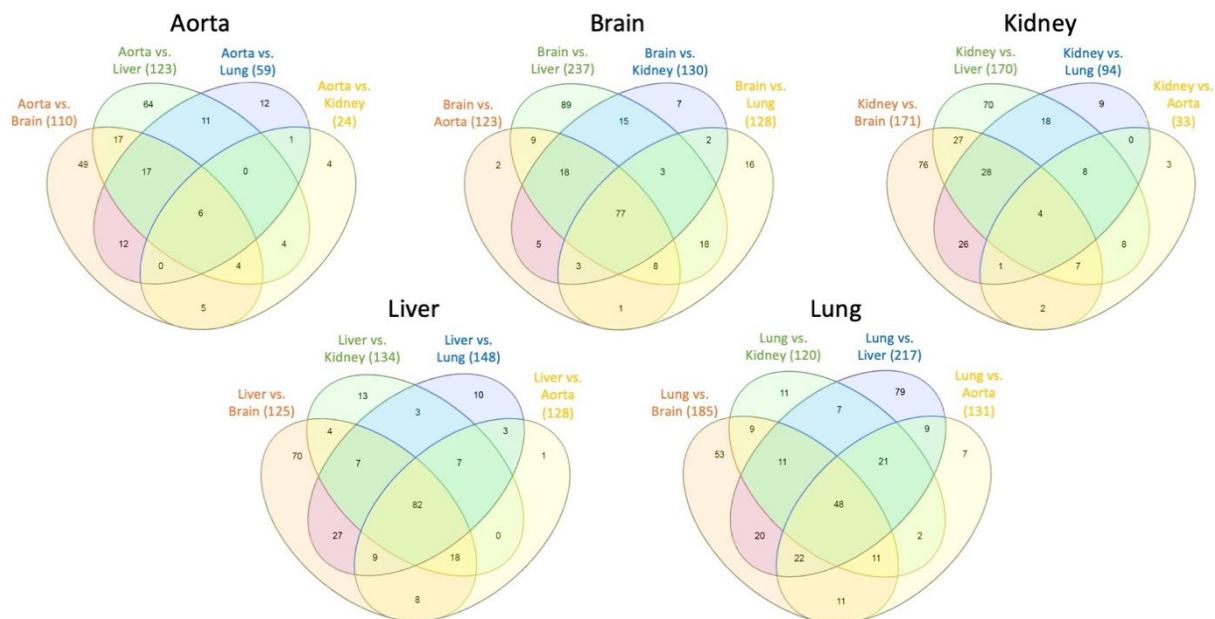


Figure 11. Visualization of the variation between transcriptomes of ECs isolated from the aorta, brain, kidney, liver, and lung in homeostatic condition.

Variations in the endothelial transcriptome were studied by analyzing the ECs data from *Tabula Muris* dataset. The amount of significantly (FDR < 0.05) and upregulated transcripts (fold change > 0,8) are shown. Data - The *Tabula Muris* Consortium *et al.*, 2018⁴⁹. Venn diagram - Heberle *et al.*, BMC Bioinformatics, 2015. ECs – Endothelial cells, FDR - False Discovery Rate.

Interestingly, further analysis revealed that some gene transcripts predicted to encode for endothelial surface proteins, namely 4 genes transcripts in the aorta, 35 in the brain, 3 in the kidney, 42 in the liver and 20 in the lung (**Table 7**). These results confirmed the existence of organ-specific transcriptomes. The genes can be found in the **Supplementary Table 1**.

However, this dataset only contains data from mice in steady state and it would be of interest to also study the gene transcripts of ECs isolated from diseased mice, which reflect the condition in which potential therapies are relevant.

Table 7. Number of organ-specific gene transcripts and transcripts encoding for endothelial surface protein.

Characterization of the endothelial transcriptome in mice in a homeostatic state was realized by analysing the data from *Tabula Muris*. The numbers of significantly (FDR < 0.05) and upregulated transcripts (FC > 0,8) are depicted. Text mining of PubMed articles was executed to determine if gene transcripts were predicted to encode for surface proteins. Data - The *Tabula Muris* Consortium *et al*, 2018, Nature. FC – Fold Change, FDR - False Discovery Rate.

Organ	Specific gene transcripts	Specific gene transcripts encoding for surface protein
Aorta	6	4
Brain	77	35
Kidney	4	3
Liver	82	42
Lung	48	20

3.2 – Small-bulk RNA-seq - The effect of an inflammatory stimulus on endothelial transcriptome of the aorta and lung

In the chapter above the transcriptomic profiles of ECs from mice in homeostasis were studied. In this chapter the EC transcriptome of a mouse exposed to acute inflammation was compared to the transcriptome of mouse in steady state. ECs from the aorta and lung were sorted from VE-cadherin-cre-rfp^{fllox/fllox} mice. The genetic construct in these mice contributed to the ability to sort ECs while the endothelial marker VE-cad is genetically labeled with RFP. The cells were sorted as single cells, combined in a small-bulk of 50 ECs, whereafter small-bulks were subjected to RNA-seq. The recovered dataset contained a total 20 samples (aorta and lung ECs, mouse in homeostasis and a mouse exposed to inflammation, five technical replicates per organ/condition). An average sequencing depth of 9,000,000 reads per sample an average of 9,470 genes per sample. Principal component analysis showed that ECs from aorta and lung of a homeostatic mouse model have a more differential tissue signature compared to the acute inflammatory mouse model (**Figure 12a**). Furthermore, the endothelial transcriptome of mice exposed to inflammation did not cluster with the mice in homeostasis, meaning that the gene transcripts of these two conditions differ extensively (**Figure 12b** and **2c**). Interestingly, organ-specific genes could still be identified for the organs exposed to LPS, opening the possibility to study disease related gene transcripts. The transcriptomic profiles of all samples were compared to each other. This resulted in the identification of upregulated and organ-specific genes in the aorta and lung within a condition and between conditions

(Table 8-9). The top-10 upregulated and organ-specific genes of the different groups can be found in **Supplementary Table 2-5**

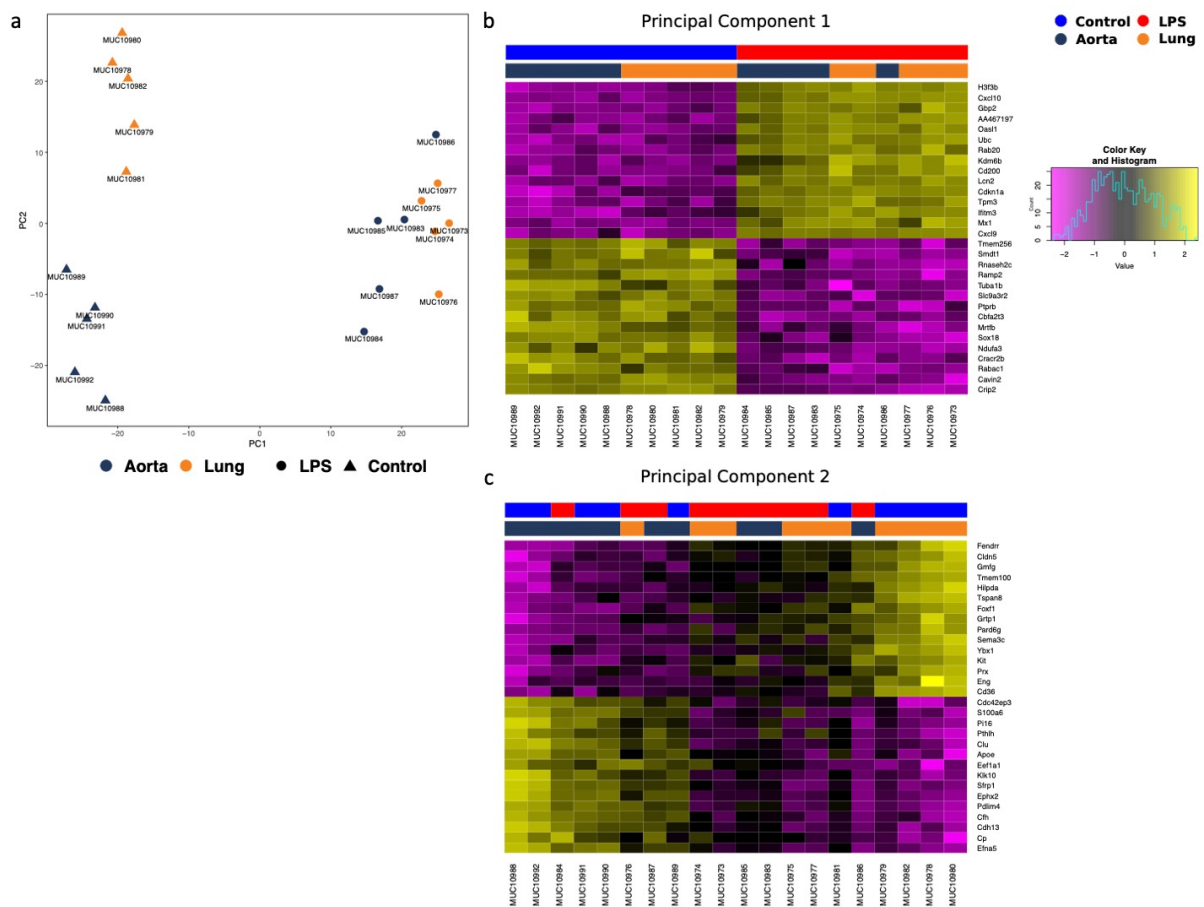


Figure 12. Tissue and acute inflammatory signature in transcriptome of ECs from mice in homeostatic condition compared to acute inflammatory condition.

Principal component analysis of the gene transcriptome from sorted ECs from the aorta and lung from a mouse in homeostatic condition (Control) and acute inflammatory condition (*i.p.* LPS injection four hours prior harvest). **(a)** Distribution of gene transcriptome of ECs in PC1 and PC2. **(b)** Heat map depicting thirty gene transcripts, which were the most upregulated in PC1. **(c)** Heat map depicting thirty gene transcripts, which were the most upregulated in PC2. (Control and LPS $n=1$, technical replicates (*MUCnumber*) = 5, Control Aorta MUC1088-1092, Control Lung MUC1078-1082, LPS Aorta MUC1083-1087, LPS Lung 1073-1077). ECs – Endothelial cells, LPS – Lipopolysaccharide, PC – Principal component.

Table 8. Upregulated and organ-specific genes within a condition.

Ctrl – Control, LPS – Lipopolysaccharide.

	Aorta Ctrl	Lung Ctrl	Aorta LPS	Lung LPS
Total	810	577	377	161
Organ-specific	178	98	81	21

Table 9. Upregulated and organ-specific genes between conditions.

Ctrl – Control, LPS – Lipopolysaccharide, vs – versus.

	Aorta Ctrl vs LPS	Lung Ctrl vs LPS	Aorta LPS vs Ctrl	Lung LPS vs Ctrl
Total	1579	1410	1309	827
Organ-specific	124	145	141	69

It is important to note, that a limiting factor in this experiment was the small number of cells that could be sorted. Increasing the number was challenging, since many cells were not recognized as ECs since the laser only captured cell when appearing in the center of the stream. Cells were not recognized as ECs and therefore not sorted when the cells shifted slightly to the left or right side of the stream. Changing the sorting strategy and sorting the ECs in bulk increased the number the number of cells drastically.

3.3 – scRNA-seq - The effect of acute and chronic inflammation together with circadian rhythmicity on endothelial transcriptome of eight organs

3.3.1 - Experimental set-up, quality control, and doublet detection

All freshly isolated organs were digested with the same optimized protocol to prevent transcriptomic differences due to tissue processing (see chapter 2.4.2). Isolated ECs from the aorta, bladder, bone, colon, kidney, liver, lung, and ileum of VE-cadherin-cre-rfp^{fllox/fllox} mice were isolated at 8 am (am) or 8 pm (pm). These animals were subjected to homeostatic (Ctrl), acute inflammatory (LPS), chronic inflammatory (hyperglycemic (STZ) or hyperlipidemic (AAV)) conditions. Organs single cell suspensions were labelled with the help of Feature Barcode technology, supporting the ability to sequence the cell simultaneously. Subsequently, cells were sorted in bulk, which resulted in avoiding the limitation of single cell sorting since enough cells could be sorted for these experiments. ECs of all organs of one treatment (homeostasis, acute inflammation, hyperglycemia, and hyperlipidemia) and timepoint (8 am or 8 pm) were pooled, resulting in eight samples. All samples were subjected to the 10x Genomics-based single-tube protocol with exclusive transcript counting through barcoding with unique molecular identifiers, whereafter all eight samples (treatments and timepoints) were pooled, creating one samples. This one sample was subjected to scRNA-seq. The recovered dataset contained a total of 52,329 cells, with an average sequencing depth of 75,000 reads per cell, an average sequencing saturation rate of 80.5%, and an average of 2,314 genes per cell. Samples were demultiplexed and subsequently analyzed with R (**Figure**

13a). The dataset was quality filtered for library size, number of detected genes, and mitochondrial read counts. (**Figure 13b**). Subsequently, graph-based clustering was performed to group cells according to their Feature Barcode profile and visualized by t-SNE plots. The eight clusters observed on the t-SNE plots equate to the eight different organs. An important step in single cell data analysis is the removal of doublets. Doublets form because of co-encapsulation of cells within a droplet, leading to a hybrid transcriptome from two or more cells or one cell (Within-sample doublet). Furthermore, cells can be labeled with two Feature Barcodes, resulting in a cell carrying the identification hashtag of two organs (Cross-sample doublet). Cells labelled by two hashtags (doublets) and non labelled cells (negative) were removed from the dataset before continuing with the downstream analysis. The dataset was separated into eight datasets (treatment and timepoint: Ctrl am and pm, LPS am and pm, AAV am and pm, STZ am and pm) before doublet detection. The doublets and cells without a hashtag were removed from the datasets and the results of Ctrl am, can be observed in **Figure 13c** (results of all datasets are shown in **Supplementary Figure 1-2**).

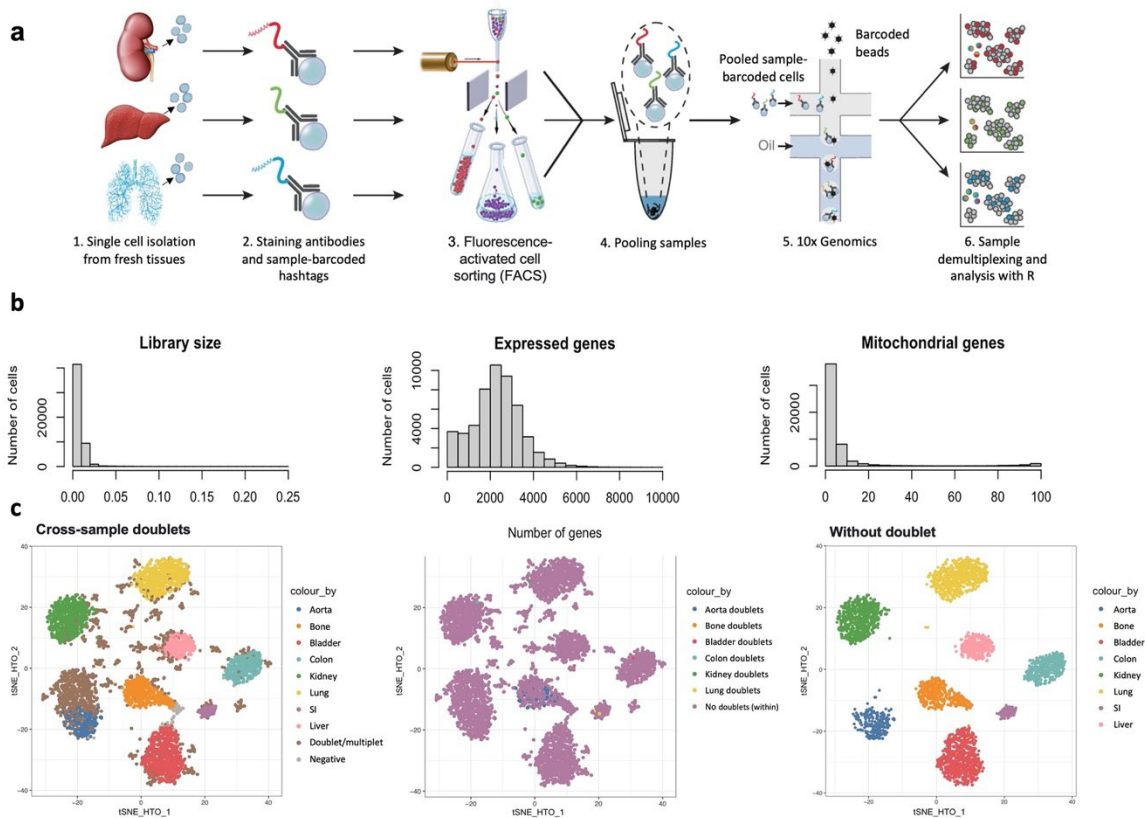


Figure 13. Experimental workflow of EC sorting, labeling with Feature barcoding technology, 10x Genomics, scRNA-seq, quality control, and doublet detection.

(a) Experimental workflow. Fresh tissues were isolated from VE-cadherin-cre-rfp^{flox/flox} mice. Single cell suspensions were hashtagged with TotalSeq™-B Feature Barcode technology. Live ECs (DAPI⁺CD45⁻CD31⁺VE-Cad) were sorted and the ECs from the different organs were pooled. The samples were subjected to 10x Genomics 3' Single Cell Gene expression kit. The barcode encodes a unique sequence representing each tissue sample, enabling sequence-based identification of each cell after pooling and profiling the different organs. Figure adapted from: Gaublomme *et al.* Nature Commun. 2019. **(b)** Overview of quality control depicting histograms of the library size, expressed genes, and genes from the mitochondrial genome. **(c)** Dimension reduction on Feature Barcoding count by using t-SNE. Portraying cross-sample doublets, within-sample doublet, and doublet free dataset. Representative images are shown for the doublet detection of ECs from mice sacrificed at am and in homeostasis (Ctrl am). Ctrl – Control, ECs – Endothelial cells, DAPI – 4',6-Diamidino-2-phenylindol, t-SNE – t-distributed stochastic neighbour embedding, VE-Cad – VE-Cadherin.

3.3.2 - Cleaning dataset

The primary goal of this study was to focus on vascular ECs. Therefore, another important step is to exclude contaminating cell types from the datasets. The separated datasets were merged into one big dataset to reduce the time needed to execute the following cleaning set. Subsequently, cells were grouped by graph-based clustering according to their gene-expression profile and t-SNE plots were used for visualization. The following cell types were deleted from the dataset based on the expression of cell type specific markers: platelets (*Pf4*, *Ppbb*), red blood cells (*Hba-a1*, *Hba-a2*, *Hbb-bs*), smooth muscle cells (*Acta2*), fibroblasts (*Col1a1*), pericytes (*Pdgfrb*), immune cells (*Ptpnc*) and lymph ECs (*Prox1*, *Pdnp*) (**Figure 14**).

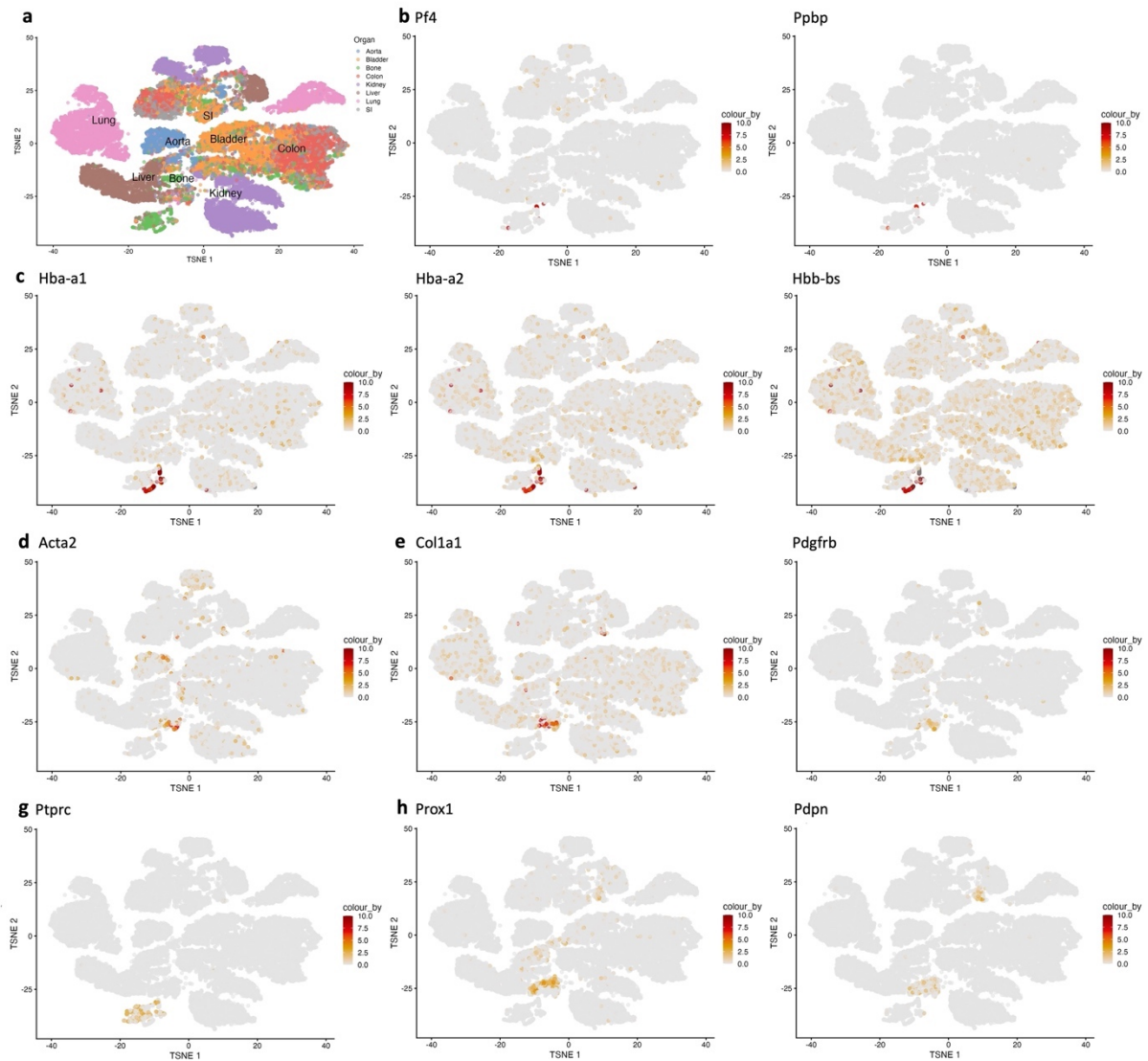


Figure 14. *In Silico* selection of cell types contaminating the endothelial cell dataset.

(a) t-SNE plots showing clustering of the organs of the pre-cleaned data; (b-h) cells are color-coded for marker genes selective for (b) platelets (*Pf4*, *Ppbp*), (c) red blood cells (*Hba-a1*, *Hba-a2*, *Hbb-bs*), (d) smooth muscle cells (*Acta2*), (e) fibroblasts (*Col1a1*), (f) pericytes (*Pdgfrb*), (g) immune cells (*Ptpnc*) and (h) lymph cells (*Prox1*, *Pdpn*). Color scale: red, high expression; grey, low expression. *Acta2* – actin alpha 2, *Col1a1* – Collagen Type I Alpha 1 Chain, ECs – Endothelial cells, *Hba-a1* – Hemoglobin A, *Hbb-bs* – Hemoglobin B, *Pdgfrb* – Platelet derived growth factor receptor beta, *Pdpn* – Podoplanin, *Pf4* – Platelet factor 4, *Ppbp* – Pro-Platelet Basic Protein, *Prox1* – Prospero Homeobox 1, *Ptpnc* – Protein tyrosine phosphatase receptor type c, TSNE – t-distributed stochastic neighbour embedding.

Next, ECs were clustered and selected based on the expression of EC markers (*Pecam1*, *Cdh5*, and *Lyve1*). All cells expressed *Cdh5* and *Pecam1* and some cells expressed *Lyve1*. Especially ECs of the lung of the acute inflammatory model expressed *Lyve1*, which is known as a lymphatic ECs marker. However, since these lung cells expressed also both ECs markers they were still included for further analysis (Figure 15).

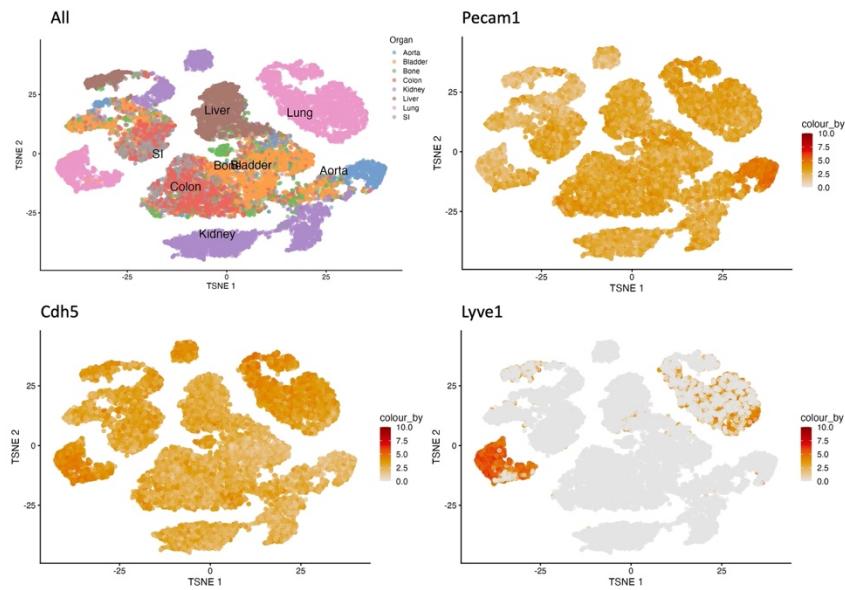


Figure 15. *In Silico* endothelial cell selection.

t-SNE plot of cells that were included from the analysis based on expression of marker genes for ECs (*Pecam1*, *Cdh5*, *Lyve1*). Color scale: red, high expression; grey, low expression. ECs – Endothelial cells, *Cdh5* – Claudin 5, *Lyve1* – Lymphatic vessel endothelial hyaluronan receptor 1, *Pecam1* – Platelet and endothelial cell adhesion molecule 1, TSNE – t-distributed stochastic neighbour embedding.

The dataset was divided into eight datasets based, namely four treatments (Ctrl, LPS, AAV, STZ) and two timepoints (am and pm). The number of cells per data set varied, the smallest subset consisted out of 1748 cells (LPS am) and the largest subset contained 3709 cells (LPS pm). In number of ECs per organ also varied per subset, namely the smallest number of cells was found in the AAV am subset where the ileum was represented by two cells and the highest number of cells was observed in the LPS pm subset from which 888 cells from the lung were detected. The largest number of cells was found in the LPS pm subset, where 888 ECs were measured in the lung. Overall, bone ECs seemed underrepresented, while the lung ECs were overrepresented in most datasets (**Table 10**).

Table 10. Overview of the number of endothelial cells per organ, treatment, and moment of organ collection.

Total number of ECs present in the dataset from mice were subjected to homeostatic (Ctrl), acute inflammatory (LPS), chronic inflammatory (hyperglycemic (STZ) or hyperlipidemic (AAV)) conditions at am or pm. AAV - Adeno associated virus, Ctrl – Control, LPS – lipopolysaccharides, STZ – Streptozotocin.

	Ctrl am	Ctrl pm	LPS am	LPS pm	STZ am	STZ pm	AAV am	AAV pm	Total
Aorta	189	132	133	79	131	79	500	187	1430
Bone	86	166	120	74	35	192	158	89	920
Bladder	676	420	264	518	479	469	382	377	3585
Colon	415	336	218	481	162	385	403	183	2583
Kidney	601	427	269	743	548	445	503	354	3890
Lung	677	673	304	888	528	520	590	488	4668
Ileum	111	284	229	598	107	146	2	76	1553
Liver	310	280	211	328	412	329	491	367	2728
Total	3065	2718	1748	3709	2402	2565	3029	2121	21357

3.3.3 - Clustering

As a first step to get more insight in the expression profiles of the genes, the data was clustered. By clustering in an unsupervised way, groups of cells could be defined with similar expression profiles. The primary purpose of clustering was to summarize the data in a more digestible format and allowing to interpret the heterogeneity of the organs within a subset. ECs from the colon and Ileum (SI) mostly clustered together, whereas the lung always clustered separated from the other organs. The kidney ECs, interestingly, appeared for all subsets as two separate clusters. The organs of the Ctrl, AAV, and STZ subsets am as well as pm appeared in the t-SNE plot in a similar location, while the LPS am and pm subsets showed a strikingly different profile (**Figure 16**).

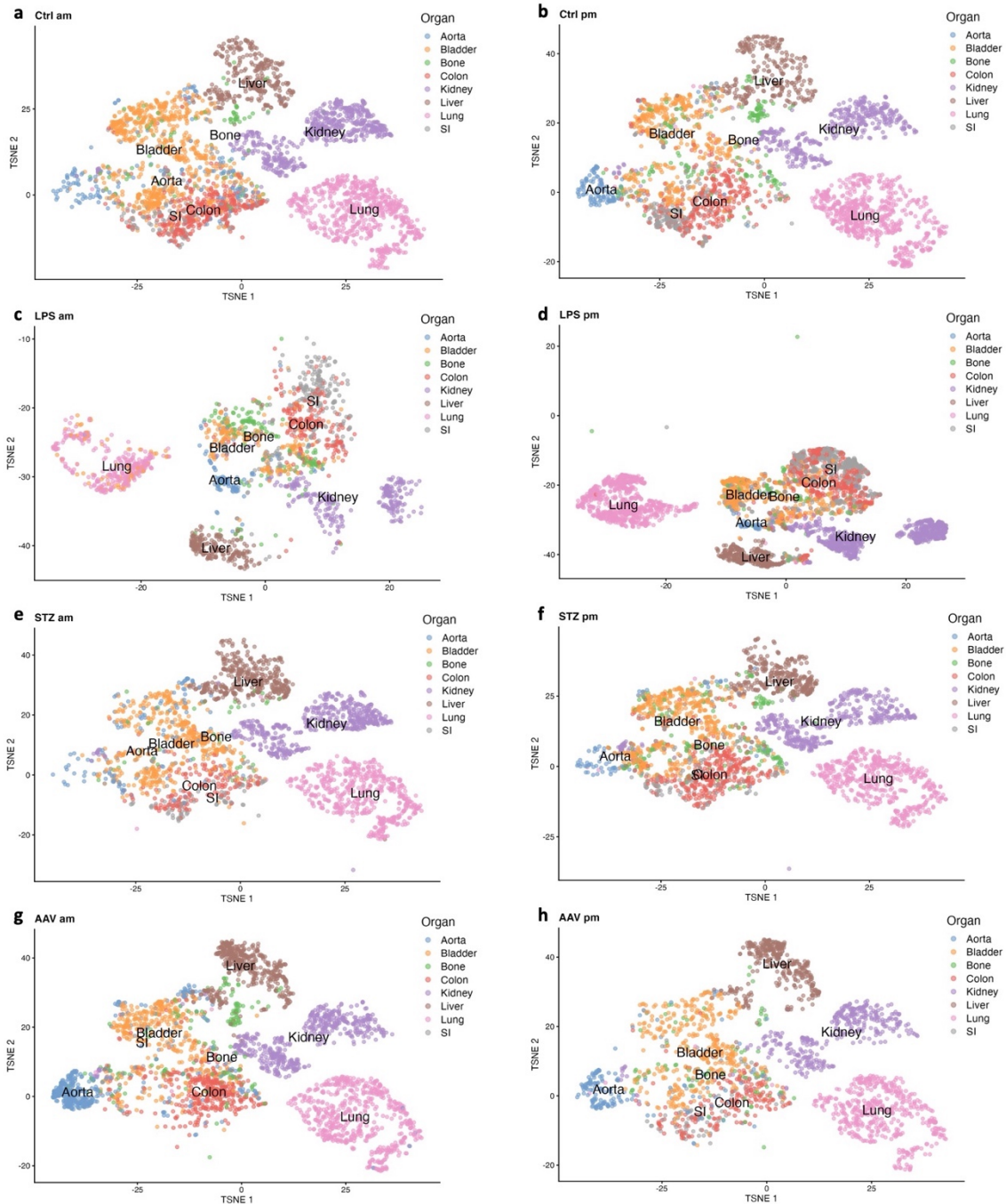


Figure 16. Clustering of endothelial cells from organs of mice in homeostasis, exposed to an inflammatory stimulus or a chronic inflammatory condition.

t-SNE plots representing the clusters of the aorta, bladder, bone, colon, kidney, liver, lung, and SI (Ileum) from mice sacrificed in homeostasis or after exposure to inflammatory conditions: Ctrl am and Ctrl pm (a-b), or acute inflammation: LPS am and LPS pm (c-d), or chronic inflammation – hyperglycemia: STZ am and STZ pm (e-f), or hyperlipidemia: AAV am and AAV pm (g-h). AAV - Adeno Associated Virus, Ctrl – Control, LPS – Lipopolysaccharides, SI – Small Intestine, STZ – Streptozotocin, t-SNE – t-distributed stochastic neighbour embedding.

3.3.4 - Differentially expressed genes

A powerful use of scRNA-seq technology lies in the ability to detect changes in the composition and/or expression between conditions, which is facilitated by the design of replicated multi-condition experiments. During this project such a multi-condition experiment was conducted, though, experiments were not replicated due to experimental costs. The lack of replicates, but the desire to detect changes in the composition or expression between organs, was obviated by designating single cells as replicates. In the endothelial dataset only organs within one subset could be compared, since sacrifices and library preparation of the different mouse experiments were conducted on different days.

Differential Gene Expression analyses were executed as a second step to get more insight in the expression profiles of the different ECs. The DE genes from one organ were compared with the DE genes of all other organs combined to identify differences in gene expression for this specific organ. Volcano plots were used to represent and visualize the results of DE analyses. The dataset consisted of 20,323 genes (variables) and a substantial number of genes were observed to be either significantly down (left) or upregulated (right), which are depicted in red. The volcano plots displaying the DE genes from aorta and lung are presented in **Figure 17**, while the plots for bladder, bone, colon, kidney, liver, and ileum (SI) can be found in **Supplementary Figure 3-10**, and an overview of the top-10 DE genes in **Supplementary Table 6, 9, 12 and 15**.

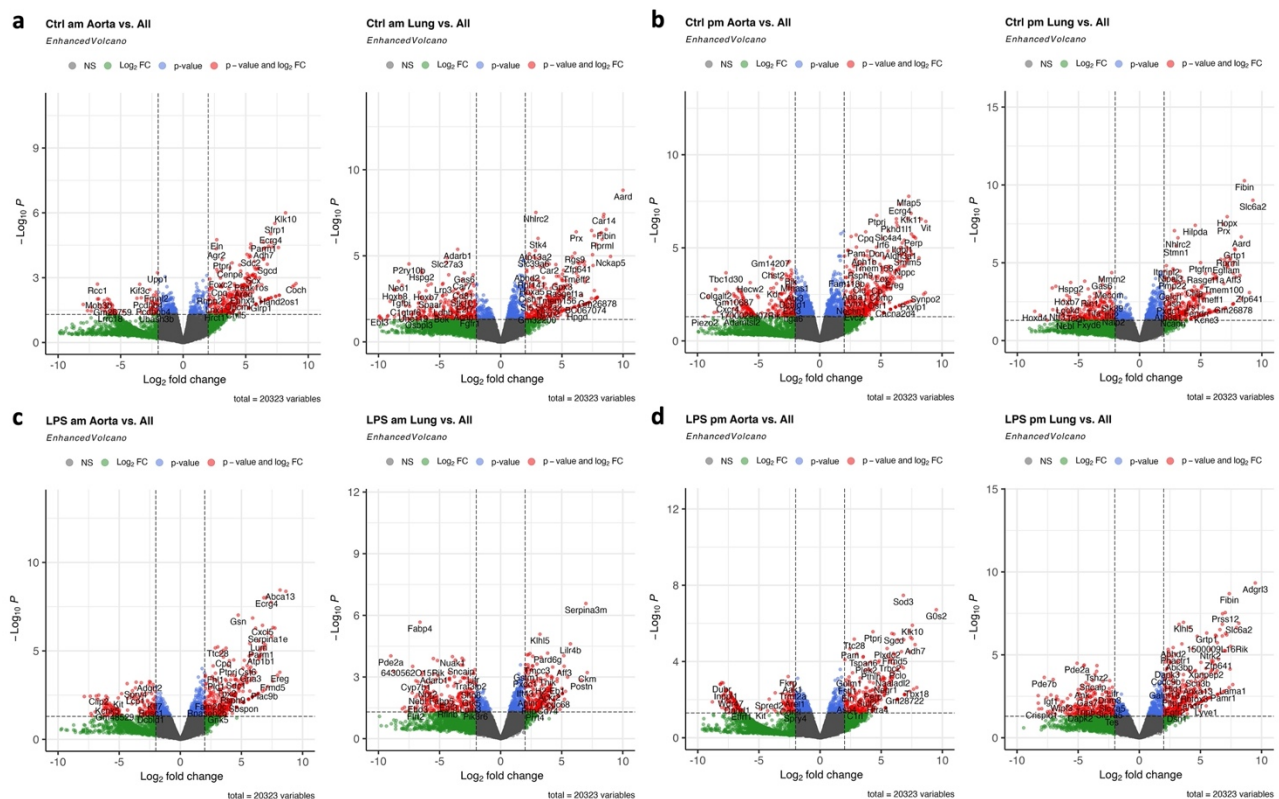


Figure 17 continues on the next page

Continuation of Figure 17

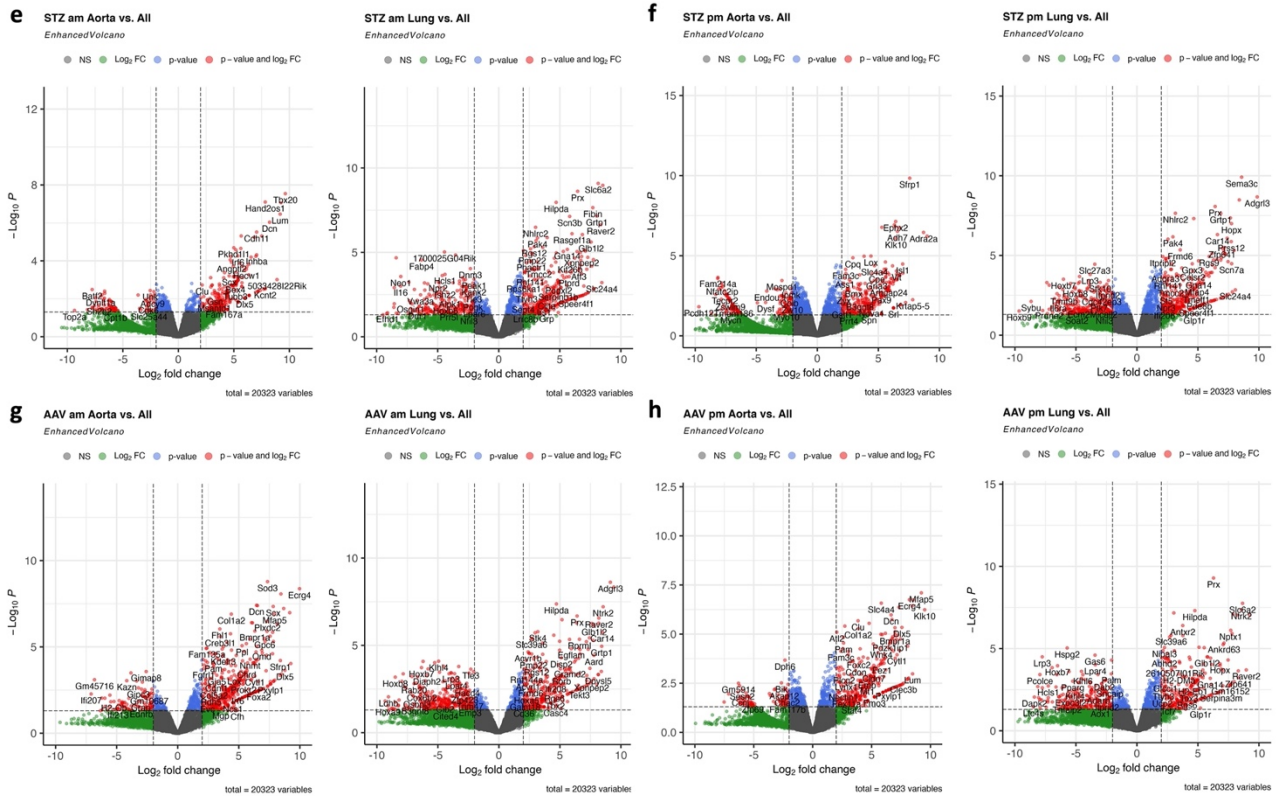


Figure 17. Differentially expressed genes of the aorta and lung.

Volcano plots representing the DE genes of the ECs of the aorta and lung collected from mice which were subjected to homeostasis (a-b) Ctrl am and Ctrl pm, acute inflammation (c-d) LPS am and LPS pm, or chronic inflammation - hyperglycemia (STZ) am and pm (e-f), or hyperlipidemia (AAV) am and pm (g-h). Gene colors: grey – p-value NS and log₂FC > -2 or < 2, green - log₂FC < -2 or > 2, blue - p-value < 0.05, red - p-value < 0.05 and log₂FC < -2 or > 2. AAV - Adeno Associated Virus, Ctrl – Control, FC – Fold Change, LPS – Lipopolysaccharides, NS – Not Significant, STZ – Streptozotocin, vs. – versus.

3.3.5 - Marker gene detection

As third approach to gain more insight in the expression profiles of the ECs, genes were identified that drove the separation between the organ clustering. These marker genes are (mostly) expressed by one organ. However, it should be considered that these marker genes are not organ-specific genes, as they can still be expressed, though lower expression, by the ECs of other organs. The identification of marker genes is based on the retrospective detection of DE genes between the organs since separation of the organs into clusters is most likely caused by more strongly DE genes in the first place. Marker genes were only selected when they were DE in all pairwise comparisons. Heatmap analysis of the top-5 upregulated candidate markers revealed distinct signatures of ECs between organs (Figures 18-21a and c). The top-1 markers were visualized with the help of violin plots. All organs are represented by such a top-1 marker, except the ECs of the ileum (SI) in the LPS am, AAV am, AAV pm, and STZ am subset and the ECs of the bone in the AAV pm subset. For these subsets no

upregulated marker genes could be found when the threshold of the FDR was set to <0.05 (**Figures 18-21b** and **d**). The given an overview of all upregulated genes, exclusion criteria of markers shown in **Figure 18-21** was limited and all upregulated genes were included. **Supplementary Table 18** depicts the numbers of marker genes found when more strict exclusion criteria were implemented and the top-10 marker genes can be found in **Supplementary Table 7, 10, 13** and **16**.

In the subset Ctrl am only three marker genes could be identified for the ECs of the bone and two for the Ileum (SI) ECs (**Figure 18a**). The top-1 marker from the aorta, kidney, liver, lung, and Ileum (SI) is only in a low extend expressed in the other organs and thereby rather specific. In contrast, the top-1 candidate genes representing the bladder, bone, and colon are less specific and are to a greater extend also expressed by ECs of other organs (**Figure 18b**). All top-5 markers genes could be found for the organs in the Ctrl pm subset (**Figure 18c**). The top-1 gene of most organs stood out reflecting some degree of specificity, however the marker genes from the bladder, colon, and Ileum (SI) ECs were also expressed by the other organ (**Figure 18d**).

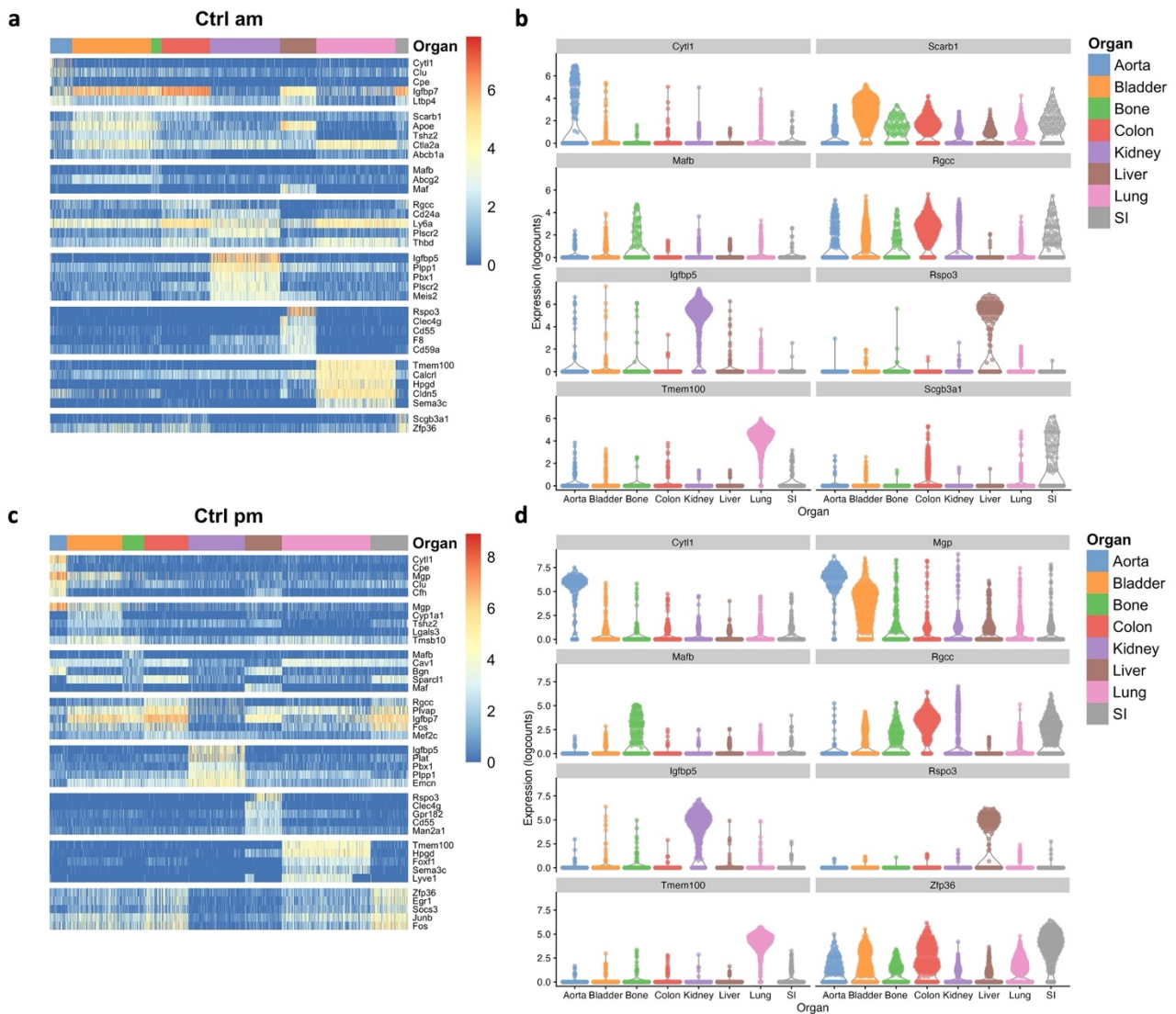


Figure 18. Upregulated marker genes of homeostatic mice.

(a and c) Gene-expression heatmap of the top 1-5 marker genes from tissues collected at **(a)** am or **(b)** pm from homeostatic mice (Ctrl). Color scale: red, high expression; blue, low expression. **(b and d)** Violin plots of the expression of top marker, highly expressed in ECs in the indicated tissues, harvested at **(b)** am or **(d)** pm. $\text{Log}_2\text{FC} > 0$ and $\text{FDR} < 0.05$. Ctrl – Control, ECs – Endothelial Cells, FDR - False Discovery Rate, SI – Small intestine (Ileum).

In the LPS am subset marker genes were found for all genes, however, for the ECs from the bone only two marker genes could be identified (**Figure 19a**). No marker genes were detected for the bone ECs of the LPS pm dataset (**Figure 19c**). Interestingly, the top-1 marker genes for this subset were less organ-specific. The violin plots showed that genes are also expressed by most other organs (**Figure 19b and d**), which is in sharp contrast to the specificity shown in the violin plots of the Ctrl and AAV subset (**Figure 18b and d and Figure 21b and d**).

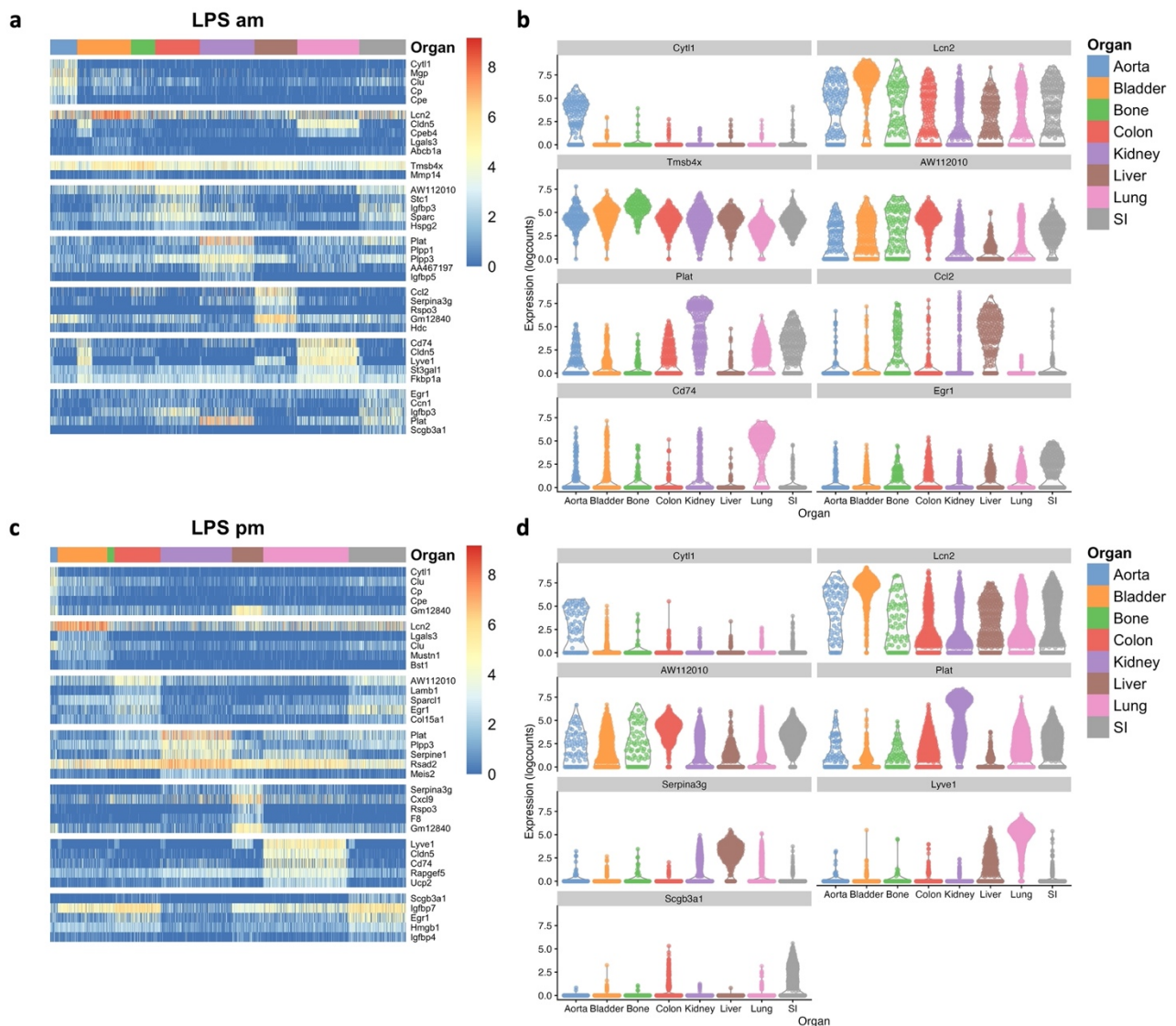


Figure 19. Upregulated marker genes of mice exposed to acute inflammation.

(a and c) Gene-expression heatmap of the top 1-5 marker genes of the indicated tissues which were harvested at (a) am or (b) pm, from a mouse exposed to endotoxin (LPS). Color scale: red, high expression; blue, low expression. (b and d) Violin plots of the expression of top marker, highly expressed in ECs in the indicated tissues at (b) am or (d) pm. Log2FC > 0 and FDR < 0.05. ECs – Endothelial Cells, FDR - False Discovery Rate, LPS - Lipopolysaccharides, SI – Small intestine (Ileum).

Marker genes could be identified for almost all organs of the STZ am dataset, only for the bone ECs no markers could be found and for the ileum (SI) only one marker was identified (Figure 20a). In the other datasets, such as STZ pm, a top-1 marker gene was found which characterized the aorta without being strongly expressed in the other organs. However, in the STZ am dataset the aorta marker looked less specific. Nevertheless, top-1 marker genes of the kidney, liver, and lung could be considered as promising candidate marker genes (Figure 20b). Marker gene analysis resulted in the detection of marker genes in all organs in the STZ pm subset. However, for the bone ECs only four markers could be found and for the ileum (SI) ECs only one (Figure 20c). The top-1 marker gene which distinguishes the colon ECs was

also expressed by all other organs, while other genes appeared to be more suitable to describe the specific organ population (**Figure 20d**).

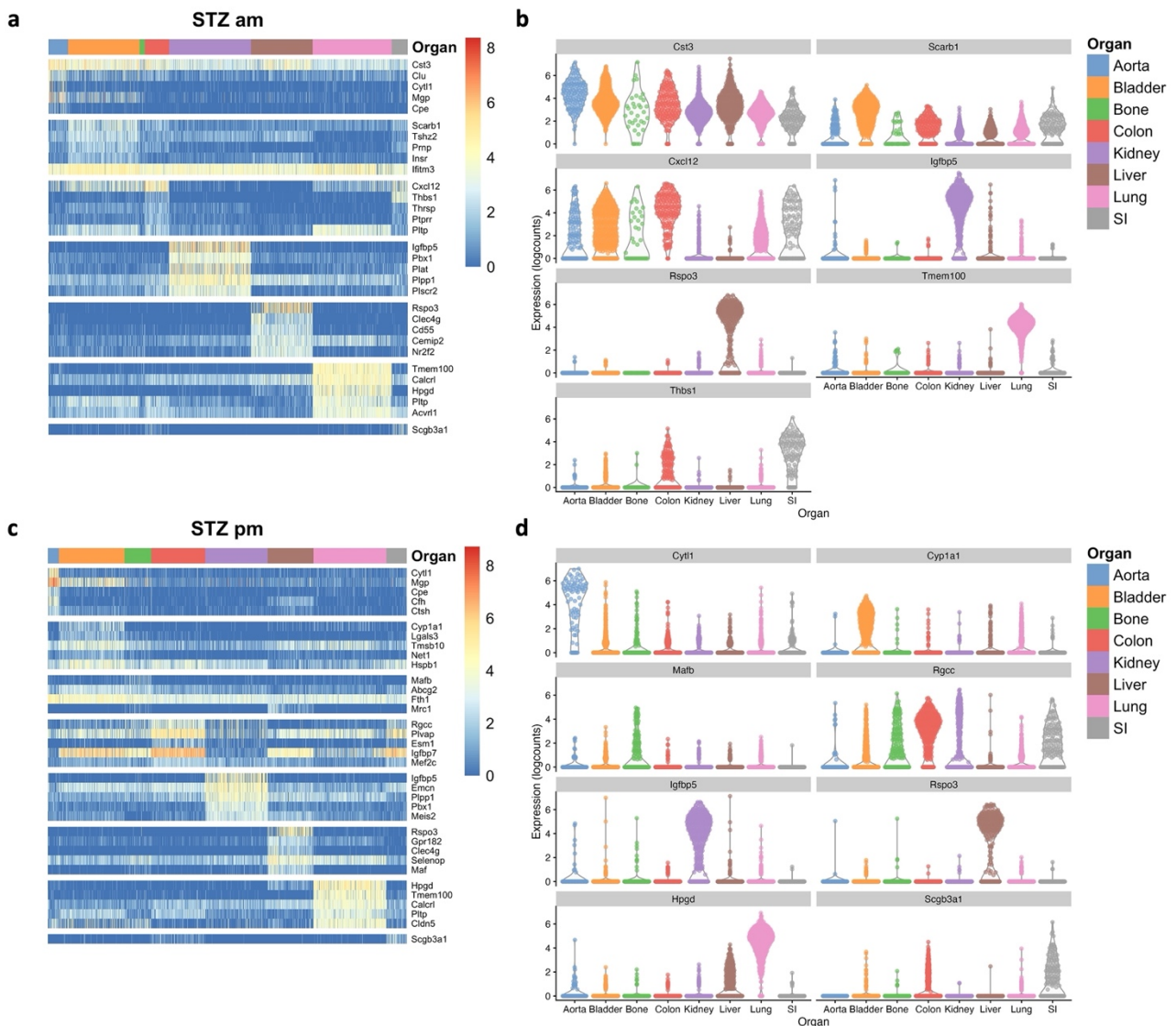


Figure 20. Upregulated marker genes of mice exposed to hyperglycemia.

(**a** and **c**) Heatmap showing the gene-expression of the top 1-5 marker genes of mice exposed to hyperglycemia (STZ) for tissue collected at (**a**) am or (**b**) pm. Color scale: red, high expression; blue, low expression. (**b** and **d**) Top marker, highly expressed in ECs in the indicated tissues, are depicted in violin plots at (**b**) am or (**d**) pm. Log2FC > 0 and FDR < 0.05. Ctrl – Control, ECs – Endothelial Cells, FDR - False Discovery Rate, SI – Small intestine (Ileum), STZ – Streptozotocin.

As mentioned above, a representing marker could not be selected for the Ileum (SI) ECs. This can be explained by the low number of Ileum (SI) cells present in the dataset ($n = 2$), therefore SI is not depicted in **Figure 21a**. The top-1 marker gene of the aorta, kidney, liver, and lung clearly represent an organ-specific EC population, since the gene seems not to be extensively expressed in the other organs (**Figure 21b**). Marker genes could only be detected for six organs of the AAV pm subset, namely the aorta, bladder, colon, kidney, liver, and lung (**Figure**

21c). Nonetheless, the top-1 marker expression appears to be fascinating specific for most of the organs (**Figure 21d**).

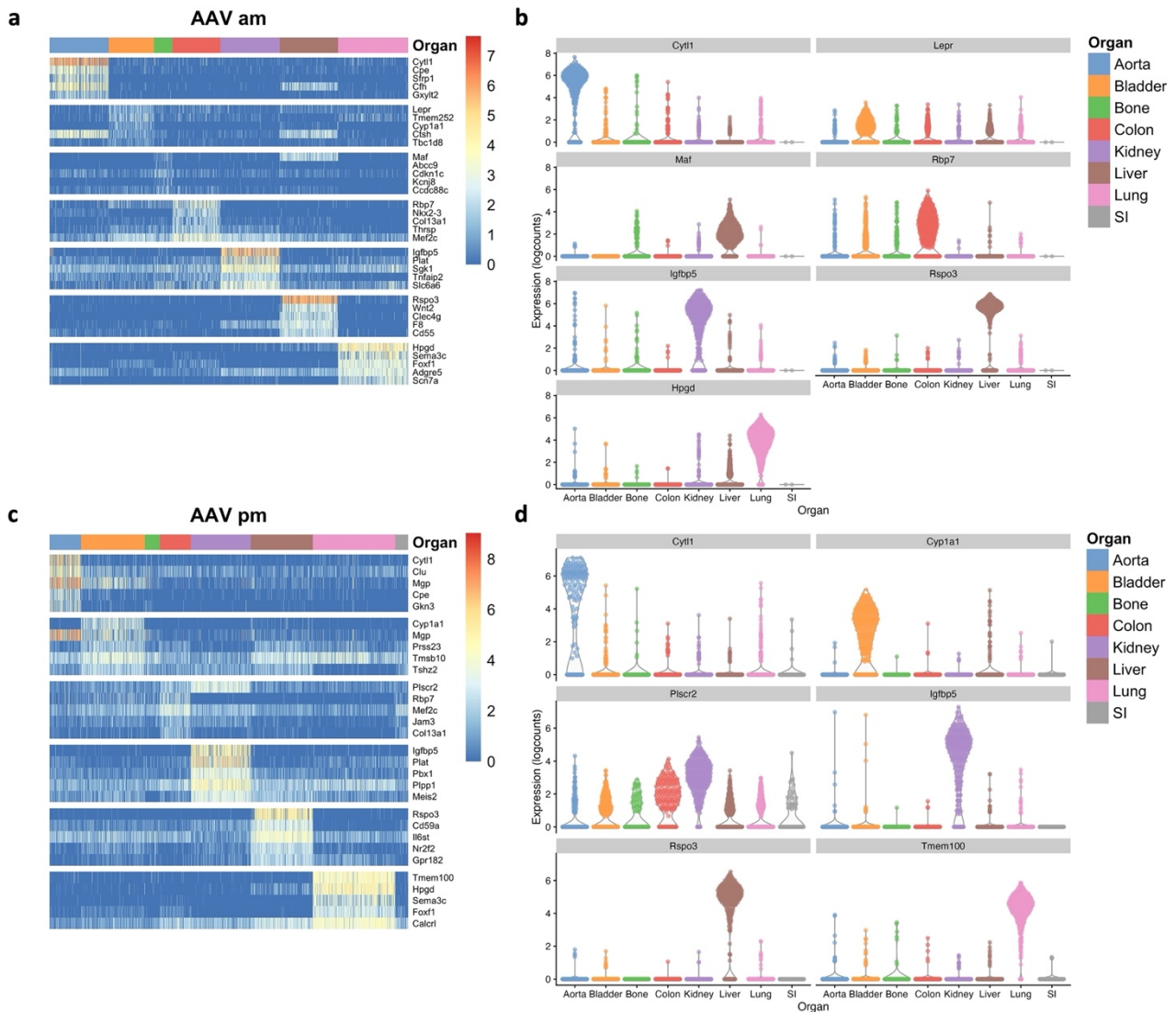


Figure 21. Upregulated marker genes of mice exposed to hyperlipidemia.

(**a** and **c**) Gene-expression heatmap of the top 1-5 marker genes for mice experiencing hyperlipidemia (AAV) of tissue which were collected at (**a**) am or (**b**) pm. Color scale: red, high expression; blue, low expression. (**b** and **d**) Violin plots depict the expression of top marker, highly expressed in ECs of the indicated tissues at (**b**) am or (**d**) pm. $\text{Log}_2\text{FC} > 0$ and $\text{FDR} < 0.05$. AAV - Adeno Associated Virus, ECs – Endothelial Cells, FDR - False Discovery Rate, SI – Small intestine (Ileum).

3.3.6 - Organ-specific genes expression

As observed in Chapter 3.3.5, various gene markers were extensively expressed by one organ. However, the marker genes are not organ-specific, as they were expressed by ECs from other organs. However, the marker genes can be incorporated in the atlas of endothelial heterogeneity, nevertheless organ-specific genes would increase the value of this atlas.

The subsets were analyzed to detect the presence of organ-specific genes. Fascinatingly, in nearly all organs' organ-specific genes were identified, with an average of 226 specific genes per organ. The only organ without organ-specific genes is the Ileum in the AAV am dataset. This can be explained by the small number of ileum ECs in this dataset (n=2). Especially the aorta, bladder, kidney lung, and liver expressed valuable organ-specific genes (**Table 11**). The top-10 organ-specific genes can be found in **Supplementary Table 8, 11, 14** and **17**.

Table 11. Overview of the number of organ-specific genes.

AAV - Adeno Associated Virus, Ctrl – Control, LPS – Lipopolysaccharides, STZ – Streptozotocin.

	Ctrl am	Ctrl pm	LPS am	LPS pm	STZ am	STZ pm	AAV am	AAV pm
Aorta	181	186	251	73	158	80	466	275
Bone	74	134	151	36	48	132	104	70
Bladder	439	277	304	310	313	312	235	317
Colon	119	130	135	137	60	164	118	89
Kidney	351	258	336	331	443	318	305	345
Lung	331	388	308	381	448	397	302	333
Ileum	41	160	176	217	52	55	0	42
Liver	246	256	254	179	344	320	309	390

The organ-specific genes with the highest number of read counts were visualized using violin plots. The number of read counts of the specific genes of many organs was rather low, making them less suitable genes to focus on for organ-specific targeting. However, the Ctrl subset showed potential genes, which could be used for organ-specific targeting. For example, in the am subset, the kidney and lung ECs expressed *Gm13470* (95 read counts) and *Adgrl3* (Adhesion G protein-coupled receptor L3, 625 read counts), respectively (**Figure 22a**). The read counts of the organs-specific genes in the pm subset reached 100 in the kidney ECs for *Lypd6* (LY6/PLAUR domain containing 6) and 117 read counts for the *Zfp641* (Zinc finger protein 641) in the lung (**Figure 22b**). In the LPS am subset contains only one gene of interest, namely *Dlk1* (Delta like non-canonical notch ligand 1) with 207 read counts, which is expressed by ECs of the kidney (**Figure 22c**). For the pm subset the read counts of the genes were too low to be of interest (**Figure 22d**).

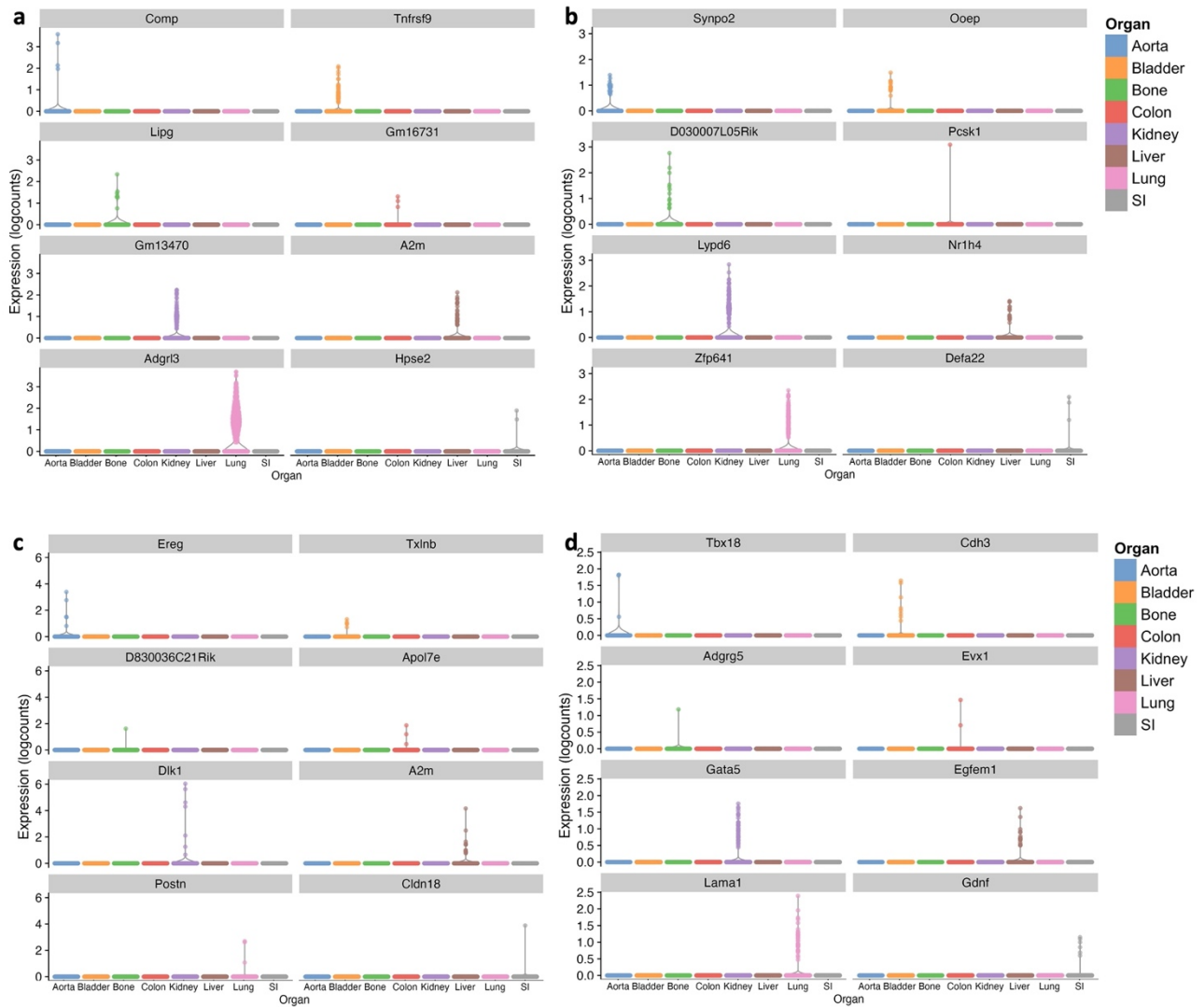


Figure 22. Organ-specific genes of mice in homeostasis and after being exposed to acute inflammatory stimulus.

Violin plots of the expression of top organ-specific marker, specifically expressed in ECs in the indicated tissues of the subset of homeostatis (a-b) Ctrl am and pm, and acute inflammation (c-d) LPS am and pm. LPS – Lipopolysaccharides, SI – Small intestine.

Interestingly, for some genes of the STZ subset the read counts were noticeably high. For example, the organ-specific gene of the ECs of the kidney and liver in the STZ subsets could be considered for targeting, due to this reasonably high read counts. For example, the kidney ECs of the am as well as the pm subset expressed *3110099E03Rik*, in the STZ am dataset the gene was counted 452 times and in the STZ pm dataset 335 times. Organ-specific genes were also identified in the liver ECs, namely 293 read counts of *Gm17167* in the STZ am, and 109 read counts of *Ajap1* (Adherens junctions associated protein 1) in the STZ pm subset (Figure 23a and b). The ECs of the aorta and liver in the AAV subsets also express genes

with reasonable number of read counts, namely 339 read counts for *Isl1* (ISL LIM homeobox 1) and 206 read counts for *Gm17167* (**Figure 23c**). In the AAV pm subset the kidney, lung and liver ECs expressed organ-specific genes, precisely the kidney ECs expressed with 191 read counts *3110099E03Rik*, the liver ECs 355 read counts for *Gata4*, and the lung ECs 96 read counts for *Raver2* (Ribonucleoprotein, PTB binding 2)(**Figure 23d**).

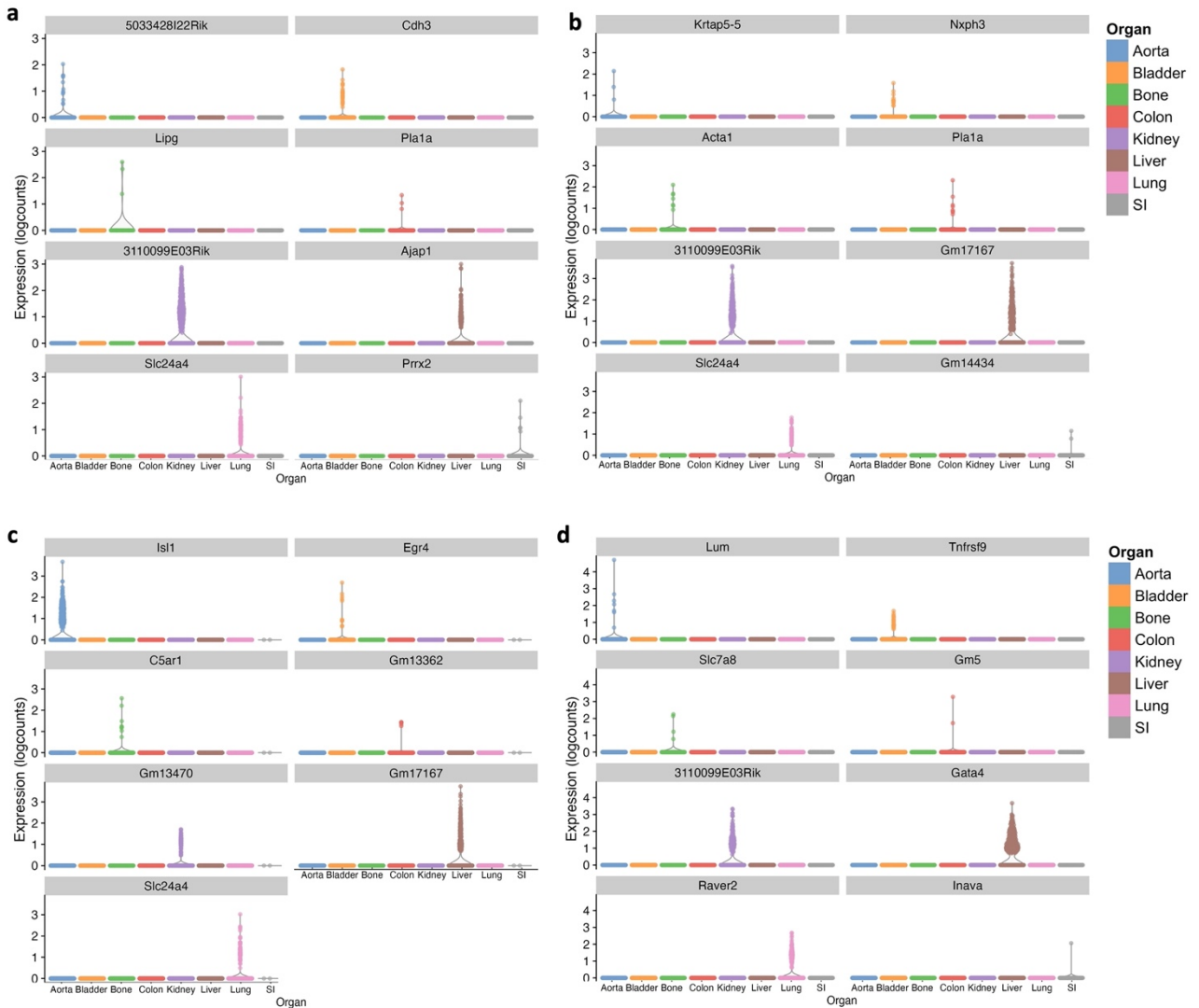


Figure 23. Organ-specific genes of mice exposed to chronic inflammatory conditions.

Violin plots of the expression of top organ-specific marker, specifically expressed in ECs in the indicated tissues of the subset hyperglycemia (STZ) am and pm (**a-b**) and hyperlipidemia (AAV) am and pm (**c-d**). AAV - Adeno Associated Virus, SI – Small intestine, STZ – Streptozotocin.

Together, these data give an overview of DE, marker genes, as well as several organ-specific genes, paving the way to the assembly of an atlas of endothelial heterogeneity.

4 - Discussion

In the past years, the EC transcriptome of various organs has been identified in physiological state. Previous studies on deciphering endothelial heterogeneity were insightful and comprehensive, due to the number of organs analyzed in parallel^{17, 30, 31} and by performing single cell analysis allowing the detection of small populations or low expressed genes^{18, 19}. However, very little is known regarding potential fluctuations in endothelial heterogeneity upon changes in the physiological state. Furthermore, the effect of environmental factors on the transcriptomic signature throughout the day are not considered. This study presents the first data on the endothelial transcriptome in steady- and inflammatory states and includes the effect of circadian rhythmicity on endothelial heterogeneity. Herewith, this study paves the way to establish a versatile atlas of heterogeneity of ECs. The ECs from this atlas cover an extensive vascular network and have an enormous yet largely untapped diagnostic and therapeutic potential.

4.1 - Endothelial transcriptome in steady state

Several recent advances contributed to the generation of transcriptomic endothelial atlases of major mammalian organs have been made over the last years. These atlases are created by studying publicly available datasets¹⁹ as well as new single cell sequencing studies^{17, 18}.

4.1.1 – Studying the endothelial transcriptome in homeostasis by means of a publicly available dataset

The endothelial transcriptome in steady state was studied with the use of the *Tabula Muris* dataset. The *Tabula Muris* consortium published an online open-access database consisting of single cell transcriptomic data of 20 organs collected from mice in homeostasis⁴⁹. In this paper several mice were used, generating a dataset which was controlled for age, environment, and epigenetic effects. They mainly focused on defining organ-specific cell types, compared the cell sorting methods, applied global clustering, and conducted transcription factor analysis of the organs. This publicly accessible *Tabula Muris* represented a new resource to study cell biology. The dataset unlocks the opportunity to compare gene expression profile of poorly characterized cell populations in cell types that are shared between tissues. In this thesis we used the *Tabula Muris* to study endothelial heterogeneity from cells isolated from different anatomical locations.

The *Tabula Muris* consortium used two methods to separate single-cells for scRNA-seq, namely FACS-sorting and microfluidic droplet-based sorting⁴⁹. The consortium reported that the use of different cell sorting methods led to high variability in the number of genes that were

detected per cell. In this thesis it was decided to preserve a coherent dataset, and consequently only including sequencing data from ECs that were sorted by means of FACS to avoid variability bias. This resulted in the identification of organ-specific genes of five organs. Additionally, surface expression was predicted based on text mining. Organ-specific genes were identified in the aorta (organ-specific genes: 6 – genes encoding for surface proteins: 4), brain (77-35), kidney (4-3), liver (82-42), and lung (48-20) (**Figure 11, Table 7, and Supplementary Table 1**). As a critical note, these organ-specific genes are identified by comparing the endothelial transcriptome of only 5 organs. These genes could potentially be expressed in ECs from organs that were not included in this analysis. The number of available organs could have been increased when data acquired by means of microfluidic droplet-based sorting would have been combined with the data obtained by FACS, since both methods showed to recapitulate average cell-type gene-expression profiles accurately⁴⁹. Future studies should therefore consider including a larger variety of organs, which will increase targeting specificity and reduced off-target effects.

Paik et al. also studied the *Tabula Muris* to evaluate the endothelial transcriptome. However, in contrast to this thesis, they incorporate the sequencing data from ECs sorted by both FACS- and microfluidic droplet-based sorting. This resulted in the ability to compare the transcriptome of 12 organs. ECs from some organs presented tissue specific DE gene (e.g. brain, kidney, liver and lung), whereas other tissues (e.g. adipose tissue, heart, aorta) showed considerable overlap in gene expression¹⁹. Additionally, another difference with our study is the fact that, Paik et al. identified overexpressed genes, while this thesis focused on identifying organ-specific genes. Interestingly, in the brain, liver, and lung an overlap was observed in the identified DE genes by Paik *et al.* and the detected organ-specific genes in this thesis. In the brain 5 genes which encode surface proteins were identified by both studies: *Slco1c1* (Solute carrier organic anion transporter family member 1C1), *Slco1a4*, *Slc22a8*, *Mfsd2a* (Major facilitator superfamily domain containing 2A), and *Slc38a3*. All top-10 DE genes in liver ECs were also identified as organ-specific genes in this thesis, from which 5 genes are encoding for surface proteins: *Dnase1l3* (Deoxyribonuclease 1 like 3), *Oit3* (Oncoprotein induced transcript 3), *Bmp2* (Bone morphogenetic protein 2), *Aass* (Amino adipate-semialdehyde synthase), *Wnt2*, encoding for surface proteins: *Clec4g* (C-Type lectin domain family 4 member G), *Fcgr2b* (Fc fragment of IgG receptor IIb), *Stab2* (Stabilin 2), *Mrc1* (Mannose receptor C-type 1), *Plxnc1* (Plexin c1). In the lung ECs 8 genes overlapped between both studies, from which three are especially interesting since they encode for surface proteins: *Grtp1* (Growth hormone regulated TBC protein 1), *Hpgd* (15-Hydroxyprostaglandin dehydrogenase), *Foxf1a* (Forkhead box F1a), *Rasgef1a* (RasGEF domain family member 1A), *Prx* (Periaxin), encoding for surface proteins: *Adrb1* (Adrenoceptor beta 1), *Scn7a* (Sodium

voltage-gated channel alpha subunit 7), and *Tmem100*¹⁹. No overlap was found between the DE genes and organ-specific genes of the ECs from the aorta and kidney¹⁹. The lack in overlap could be explained by the fact that only top-10 genes were compared between studies. Nevertheless, the overlap found is fascinating and shows that bioinformatic analysis of the *Tabula Muris* dataset can be reproduced.

Both approaches have different advantages. The approach by Paik *et al.* resulted in the selection of a larger pool of organs, leading to the availability of a more robust genetic transcript, whereas the approach of this thesis, by selecting organ-specific genes, could allow organ-specific targeted drug delivery without interfering with any other organ. However, both approaches also have specific limitations. In the organ-specific selection approach only a small number of genes were identified and the genes that were found had a low sequence fragment assigned (counts) of genes per cell. Not all detected genes are encoding for surface proteins, while these genes would be especially of interest since these proteins are potential and promising targets for organs-specific drug delivery, possessing greater target specificity and thereby reducing the risk of side effects. Furthermore, due to the low read counts, possible proteins might not be expressed by all ECs of the organ. The targeting efficiency therefore decreases, and treatment will only reach a limited number of cells of the vascular bed. A limitation of the study by Paik *et al.* is the use of different cell sorting methods, which might have led to a technical variability bias.

Combining the DE genes identified by Paik *et al.*¹⁹ and the organ-specific genes of this study would contribute to the realization of an organ-specific genetic fingerprint and contribute to the establishment of an atlas of endothelial heterogeneity. However, combining data will not come without a disadvantage. The use of different sample preparations and/or analyzing methods might result in technical variations in the dataset, which can be confused with biological effects. Furthermore, it should be considered that both studies did not validate whether the identified genes were also translated, resulting in protein expression on the endothelial surface. Furthermore, the variation between identified genes by the two analysis approaches highlights the necessity to compare multiple studies and consider a large variety of organ to identify robust organ-specific endothelial markers.

4.1.2 – Original scRNA-seq studies to determine the endothelial transcriptome in homeostasis

Recently, single cell EC transcriptome atlas of multiple tissues were generated to decipher the EC diversity between and within tissues. Kalucka *et al.* contributed to the knowledge on the murine endothelial transcriptome by performing scRNA-seq experiments including various

organs¹⁸. An overlap was observed between their study and the data acquired by means of the *Tabula Muris* in this thesis (**Supplementary Table 1**). A similar overlap was observed when results from Paik *et al.* were compared to the results from Kalucka *et al.*, characterized a high degree of overlap of markers in brain, kidney, and liver ECs, medium for the lung, and low for ECs of the heart^{18, 19}, demonstrating a certain degree of reproducibility of the studies.

This thesis also studied the transcriptomic signature of murine ECs and broadened the knowledge on ECs heterogeneity by creating new transcriptomic datasets. In this thesis eight organs were selected to study the endothelial transcriptome, namely the aorta, bladder, bone, colon, ileum, kidney, liver, and lung. Single cells were sorted as bulk and subjected to 10x Genomics, followed by scRNA-seq. DE genes (**Figure 17a** and **Supplementary Figure 3**), organ markers (**Figures 18a-b**) and organ-specific genes (**Table 11** and **Figure 22a**) were identified. These genes can be classified in three different degrees by which they represent an organ. Firstly, DE genes are selected based on the statistically significant observed differences by means of expression levels (read counts and log₂FC) between organs. Secondly, marker genes represent one organ to a larger extent than other organs. They drive the separation between clusters and allow to assign a biological meaning to each cluster based on their functional annotation. Marker genes as well as DE genes are not organ-specific and are also represented in other organs. Lastly, organ-specific genes which are expressed in ECs from one organ while absent in the transcriptomes of other tissues.

4.1.2.1 Differentially expressed genes

DE genes could be identified for all organs (log₂FC > 2, p-value < 0.05) (**Figure 17a** and **Supplementary Figure 3**). The top-10 DE genes were compared to other sequencing studies (**Supplementary Table 6**). Four genes were identified by both Cleuren *et al.* and in our dataset, namely *Gata5* in kidney ECs and *Sprrr2b* (Small proline rich protein 2B), *Tmem132e*, and *Wnt9b* in the ECs of the liver. Cleuren *et al.* identified these genes as organ-specific genes, while in our dataset these genes were DE genes. This might be explained by a variety of factors. Firstly, the studies focused on a different number of organs (**Figure 2**). Cleuren *et al.* only included five organs into their study while our study included eight organs¹⁷. Secondly, the selected organs varied between studies, with only three overlapping organs, namely the kidney, liver, and lung. In our data, *Gata5*, *Sprrr2b*, *Tmem132e*, and *Wnt9* were observed to be expressed in the ECs of the aorta, bladder, bone, colon, ileum, and lung, which are organs that were not included in the work from Cleuren and colleagues. This highlights the relation between the organ included in the study and the eventually identified genes. Including a larger variety of organs will increase the specificity of the selection of DE, marker, and/or organ-specific genes. Thirdly, Cleuren *et al.* used TRAP to isolate the actively translated mRNAs,

thereby studying the translome, while our study focused on the transcriptome. Organs are mechanically dissociated for the TRAP procedure, while our study used enzymatic digestion. Altogether, it is very interesting that an overlap of genes could be observed considering the number of variations between the experimental setup from Cleuren *et al.* and our work.

Two other studies identified DE genes in a homeostatic mouse model. Paik *et al.* and our work selected *Oit3* as a DE gene of liver ECs. In addition, *Slc6a2* was identified as a DE gene for lung ECs by Jambusaria *et al.* and our study. Interestingly, some genes were identified by multiple studies. For example, *Grtp1* and *Prx* were identified as DE genes in lung ECs by Paik *et al.*, Jambusaria *et al.*, and in our dataset^{19, 20}. Furthermore, *Aard* was detected in the lung ECs by Cleuren *et al.* as an organ-specific gene, and by Jambusaria *et al.* and in our dataset as a DE gene, but not organ-specific^{17, 20}. Interestingly, both Cleuren *et al.* and Jambusaria *et al.* studied the brain, heart, and lung ECs, therefore it would have been expected that both studies would classify *Aard* as a lung-specific gene. The difference might be explained by the fact that both studies used different mouse models to extract ribosome-associated RNA, namely TRAP by Cleuren *et al.* while Jambusaria *et al.* used RiboTag. The methods might have influenced the recovered RNA, resulting in the detection of *Aard* to be organ-specific or DE.

4.1.2.2 Marker genes

The genes were ranked for each organ, whereafter top-10 organ marker genes were compared with the literature (**Supplementary Table 7**). In our dataset marker genes were found in all organs ($\log_2FC > 0$). However, a top-10 of marker genes could not be generated for the bone and ileum (SI) ECs, since only 3 and 2 genes could be identified, respectively (**Figure 18**). Furthermore, a broad variation in the number of marker genes could be observed, as for example in the aorta ECs were represented by only one marker gene while the lung ECs were represented by 51 marker genes (**Supplementary Table 18**). The high number of genes representing the lung could be explained by the unique design of the pulmonary system. This circulatory system is designed to perform certain specific functions that are distinctive for the lung, such as ventilation and gas exchange, furthermore, the arteries transport oxygen-poor blood, while the veins transport oxygen-rich blood, which is opposite to the blood transported in the vascular system of other organs¹⁶⁵. The low number of genes identified in the colon could be justified by the comparable heterogeneity of ECs of the ileum. The limited identified marker genes for bone ECs could be a result of the lower number of cells in the dataset (**Table 10**).

To test the reproducibility of scRNA-seq followed by the identification of marker genes, the top-10 marker genes of three studies comparing the genetic profile of ECs¹⁸⁻²⁰ were compared to a top-10 of marker genes of this thesis. For the latter, genes were selected which had a log₂FC bigger than zero. Comparing the data of Kalucka *et al.* with the marker genes found in this thesis, resulted in the identification of a total of 11 genes which were classified as marker genes in both studies. Interestingly, even though only a limited amount of marker genes could be identified, four of these marker genes represented the colon (*Cd24a* and *Rbp7* (Retinol binding protein 7)) and ileum (*Zfp36* (Zinc finger protein 36) and *Scgb3a1* (Secretoglobin Family 3A Member 1)) ECs. Furthermore, an overlap in genes was observed in the liver (*ApoE*, *Gpr182* (G protein-coupled receptors 182), and *Maf* (MAF BZIP transcription factor)), lung (*Tspan7* (Tetraspanin 7)), and kidney (*Meis2* (Meis homeobox 2), *Emcn* (Endomucin), and *Plscr2* (Phospholipid scramblase 2))¹⁸. Furthermore, the study by Paik *et al.* identified a gene representing kidney ECs (*Dkk* (Dickkopf WNT signaling pathway inhibitor)), which was also found in the top-10 kidney EC marker genes in our study¹⁹. Fascinatingly, some genes classified as marker genes were present in our dataset as well as multiple other studies. Paik *et al.*, Kalucka *et al.* and this thesis identified *Igfbp5* (Insulin-like growth factor-binding protein) and *Clec4g* to characterize the kidney and liver ECs, respectively^{18, 19}. The lung ECs were marked by *Sema3c* (Semaphorin 3C) in data from Kalucka *et al.*, Jambusaria *et al.* and in our dataset^{18, 20}. Additionally, *Tmem100*, *Hpgd*, and *Foxf1(a)* distinguished lung ECs and was detected in the dataset of four studies, namely Paik *et al.*, Kalucka *et al.*, Jambusaria *et al.*, and this thesis¹⁸⁻²⁰. Remarkably, *Mafb* was acknowledged as a marker gene and DE gene of bone ECs in this thesis. However, Kalucka *et al.* observed this gene as a gene representing ECs of the spleen¹⁸. This could be explained by the fact that, this thesis did not include spleen ECs, whereas Kalucka *et al.* did not include bone ECs to their study¹⁸. This observation further emphasizes importance to include multiple organs into the equation, highlighting the influence of the organ selection in the study on the eventually detection of genes of interest. Additionally, some overlap was observed between marker genes and DE gene. In this thesis *Pbx1* was identified as a marker gene as well as DE gene of kidney ECs, which is confirmed by Paik *et al.* and Kalucka *et al.* which also identified *Pbx1* to be a gene representing the ECs of the kidney^{18, 19}.

4.1.2.3 Organ-specific genes

Organs-specific genes are of interest since these genes can contribute to the identification of proteins which can be used for organ-specific targeting without interfering with other organs. The organ-specific genes with the highest count number were visualized using violin plots and a top-10 of organ-specific genes can be found in **Supplementary Table 8**. However, the read counts for most genes were relatively low (**Figure 22a**), making the genes less attractive as

potential targeting sites since these genes will not be ubiquitous expressed through-out the vasculature of the organ. However, some potential genes were found to have a reasonable count number. For example, *Gm13470* (95 read counts) was specifically expressed in the kidney ECs and *Adgrl3* (625 read counts) in the lung ECs. Unfortunately, *Gm13570* is a non-coding RNA, which are not of our interest, and thus the dataset should be filtered to remove gene encoding for non-coding RNA. Nevertheless, *Adgrl3* is a gene coding for a cell surface protein. It is a member of the latrophilin subfamily of G-protein-coupled receptors (GPCR) and latrophilins function in signal transduction and cell adhesion. *Adgrl3*, also known as *Lphn3* (Latrophilin 3), is mainly studied in brain and polymorphisms have been linked to an increased risk of attention-deficit/hyperactivity disorder (ADHD) and substance use disorders. ADGRL3 is expressed on neurons and involved in transcellular adhesion, glutamatergic synapse development and has putative roles in neuronal migration and synapse development¹⁶⁶⁻¹⁶⁸. No literature is available on the expression of *Adgrl3* in ECs of the lung and/or brain, however in our dataset this gene seems to be specifically expressed on lung ECs. The expression of *Adgrl3* in other organs was verified with the help of the online *Tabula Muris* tool. The brain and the lung ECs both expressed *Adgrl3* as 8.95% of the brain ECs expressed *Adgrl3* and 14.14% lung ECs. Nevertheless, the expression was also observed in ECs of other organs, though to a very low extend, namely aorta (3.72%), bladder (0.29%), kidney (1.59%), and the gene was not detected in liver ECs⁴⁹. In our study find *Adgrl3* to be exclusively expressed by the ECs of the lung. The expression of the ADGRL3 protein on the EC surface should be verified, while due to its very specific expression in only two organs, it could be a very promising target to deliver drugs exclusively to the lung and/or brain. The blood brain barrier permeability may protect the brain from exposure to drugs and might makes this targeting approach even lung specific.

Cleuren *et al.* identified three genes which were also detected in our dataset. Both studies found *Lgr5* as a kidney ECs specific gene and the organ-specific expression of *Gm26878* in lung ECs. However, also here, it should be considered that the number and type of organs influence which organ-specific genes are detected. *A2m* was detected as an organ-specific gene in both the data of this thesis as well as in the dataset from Cleuren *et al.*. Nevertheless in our study *A2m* was found to be expressed specifically in aortic ECs, while Cleuren *et al.* detected *A2m* specifically in heart ECs. This contradicting result is presumably a consequence of the organs included in the studies, as this thesis did not include the heart and Cleuren *et al.* did not include the ECs of the aorta¹⁷.

Organ-specific genes could only be identified in a limited number of organs and therefore this approach may be too strict to select genes of interest for organ-specific drug delivery. Other

approaches, such as organ markers and DE genes detection might be sufficient to create an EC transcriptomic atlas and contribute to organ drug delivery.

The overlap between studies is fascinating and gives the impression that increasing the number of organs will contribute to the specificity of the identification of marker genes and DE gene. While the number of organ-specific genes might decrease, the required specificity of identified organ-specific genes will drastically increase. Including a large variety of organs in one study is costly, which could be circumvented by combining publicly available datasets and creating one big database. Possible advantages and disadvantages will be discussed in the following chapter.

4.1.2.4 Combining forces

There is a necessity for the identification of robust markers of tissue-specific ECs. Combining multiple studies will contribute to the identification of such markers. However, it must be considered that sample preparation varies between and even within studies and it has been shown that the use of different protocols can influence the genetic profile^{17, 51, 52, 169}. Therefore, the question arises whether results from the studies discussed above could be combined and/or compared as the *Tabula Muris* consortium as well as Kalucka *et al.* used different protocols between but also within their study to digest the organs to achieve single cell dissociation. Cleuren *et al.* investigated whether digestion protocols can affect the gene expression profile. They compared the endothelial gene expression from samples prepared by chemical tissue digestion with those from samples acquired from intact organs by means of TRAP. Interestingly, brain and liver ECs were identified as more similar based on the method of sample preparation (mechanical vs chemical tissue cell dissociation) than by type of organ¹⁷.

For this thesis the variation was controlled by using the same enzymatic dissociation protocol for all organs. However, the enzymatic digestion can still influence the genetic profile. Furthermore, the potential shifts in the endothelial expression profile during the dissociation is not the only limitation of current scRNA-seq methods. These methods also limit detection of low abundance transcripts as they exhibit a relatively limited sensitivity¹⁷⁰. Other approaches, which use a mechanical dissociation protocol, might overcome these limitations. The TRAP approach might be favored over the current dissociation methods used for scRNA-seq sample preparation, since TRAP prepared samples appear to give a more accurate overview of EC profiles, including low abundance transcripts, across vascular beds¹⁷. Another possible method to dissociate tissues would be RiboTag affinity purification. An advantage of the ribosomal purification techniques, like TRAP or RiboTag, is that non-coding regulatory genes

are not detected¹⁷¹. However, a limitation of these studies is the lower FC of DE cell type-enriched genes compared to other dissociation methods¹⁷¹. Furthermore, crossing mice of interest (Cre driver mouse line) with the RiboTag mouse line is time consuming and mRNA profiling using the RiboTag viral vector is costly¹⁷². For our study TRAP or RiboTag would not be used since these mouse models were not available to us.

To create an endothelial transcriptomic atlas which can be used to define targets for organ-specific drug delivery, another aspect must be considered. The studies above only examined the transcriptome for ECs isolated from mice in homeostasis. A genetic fingerprint of the transcriptome of ECs isolated from diseased mice would be of interest, while drugs will mostly be administered to diseased individuals instead of health ones.

4.2 – The endothelial transcriptome of mice exposed to inflammatory stimuli

In the following chapter, the endothelial transcriptome of mice exposed to an acute inflammatory stimulus (endotoxin) and chronic inflammatory stimuli, namely hyperlipidemia and hyperglycemia, was studied.

4.2.1 – Acute inflammation

Understanding the organotypic endothelial heterogeneity that exists during normal physiological conditions as well as during an inflammatory state is essential for understanding endothelial plasticity in homeostasis and tissue-specific responses to inflammation. This chapter will discuss two experiments which studied the transcriptome of ECs isolated from mice exposed to endotoxins. For the first experiment cells were sorted as single cells and pooled in small bulks. In the second experiment, cells were sorted as bulk, however with the help of 10x Genomics labelled as single cells and sequenced resulting in a single cell dataset.

4.2.1.1 Sequencing of a small bulk endothelial cells exposed to endotoxin

The effect of an acute inflammatory condition on the endothelial transcriptome of the aorta and lung were studied. For this pilot-study, all samples were collected on the same day and cells were dissociated with the same protocol, resulting in the opportunity to compare the genetic profiles. Endothelial heterogeneity in response to the systemic inflammatory stress induced by LPS blunted but could still be studied since the endothelium in each tissue maintained a distinct organ-specific molecular identity. Our study was not the only one observing the transcriptome of different organs becoming more similar upon LPS activation¹⁷³. However, organ-specific and upregulated genes could still be identified between and within conditions and organs (**Table 8-9** and **Supplementary Table 2-5**). Most organ-specific genes

were found in ECs of the aorta sorted from a mouse in homeostasis (178), while the least were found in the lung ECs of a mouse exposed to endotoxin (21). The highest number of specific genes were identified in the lung ECs of the homeostatic conditions (145), when compared to ECs collected from a mouse supplemented with endotoxin. The opposite comparison resulted in the lowest number of specific genes (69).

Some other studies also focused on the influence of inflammation on endothelial heterogeneity. Jambusaria *et al.* studied the influence on the endothelial transcriptome 6 hours post systemic LPS supplementation (early response) and 24 hours post systemic LPS injection (late response), by comparing to the endothelial transcriptome of a mouse in homeostasis. Interestingly, three marker genes identified by Jambusaria *et al.* overlapped with genes found in this thesis. However, the organs expressing these genes did not match. Jambusaria *et al.* found *Cxc/9* to be expressed by lung ECs in an early as well as a late inflammatory response. In our dataset this gene seemed DE in the aorta as well as the lung ECs isolated from mice which were exposed to LPS. *I/6* (Interleukin 6) was found in the brain ECs in an early inflammatory response and *Apod* (Apolipoprotein d) in the heart in a late inflammatory response, in the study by Jambusaria *et al.*²⁰. In our study these genes were classified as organ-specific genes of the ECs of the aorta in a setting of acute inflammation. The variation can be explained by the number and type of organs used in both studies. Jambusaria *et al.* included ECs of the brain, heart, and lung²⁰, while in this pilot-study ECs from only the aorta and lung were included. Here we again see the importance of comparing a larger variety of organs to determine the transcriptome and to generate an overview of genes representing one organ. They did not mention a reduction of EC heterogeneity upon exposure to LPS.

Cleuren *et al.* also studied the influence of inflammation on endothelial heterogeneity and compared the endothelial transcriptomes of cells collected during homeostasis and acute inflammation 4 hours after LPS administration. They found that upregulated genes by endotoxin included several adhesion molecules which are required for leukocyte recruitment and migration and genes involved in maintenance of the EC barrier were downregulated. Only a general list of genes previously identified to be affected in endotoxemia was published¹⁷. Genes in this list did not correspond with the genes identified in our study. However, this list did not focus on identifying genes representing a particular organ but focused more on general upregulated and downregulated genes among all organs. Therefore, it was hard to compare both studies.

Toledo et al. studied the effect of MRSA induced sepsis (24 hours post infection) on the vascular cell surface proteome²¹. They identified organ-specific vascular targets with the use of biotinylation of the vasculature followed by a proteomics workflow. Their data indicated that MRSA-sepsis triggered the proteome remodeling of the vascular cell surfaces extensively, in a tissue-specific manner. The proteins CXCL9 and LCN2 were detected in the liver and kidney, respectively. Interestingly, in our study genes corresponding to these proteins were also detected as DE genes, however in the aorta as well as the lung ECs. As a sidenote, our study did not include the ECs from the liver and kidney, while Toledo *et al.* did not study the ECs of the aorta and lung²¹.

Kaur *et al.*, studied the effect of different inflammatory stimuli and investigated the activation of ECs and SMC in murine models of sepsis and atherosclerosis¹⁷³. The inflammatory conditions led to characteristic changes in the GPCR repertoire. More specifically, depending on their anatomical location and expression to a certain stimulus, ECs showed remarkable variances in the GPCR repertoire. Interestingly, *Glp1r* (Glucagon-like peptide-1 receptor) was observed to be specifically upregulated in lung ECs exposed to sepsis. In our study we also identified *Glp1r* to be a DE gene in the lung upon inflammatory conditions. Clear changes in the expression of the GPCR as well as function-related genes were observed when ECs from healthy aortae were compared to atherosclerotic aortae. In addition, comparing the transcriptome of acutely or chronically activated ECs showed expression changes in selected GPCRs and adhesion molecules¹⁷³. This shows the importance to study next to a variety of organs, also different chronic inflammatory models in this study.

The purpose of this pilot study was to verify if acute inflammation can influence the endothelial transcriptome. Promising differences were observed comparing the transcriptomes of the ECs isolated from a homeostatic and acute inflammatory condition. This further triggered our interest to also study the effect of other inflammatory stimuli on the transcriptomic profile. However, the set-up of the pilot study limited the quantity of ECs. Single cell sorting limited this experiment drastically since many cells were not recognized as ECs during FACS. Cell numbers could be increased by culturing the sorted ECs. *In vitro* culturing, although this would remove ECs from their organ-specific microenvironment. This would be a major limitation as microenvironmental cues from the neighboring tissues are believed to be a co-regulator of EC heterogeneity, contributing to microvascular adaptations of the ECs to local needs¹⁷⁴. Thereby, removal of the ECs from their microenvironment can lead to a modulation of mRNA levels¹⁷⁵, stability¹⁷⁶, and induce rapid gene expression drift^{177, 178}. Therefore, another sorting strategy was essential to obtain a reasonable number of ECs.

4.2.1.2 10x Genomics and scRNA-seq

To overcome the limiting factor of the number of available ECs the cells were sorted in bulk and subjected to 10x Genomics to keep the opportunity to analyze the data as single cells. Further analysis resulted in the selection of DE genes (**Figure 19a-b** and **Supplementary Table 9**), marker genes (**Figure 17c**, **Supplementary figure 5** and **Supplementary Table 10**), and organ-specific genes (**Figure 22c** and **Supplementary Table 11**).

Organ-specific, markers, and DE genes could be identified for all organs. Preferably comparison would be made between the gene transcripts identified in this thesis with the literature, to confirm reproducibility and consistency of the transcripts. However, only three studies focused on the effect of endotoxin on the endothelial transcriptomic, all with different experimental approaches. In this study we compared the transcriptome of 8 organs from a mouse subjected to acute inflammation by injection of LPS 4 hours before organ collection. As described above, Cleuren *et al.* and Jambusaria *et al.* focused on the influence of inflammation on endothelial heterogeneity and compared the endothelial transcriptomes of cells collected during homeostasis and acute inflammation^{17, 20}. Unfortunately, due to our experimental set-up, no comparison can be made between treatments. The main limitation, making a direct comparison impossible, is the fact that organs of mice in homeostasis and of mice subjected to an acute inflammatory stimulus were collected, processed, sorted, and subjected to 10x Genomics on different days, without the inclusion of an internal control, such as ERCC. Therefore, no batch correction could be executed since biological effects could not be distinguished from technical variations. However, both Cleuren *et al.* and Jambusaria *et al.* also studied the difference between genetic profiles of organs exposed to sepsis^{17, 20}. Detected genes in the sample of the acute inflammatory conditions of the two studies and our study were compared. Three genes detected by Cleuren *et al.* were also present in our dataset. They found that *Cldn5* and *Tfpi* (Tissue factor pathway inhibitor) were downregulated in all organs, and *Plat* (Plasminogen activator, tissue type) was upregulated in the lung¹⁷. We found *Cldn5* as a marker gene for ECs of the bladder, *Plat* for kidney ECs, and *Tfpi* as a DE gene of ECs of the bone. These differences can most likely be explained by a distinctive focus of the studies and the selected organs included in the studies. No overlapping genes could be identified when comparing the data from Jambusaria *et al.* to our data, which might be a result of the variation in organs selection in both studies and the fact that cells were collected 6- and 24 hours after LPS exposure. An additional difference between the studies of Cleuren *et al.* and Jambusaria *et al.* is the fact that they studied the translatoome, while our study focused on the transcriptome.

Toledo et al. data indicated that in a MRSA induced sepsis model the protein LCN2 was detected in the kidney²¹. Interestingly, the gene encoding for this protein was in our dataset identified as a DE gene and marker gene for bladder ECs. Even though our dataset contained kidney ECs, Toledo *et al.* did not include bladder ECs in their study, which explains the difference between the studies.

The three out of four studies used LPS induced sepsis to study the effect of acute inflammation on the EC transcriptome. However, the question arises how additional or different disease models would influence transcriptome responses in different vascular bed. This will be of great value to expand our knowledge on the genetic profile of ECs in different diseased states. Thereby, contributing to finding possible targets to deliver drugs in a certain organ to treat a certain disease.

4.2.2 – Chronic inflammation

This chapter discusses the endothelial transcriptomes of two mouse models experiencing chronic inflammatory diseases. The mice were exposed to hyperglycemia or hyperlipidemia, to induce diabetes or atherosclerosis, respectively. Cells were sorted as bulk, subjected to 10x Genomics, followed by scRNA-seq.

4.2.2.1 Hyperglycemia and diabetes

Hyperglycemia and glucose intolerance are the main clinical and diagnostic features of diabetes⁷¹. It has been reported that diabetes has an influence on ECs, although the effect of diabetes on organ-specific endothelial heterogeneity has not been studied yet. Mice were injected for five consecutive days with STZ leading to the destruction of β cells, resulting in insulin deficiency and the induction of a hyperglycemic state⁸². The dataset of the organs collected in the morning was analyzed and DE genes were identified for all organs (**Figure 17e-f**, **Supplementary Figure 7**, and **Supplementary Table 12**). Marker genes could be identified in seven out of eight organs, since for the bone ECs no markers could be found, and the ileum (SI) was unfortunately only represented by one marker gene (**Figure 20a** and **Supplementary Table 13**). Organ specific genes were identified in all organs and ranged from 48 genes representing the ECs of the bone to 448 genes that distinguished the lung ECs (**Table 11**). Genes with a reasonable number of read counts were found in the kidney and liver ECs, namely *3110099E03Rik* (452 count) and *Gm17167* (293 read counts), respectively. However, both genes are not eligible for drug delivery, since both genes are long non-coding RNAs, which are not translated into proteins.

There is no literature available which studied the influence of diabetes or hyperglycemia on the transcriptome of ECs isolated from a variety of organs. Some studies focused on a specific organ, such as the retina¹⁷⁹, pancreas¹⁸⁰, kidney¹⁸¹, and ECs of the cubital vein¹⁸². However, the experiment set-up of the studies listed above vary drastically. A coherent dataset reflecting one disease model while using one coherent tissue dissociation protocol is not available. To give a small insight in the available literature, Sun *et al.* sorted cells from STZ-induced diabetic murine retinas. All cells of the retina were sequenced, from which 5% were ECs. Many genes were deregulated in diabetic vascular ECs, and the differentially expressed genes were paired to the pathways functioning in metabolism, shear stress and vascular permeability¹⁷⁹. On the other hand, Jonsson *et al.* studied pancreatic cells isolated from brain death individuals with normoglycemia or impaired glucose tolerance, which is defined as a diagnosis of T2D. Interestingly, although many differences were observed between exocrine and -islet tissue ECs, no differences were found between normoglycemic donors and donors with impaired glucose tolerance at gene as well as gene set level¹⁸⁰. Another human study, by Parker *et al.*, investigated the transcriptomic landscape of diabetic nephropathy. DE genes in the kidney ECs included extracellular matrix components, glucose transporters, and regulators of angiogenesis¹⁸¹. Furthermore, Beckman *et al.* isolated human ECs from the cubital vein from diabetic and healthy individuals. Allowing to compare endothelial transcripts, resulting in the identification of 51 upregulated and 101 downregulated genes in T2D. Gene set enrichment analysis classified, among others, TGF β signaling to be positively and oxidative phosphorylation negatively enriched¹⁸². The existing literature on the influence of diabetes and hyperglycemia on the endothelial transcriptome on a variety of organs is limited. Furthermore, as mentioned above, the available literature disagrees on whether hyperglycemia and/or diabetes affects EC heterogeneity. Studies that suggest an effect of diabetes on EC heterogeneity study different organs and identify different pathway to be affected. Our dataset, studying the endothelial transcriptome of multiple organs, is therefore an extremely novel addition to this, barely touched upon, field.

Diabetes is comprised out of a group of metabolic disorders making it difficult to select the right model to study this disease. In our study we decided to use a STZ-induced diabetes model. This model is fast, cheap, and can be applied to almost any mouse strain. An interesting side note, female mice have been omitted from the STZ model since they were reported to be resistant to the diabetogenic actions of STZ¹⁸³⁻¹⁸⁷. Consequently, only male mice were used in our study. However, resistance of female mice can be overcome by increasing the dose of STZ¹⁸⁸ but a higher dose of STZ could lead to hepatotoxicity and nephrotoxicity⁸¹. STZ-induced diabetes studies in male mice are therefore preferred.

Fascinatingly, nearly 80% of all deaths among diabetic patients is accounted for by atherosclerosis¹⁸⁹. Persistent exposure to hyperglycemia is acknowledged as a major feature in the pathogenesis of diabetes associated atherosclerosis. Hyperglycemia induces many alterations at cellular level in vasculature, which possibly accelerate the atherosclerotic lesion formation¹⁸⁹⁻¹⁹¹. Growing evidence indicates that EC dysfunction is a critical early event to diabetes-associated development of atherosclerosis¹⁹². Zhao *et al.* studied the transcriptomic changes in diabetic atherosclerosis, by performing a scRNA-seq study using ECs from mouse aorta and heart after inducing diabetic atherosclerosis by feeding the mice a diabetogenic high-fat diet with cholesterol. The study concluded that ECs were highly heterogeneous and plastic, both in atherosclerotic as well as homeostatic conditions¹⁹³. This rises the interest to study the endothelial transcriptome of multiple organs in an atherosclerotic setting.

4.2.2.2 Hyperlipidemia and atherosclerosis

Hyperlipidemia can originate from a genetic or acquired disorders and is characterized by high levels of circulating lipids and is a known risk factor for CVDs, such as atherosclerosis⁸⁹.

For this thesis, mice were injected with a AAV8 carrying a gain-of-function mutation of PCSK9¹⁰³ and fed a HFD to exacerbate hyperlipidemia. After analyzing the dataset of the organs collected in the morning, DE genes were identified and found to be present in all organs (**Figure 17g-h, Supplementary Figure 9, and Supplementary Table 15**). No marker gene could be identified for the ileum (SI) (**Figure 21a and Supplementary Table 16**), which could be explained by the low number of cells (**Table 10**). Interestingly, marker genes representing the aorta (*Cyt11*, Cytokine like 1), kidney (*Igfbp5*), liver (*Rspo3*, R-Spondin 3), and lung (*Hpgd*) seem to clearly represent EC population of one specific organ, since the genes are not extensively expressed in the other organs (**Figure 21b**). Furthermore, all genes are encoding surface proteins, making them potential interesting targets for drug delivery. Additionally, all organs were represented by organ-specific genes and the number of genes ranged from 42 genes in the ileum ECs to 490 genes distinguishing the liver ECs (**Table 11**). The read counts of the organ-specific gene of the ECs of the aorta and liver could be considered for targeting, since the read counts of these genes are reasonably high, namely 339 read counts for *Is1* and 206 read counts for *Gm17167* (**Figure 23c**), respectively. *Is1* is a protein coding gene and its protein seems to be expressed on the cell surface, on the other hand, *Gm17167*, is a long non-coding RNA and will therefore not be of interest for further analysis.

This is the first study which studied the endothelial transcriptome in a variety of organs in an atherosclerotic setting. However, the transcriptome of human atherosclerotic plaques¹⁹⁴, and

the adventitia¹⁹⁵ and ascending aorta¹⁹⁶ in mouse models of atherosclerosis are already studied. Depuydt *et al.* studied the transcriptome of the human plaque and applied scRNA-seq to all cells in advanced human atherosclerotic plaques¹⁹⁴. However, their study focused more on a general genetic profile of all cells in the plaque. It would have been fascinating to compare the data to the transcriptome of a healthy carotid artery, however, these samples are hardly available. Another interesting comparison could have been stable versus an unstable plaque. Patients are at risk when a stable plaque becomes unstable, and eventual rupture of the unstable plaque can lead to myocardial infarction or stroke^{59, 94, 95}. Defining how this switch from stable to an unstable plaque occurs, might lead to a better understand and even the development treatment reducing plaque destabilization. Studying the difference between these two plaques stages is therefore an interesting focus for future research. In addition to this human study, Gu *et al.* compared the adventitia of wild type and *Apoe*^{-/-} mice. They performed gene ontology analysis and were able to identify enrichment of chemokine activity, CCR chemokine receptor activity, and arachidonic acid binding as early changes of the adventitial ECs in atherosclerosis¹⁹⁵. Additionally, Kan *et al.* studied the heterogeneity in the ascending aortas of normal and HFD fed C57BL/6J mice. They observed a unique transcriptome profile after HFD feeding, suggesting a corresponding functional signature¹⁹⁶. All these studies underpin the ability of hyperlipidemia to change the transcriptomic profile of the ECs.

The consequence of disturbed flow on the carotid artery heterogeneity was also studied. Li *et al.* observed a shift in heterogeneity upon disturbed flow, and two disturbed-flow-derived EC subpopulations were identified. The two most significantly enriched genes representing these subpopulations were *Cd36* and *Dkk2*. *Cd36* encodes a receptor for oxidized LDL involved in lipid metabolism^{197, 198} and *Dkk2* has been reported to play a fundamental role in controlling angiogenesis¹⁹⁹. Moreover, *Dkk2* was also detected in our dataset, however, it was not expressed in the top-10 DE genes, marker genes, or organs specific genes of ECs of the aorta but in the top-10 marker gene list representing the kidney ECs. Highlighting the importance of studying the effect of hyperlipidemia in a variety of organs.

Similar to the hyperglycemic mouse models, there is also a wide variety of mouse models that can be used to study atherosclerosis. We chose for a model of PCSK9-AAV8¹⁰³ followed by a Western-type diet, since it is very versatile and efficient model. Our VE-cadherin-cre-rfp^{flox/flox} mice are not on an *Apoe*^{-/-} or *Ldlr*^{-/-} background. With injection of PCSK9-AAV8, hyperlipidemia and atherosclerosis can be easily induced in animals with a non-atherosclerotic genetic background. Furthermore, a single dose of PCSK9-AAV8 is robust and stabile even one-year post-infection, without any major biosafety concerns¹⁰⁴. This makes the PCSK9-AAV

model an optimal model for this study. However, other studies mainly use *ApoE*^{-/-} or *Ldlr*^{-/-} mouse models to study atherosclerosis. The choice for the PCSK9-AAV mouse model is therefore also a limitation, while comparisons with other studies could be difficult. This emphasizes the importance of future studies to aim to use homogenous mouse model between studies to enable comparison and reproducibility between studies.

4.3 Circadian

In addition to pathological effects (i.e. acute inflammation, hyperglycemia, hyperlipidemia) on EC heterogeneity, it has also been observed that the time of the day can have a major influence on ECs. This circadian control has major effects on ECs regulatory functions^{122, 147-150} and a striking 40% of all protein-coding genes are controlled in a circadian and organ-specific manner¹¹⁹. Based on its importance, this circadian component has also been investigated in this thesis.

The number of sorted cells seemed not to be influenced by circadian rhythmicity, while no pattern can be recognized between the number of cells sorted and different times of the day (**Table 10**). Correspondingly, Hasper *et al.* observed in vessels of the lung that the number of ECs did not oscillate over time¹³⁶. The transcriptome of ECs collected at 8 am and 8 pm can unfortunately not be directly compared, since the experiments were executed on different days. A different experimental set-up should be selected to create a dataset where ECs collected at different timepoints could be compared. Time shifted light cabinets should be used to facilitate simultaneous experiments. One group would be placed in a 12h shifted cyclers. Another option to synchronize experiments could be the use of LEDDY cages, which have a fully programmable IVC light control system. These red tinted cages contain a programmable LED source, which allows to set dedicated light cycles in the individual cage. LEDDY cages were unfortunately not available in our animal facility. Furthermore, only one light cabinet was present, not allowing to preserve the same housing conditions between the morning and afternoon group.

Even though the transcriptome could not be compared between timepoints, organs within one treatment and timepoint could be compared. DE genes could be identified in ECs isolated from all conditions (homeostasis, acute inflammation, and chronic inflammation (hyperglycemia and hyperlipidemia) and organs (**Figure 17b, d, f, h** and **Supplementary Figure 4, 6, 8, 10**). Additionally, marker genes were detected for all organs in the ECs isolated from mice in homeostasis and mice exposed to hyperglycemia (**Figure 18c** and **Figure 21c**). In the acute inflammatory dataset, no markers were found for bone ECs, and in the hyperlipidemic dataset

no marker genes are available for the ECs of the bone and ileum (SI) (**Figure 19c** and **Figure 20c**). Interestingly, the top-1 marker genes of ECs homeostatic, hyperlipidemic and hyperglycemic subset seemed to be more specific than the genes representing the acute inflammatory subset (**Figure 18-21d**). The distinct organ-specific molecular identity seems to be partly lost, similar as in the ECs harvested in the morning. Interestingly, circadian rhythmicity seems not to influence the total amount of organ-specific genes per treatment (**Table 10**). Some organ-specific genes could be identified in the kidney and lung ECs of the homeostatic dataset: *Lypd6* and *Zfp641*, respectively, reached both a reasonable number of read counts (**Figure 22b**). In the hyperglycemic dataset liver ECs exclusively expressed *Ajap1* (**Figure 23b**). The gene *3110099E03Rik* was identified to be specific for kidney ECs in the hyperglycemic as well as the hyperlipidemic subset (**Figure 23b** and **d**). Furthermore, in the hyperlipidemic subset specific genes were found in the lung *Gata4* and liver ECs (*Raver2*)(**Figure 23d**). The gene counts of the organ-specific genes in the acute inflammatory dataset were too low to be of interest for possible organ targeting.

The circadian rhythmicity of ECs is barely studied, literature regarding the endothelial transcriptome mainly focusses on one timepoint. Most studies focus on the role of circadian rhythmicity on leukocyte recruitment. However, due to the role of ECs in leukocyte recruitment some studies touch upon the circadian protein expression on ECs. For example, He *et al.* verified the rhythmic protein expression of some EC-adhesion molecules, as ICAM-1/2 (Intercellular Adhesion Molecule 1/2), Selectins and VCAM-1 (Vascular cell adhesion protein 1), in various organs. They observed that adhesion molecules were not explicitly expressed by all organs and one third of the included proteins showed to oscillate during a 24-hour timeframe²². The lymphatic vasculature also seems to be controlled by rhythmicity. Recent observations indicated that lymphocyte recruitment in the lymphatics of the skin is controlled by the circadian clocks. Cell-intrinsic circadian oscillations were observed in the skin lymphatic ECs and dendritic cells. Furthermore, afferent lymphatic ECs in the gut, lung, lymph nodes and skin showed tissue-specific temporal expression of adhesion molecules²⁰⁰. These data provide an interesting perspective on molecule identification for possible organ-specific drug delivery targeting vascular ECs. Eventually this data can contribute to time-optimized drug delivery, which may harbor an immense benefit considering that many pharmacological targets oscillate and not even to mention the short half-lives of many drugs¹¹⁹. Additionally, this way of drug deliver will enhance therapeutic efficacy since target expression will most probably not be granted throughout the day. Further, optimized delivery might potentially permit to reduce side effects. Altogether, knowledge on temporal gene expression will be a vast addition to our endothelial transcriptomic atlas.

4.4 Limitations and future perspectives

This thesis studied EC heterogeneity and provided the scientific field with a novel overview of DE, marker, and organ-specific genes expressed by ECs of a homeostatic, acute inflammatory, and two chronic inflammatory (hyperglycemic and hyperlipidemic) mouse models while incorporating circadian rhythmicity of the genetic profile. Though this study also faces some limitations. First, only 8 mouse tissues were included in this study. Although this dataset is still a valuable addition to future opportunities in tissue specific targeting, this is an important sidenote as gene expression in not included tissues is not evaluated yet and can therefore cause off-target effects. Second, this study was not designed to compare conditions with each other, and comparisons could only be made between tissues within one condition. Future studies should incorporate an internal control which allows removal of technical variation while preserving biological variation, permitting comparison between organs of different treatments. Third, additional protein analysis and functional validation, required to confirm the putative role of the EC phenotypes, are lacking. Phenotypes are now assigned based on only transcriptomic data. Proteins can be used for targeted drug delivery and surface expression should therefore be confirmed in future studies. Fourth, the heterogenetic complexity of vascular beds within one organ, i.e. the presence of arteries, veins, and capillaries, was not studied. More insight in the complexity of the vasculature would shed a light on the difference between organs and would contribute to a more robust atlas of the vasculature. Finally, single cell preparation by enzymatic tissue dissociation and FACS-based ECs enrichment might result in the detection of non-coding genes or genes which do not encode for surface proteins. This limitation can be avoided by means of using the TRAP or RiboTag method, which studies the actively translated mRNAs, which increase the chance to detect genes encoding for surface proteins. Nonetheless, this data adds a new dimension to the field of endothelial heterogeneity by studying the effect of chronic inflammation and circadian rhythmicity on the EC transcriptome. Thereby adding novel information to the EC heterogeneity field, which contributes to the development of as EC transcriptomic atlas. Eventually, selecting genes encoding for surface proteins might result in the establishment of organ-specific 'ZIP'-codes, which can be used to target one organ without interfering with other organs. This would allow to take a first step towards organ-specific drug delivery.

References

1. Anggard EE. The endothelium--the body's largest endocrine gland? *J Endocrinol.* 1990;127(3):371-5.
2. McCarron JG, Lee MD, Wilson C. The Endothelium Solves Problems That Endothelial Cells Do Not Know Exist. *Trends Pharmacol Sci.* 2017;38(4):322-38.
3. Wisse E. An electron microscopic study of the fenestrated endothelial lining of rat liver sinusoids. *J Ultrastruct Res.* 1970;31(1):125-50.
4. dela Paz NG, D'Amore PA. Arterial versus venous endothelial cells. *Cell Tissue Res.* 2009;335(1):5-16.
5. Jakab M, Augustin HG. Understanding angiodiversity: insights from single cell biology. *Development.* 2020;147(15).
6. Florey. The endothelial cell. *Br Med J.* 1966;2(5512):487-90.
7. Hennigs JK, Matuszcak C, Trepel M, Korbelin J. Vascular Endothelial Cells: Heterogeneity and Targeting Approaches. *Cells.* 2021;10(10).
8. Chang SH, Feng D, Nagy JA, Sciuto TE, Dvorak AM, Dvorak HF. Vascular permeability and pathological angiogenesis in caveolin-1-null mice. *Am J Pathol.* 2009;175(4):1768-76.
9. Cao Z, Lis R, Ginsberg M, Chavez D, Shido K, Rabbany SY, et al. Targeting of the pulmonary capillary vascular niche promotes lung alveolar repair and ameliorates fibrosis. *Nat Med.* 2016;22(2):154-62.
10. Eremina V, Baelde HJ, Quaggin SE. Role of the VEGF--a signaling pathway in the glomerulus: evidence for crosstalk between components of the glomerular filtration barrier. *Nephron Physiol.* 2007;106(2):p32-7.
11. Ricard N, Scott RP, Booth CJ, Velazquez H, Cilfone NA, Baylon JL, et al. Endothelial ERK1/2 signaling maintains integrity of the quiescent endothelium. *J Exp Med.* 2019;216(8):1874-90.
12. Tirziu D, Chorianopoulos E, Moodie KL, Palac RT, Zhuang ZW, Tjwa M, et al. Myocardial hypertrophy in the absence of external stimuli is induced by angiogenesis in mice. *J Clin Invest.* 2007;117(11):3188-97.
13. Greene AK, Wiener S, Puder M, Yoshida A, Shi B, Perez-Atayde AR, et al. Endothelial-directed hepatic regeneration after partial hepatectomy. *Ann Surg.* 2003;237(4):530-5.
14. Aird WC. Endothelial cell heterogeneity. *Cold Spring Harb Perspect Med.* 2012;2(1):a006429.
15. Aird WC. Phenotypic heterogeneity of the endothelium: II. Representative vascular beds. *Circ Res.* 2007;100(2):174-90.

16. DeLeve LD, Wang X, Hu L, McCuskey MK, McCuskey RS. Rat liver sinusoidal endothelial cell phenotype is maintained by paracrine and autocrine regulation. *Am J Physiol Gastrointest Liver Physiol*. 2004;287(4):G757-63.
17. Cleuren ACA, van der Ent MA, Jiang H, Hunker KL, Yee A, Siemieniak DR, et al. The in vivo endothelial cell transcriptome is highly heterogeneous across vascular beds. *Proc Natl Acad Sci U S A*. 2019;116(47):23618-24.
18. Kalucka J, de Rooij L, Goveia J, Rohlenova K, Dumas SJ, Meta E, et al. Single-Cell Transcriptome Atlas of Murine Endothelial Cells. *Cell*. 2020;180(4):764-79 e20.
19. Paik DT, Tian L, Williams IM, Rhee S, Zhang H, Liu C, et al. Single-Cell RNA Sequencing Unveils Unique Transcriptomic Signatures of Organ-Specific Endothelial Cells. *Circulation*. 2020;142(19):1848-62.
20. Jambusaria A, Hong Z, Zhang L, Srivastava S, Jana A, Toth PT, et al. Endothelial heterogeneity across distinct vascular beds during homeostasis and inflammation. *Elife*. 2020;9.
21. Toledo AG, Golden G, Campos AR, Cuello H, Sorrentino J, Lewis N, et al. Proteomic atlas of organ vasculopathies triggered by *Staphylococcus aureus* sepsis. *Nat Commun*. 2019;10(1):4656.
22. He W, Holtkamp S, Hergenhan SM, Kraus K, de Juan A, Weber J, et al. Circadian Expression of Migratory Factors Establishes Lineage-Specific Signatures that Guide the Homing of Leukocyte Subsets to Tissues. *Immunity*. 2018;49(6):1175-90 e7.
23. Drechsler M, Megens RT, van Zandvoort M, Weber C, Soehnlein O. Hyperlipidemia-triggered neutrophilia promotes early atherosclerosis. *Circulation*. 2010;122(18):1837-45.
24. Ortega-Gomez A, Salvermoser M, Rossaint J, Pick R, Brauner J, Lemnitzer P, et al. Cathepsin G Controls Arterial But Not Venular Myeloid Cell Recruitment. *Circulation*. 2016;134(16):1176-88.
25. Winter C, Silvestre-Roig C, Ortega-Gomez A, Lemnitzer P, Poelman H, Schumski A, et al. Chrono-pharmacological Targeting of the CCL2-CCR2 Axis Ameliorates Atherosclerosis. *Cell Metab*. 2018;28(1):175-82 e5.
26. Minami T, Aird WC. Endothelial cell gene regulation. *Trends Cardiovasc Med*. 2005;15(5):174-84.
27. Breier G, Breviario F, Caveda L, Berthier R, Schnurch H, Gotsch U, et al. Molecular cloning and expression of murine vascular endothelial-cadherin in early stage development of cardiovascular system. *Blood*. 1996;87(2):630-41.
28. Huminiecki L, Gorn M, Suchting S, Poulsom R, Bicknell R. Magic roundabout is a new member of the roundabout receptor family that is endothelial specific and expressed at sites of active angiogenesis. *Genomics*. 2002;79(4):547-52.

29. Lampugnani MG, Resnati M, Raiteri M, Pigott R, Pisacane A, Houen G, et al. A novel endothelial-specific membrane protein is a marker of cell-cell contacts. *J Cell Biol.* 1992;118(6):1511-22.
30. Nolan DJ, Ginsberg M, Israely E, Palikuqi B, Poulos MG, James D, et al. Molecular signatures of tissue-specific microvascular endothelial cell heterogeneity in organ maintenance and regeneration. *Dev Cell.* 2013;26(2):204-19.
31. Marcu R, Choi YJ, Xue J, Fortin CL, Wang Y, Nagao RJ, et al. Human Organ-Specific Endothelial Cell Heterogeneity. *iScience.* 2018;4:20-35.
32. Lukowski SW, Patel J, Andersen SB, Sim SL, Wong HY, Tay J, et al. Single-Cell Transcriptional Profiling of Aortic Endothelium Identifies a Hierarchy from Endovascular Progenitors to Differentiated Cells. *Cell Rep.* 2019;27(9):2748-58 e3.
33. Tikhonova AN, Dolgalev I, Hu H, Sivaraj KK, Hoxha E, Cuesta-Dominguez A, et al. The bone marrow microenvironment at single-cell resolution. *Nature.* 2019;569(7755):222-8.
34. Sabbagh MF, Heng JS, Luo C, Castanon RG, Nery JR, Rattner A, et al. Transcriptional and epigenomic landscapes of CNS and non-CNS vascular endothelial cells. *Elife.* 2018;7.
35. Vanlandewijck M, He L, Mae MA, Andrae J, Ando K, Del Gaudio F, et al. A molecular atlas of cell types and zonation in the brain vasculature. *Nature.* 2018;554(7693):475-80.
36. He L, Vanlandewijck M, Mae MA, Andrae J, Ando K, Del Gaudio F, et al. Single-cell RNA sequencing of mouse brain and lung vascular and vessel-associated cell types. *Sci Data.* 2018;5:180160.
37. Schupp JC, Adams TS, Cosme C, Jr., Raredon MSB, Yuan Y, Omote N, et al. Integrated Single-Cell Atlas of Endothelial Cells of the Human Lung. *Circulation.* 2021;144(4):286-302.
38. Su T, Stanley G, Sinha R, D'Amato G, Das S, Rhee S, et al. Single-cell analysis of early progenitor cells that build coronary arteries. *Nature.* 2018;559(7714):356-62.
39. Tombor LS, John D, Glaser SF, Luxan G, Forte E, Furtado M, et al. Single cell sequencing reveals endothelial plasticity with transient mesenchymal activation after myocardial infarction. *Nat Commun.* 2021;12(1):681.
40. Dumas SJ, Meta E, Borri M, Goveia J, Rohlenova K, Conchinha NV, et al. Single-Cell RNA Sequencing Reveals Renal Endothelium Heterogeneity and Metabolic Adaptation to Water Deprivation. *J Am Soc Nephrol.* 2020;31(1):118-38.
41. Karaiskos N, Rahmatollahi M, Boltengagen A, Liu H, Hoehne M, Rinschen M, et al. A Single-Cell Transcriptome Atlas of the Mouse Glomerulus. *J Am Soc Nephrol.* 2018;29(8):2060-8.

42. Menon R, Otto EA, Hoover P, Eddy S, Mariani L, Godfrey B, et al. Single cell transcriptomics identifies focal segmental glomerulosclerosis remission endothelial biomarker. *JCI Insight*. 2020;5(6).
43. Brandes R, Vold RR, Kearns DR, Rupprecht A. Static disorder and librational motions of the purine bases in films of oriented Li-DNA. *J Mol Biol*. 1988;202(2):321-32.
44. Ramachandran P, Dobie R, Wilson-Kanamori JR, Dora EF, Henderson BEP, Luu NT, et al. Resolving the fibrotic niche of human liver cirrhosis at single-cell level. *Nature*. 2019;575(7783):512-8.
45. Guo M, Du Y, Gokey JJ, Ray S, Bell SM, Adam M, et al. Single cell RNA analysis identifies cellular heterogeneity and adaptive responses of the lung at birth. *Nat Commun*. 2019;10(1):37.
46. Goveia J, Rohlenova K, Taverna F, Treps L, Conradi LC, Pircher A, et al. An Integrated Gene Expression Landscape Profiling Approach to Identify Lung Tumor Endothelial Cell Heterogeneity and Angiogenic Candidates. *Cancer Cell*. 2020;37(1):21-36 e13.
47. Khan S, Taverna F, Rohlenova K, Treps L, Geldhof V, de Rooij L, et al. EndoDB: a database of endothelial cell transcriptomics data. *Nucleic Acids Res*. 2019;47(D1):D736-D44.
48. Han X, Wang R, Zhou Y, Fei L, Sun H, Lai S, et al. Mapping the Mouse Cell Atlas by Microwell-Seq. *Cell*. 2018;172(5):1091-107 e17.
49. Tabula Muris C, Overall c, Logistical c, Organ c, processing, Library p, et al. Single-cell transcriptomics of 20 mouse organs creates a Tabula Muris. *Nature*. 2018;562(7727):367-72.
50. Rajotte D, Arap W, Hagedorn M, Koivunen E, Pasqualini R, Ruoslahti E. Molecular heterogeneity of the vascular endothelium revealed by in vivo phage display. *J Clin Invest*. 1998;102(2):430-7.
51. Adam M, Potter AS, Potter SS. Psychrophilic proteases dramatically reduce single-cell RNA-seq artifacts: a molecular atlas of kidney development. *Development*. 2017;144(19):3625-32.
52. van den Brink SC, Sage F, Vertesy A, Spanjaard B, Peterson-Maduro J, Baron CS, et al. Single-cell sequencing reveals dissociation-induced gene expression in tissue subpopulations. *Nat Methods*. 2017;14(10):935-6.
53. Semenza GL. Vascular responses to hypoxia and ischemia. *Arterioscler Thromb Vasc Biol*. 2010;30(4):648-52.
54. Pober JS, Sessa WC. Evolving functions of endothelial cells in inflammation. *Nat Rev Immunol*. 2007;7(10):803-15.

55. Fraisl P, Mazzone M, Schmidt T, Carmeliet P. Regulation of angiogenesis by oxygen and metabolism. *Dev Cell*. 2009;16(2):167-79.
56. Dobie R, Wilson-Kanamori JR, Henderson BEP, Smith JR, Matchett KP, Portman JR, et al. Single-Cell Transcriptomics Uncovers Zonation of Function in the Mesenchyme during Liver Fibrosis. *Cell Rep*. 2019;29(7):1832-47 e8.
57. Ortega-Gomez A, Perretti M, Soehnlein O. Resolution of inflammation: an integrated view. *EMBO Mol Med*. 2013;5(5):661-74.
58. Nourshargh S, Alon R. Leukocyte migration into inflamed tissues. *Immunity*. 2014;41(5):694-707.
59. Kadl A, Leitinger N. The role of endothelial cells in the resolution of acute inflammation. *Antioxid Redox Signal*. 2005;7(11-12):1744-54.
60. Buras JA, Holzmann B, Sitkovsky M. Animal models of sepsis: setting the stage. *Nat Rev Drug Discov*. 2005;4(10):854-65.
61. Cross A. Endotoxin: Back to the Future. *Crit Care Med*. 2016;44(2):450-1.
62. Charbonney E, Tsang JY, Li Y, Klein D, Duque P, Romaschin A, et al. Endotoxemia Following Multiple Trauma: Risk Factors and Prognostic Implications. *Crit Care Med*. 2016;44(2):335-41.
63. Okuda S, Sherman DJ, Silhavy TJ, Ruiz N, Kahne D. Lipopolysaccharide transport and assembly at the outer membrane: the PEZ model. *Nat Rev Microbiol*. 2016;14(6):337-45.
64. Zhang H, Niesel DW, Peterson JW, Klimpel GR. Lipoprotein release by bacteria: potential factor in bacterial pathogenesis. *Infect Immun*. 1998;66(11):5196-201.
65. Raetz CR, Whitfield C. Lipopolysaccharide endotoxins. *Annu Rev Biochem*. 2002;71:635-700.
66. Merle NS, Paule R, Leon J, Daugan M, Robe-Rybkin T, Poillierat V, et al. P-selectin drives complement attack on endothelium during intravascular hemolysis in TLR-4/heme-dependent manner. *Proc Natl Acad Sci U S A*. 2019;116(13):6280-5.
67. Mantovani A, Cassatella MA, Costantini C, Jaillon S. Neutrophils in the activation and regulation of innate and adaptive immunity. *Nat Rev Immunol*. 2011;11(8):519-31.
68. Fox S, Leitch AE, Duffin R, Haslett C, Rossi AG. Neutrophil apoptosis: relevance to the innate immune response and inflammatory disease. *J Innate Immun*. 2010;2(3):216-27.
69. Fadok VA, Bratton DL, Konowal A, Freed PW, Westcott JY, Henson PM. Macrophages that have ingested apoptotic cells in vitro inhibit proinflammatory cytokine production through autocrine/paracrine mechanisms involving TGF-beta, PGE2, and PAF. *J Clin Invest*. 1998;101(4):890-8.

70. Michlewska S, Dransfield I, Megson IL, Rossi AG. Macrophage phagocytosis of apoptotic neutrophils is critically regulated by the opposing actions of pro-inflammatory and anti-inflammatory agents: key role for TNF-alpha. *FASEB J*. 2009;23(3):844-54.
71. Giri B, Dey S, Das T, Sarkar M, Banerjee J, Dash SK. Chronic hyperglycemia mediated physiological alteration and metabolic distortion leads to organ dysfunction, infection, cancer progression and other pathophysiological consequences: An update on glucose toxicity. *Biomed Pharmacother*. 2018;107:306-28.
72. Leon BM, Maddox TM. Diabetes and cardiovascular disease: Epidemiology, biological mechanisms, treatment recommendations and future research. *World J Diabetes*. 2015;6(13):1246-58.
73. Alam U, Asghar O, Azmi S, Malik RA. General aspects of diabetes mellitus. *Handb Clin Neurol*. 2014;126:211-22.
74. Patterson C, Guariguata L, Dahlquist G, Soltesz G, Ogle G, Silink M. Diabetes in the young - a global view and worldwide estimates of numbers of children with type 1 diabetes. *Diabetes Res Clin Pract*. 2014;103(2):161-75.
75. Primavera M, Giannini C, Chiarelli F. Prediction and Prevention of Type 1 Diabetes. *Front Endocrinol (Lausanne)*. 2020;11:248.
76. Craig ME, Hattersley A, Donaghue KC. Definition, epidemiology and classification of diabetes in children and adolescents. *Pediatr Diabetes*. 2009;10 Suppl 12:3-12.
77. American Diabetes A. 2. Classification and Diagnosis of Diabetes: Standards of Medical Care in Diabetes-2018. *Diabetes Care*. 2018;41(Suppl 1):S13-S27.
78. Khawandanah J. Double or hybrid diabetes: A systematic review on disease prevalence, characteristics and risk factors. *Nutr Diabetes*. 2019;9(1):33.
79. King AJ. The use of animal models in diabetes research. *Br J Pharmacol*. 2012;166(3):877-94.
80. Lenzen S. The mechanisms of alloxan- and streptozotocin-induced diabetes. *Diabetologia*. 2008;51(2):216-26.
81. Dufrane D, van Steenberghe M, Guiot Y, Goebbels RM, Saliez A, Gianello P. Streptozotocin-induced diabetes in large animals (pigs/primates): role of GLUT2 transporter and beta-cell plasticity. *Transplantation*. 2006;81(1):36-45.
82. Paik SG, Fleischer N, Shin SI. Insulin-dependent diabetes mellitus induced by subdiabetogenic doses of streptozotocin: obligatory role of cell-mediated autoimmune processes. *Proc Natl Acad Sci U S A*. 1980;77(10):6129-33.
83. Wu J, Yan LJ. Streptozotocin-induced type 1 diabetes in rodents as a model for studying mitochondrial mechanisms of diabetic beta cell glucotoxicity. *Diabetes Metab Syndr Obes*. 2015;8:181-8.

84. Cooper ME, Vranes D, Youssef S, Stacker SA, Cox AJ, Rizkalla B, et al. Increased renal expression of vascular endothelial growth factor (VEGF) and its receptor VEGFR-2 in experimental diabetes. *Diabetes*. 1999;48(11):2229-39.
85. Hovind P, Tarnow L, Oestergaard PB, Parving HH. Elevated vascular endothelial growth factor in type 1 diabetic patients with diabetic nephropathy. *Kidney Int Suppl*. 2000;75:S56-61.
86. Gooch JL, Pergola PE, Guler RL, Abboud HE, Barnes JL. Differential expression of calcineurin A isoforms in the diabetic kidney. *J Am Soc Nephrol*. 2004;15(6):1421-9.
87. Kikuchi Y, Ikee R, Hemmi N, Hyodo N, Saigusa T, Namikoshi T, et al. Fractalkine and its receptor, CX3CR1, upregulation in streptozotocin-induced diabetic kidneys. *Nephron Exp Nephrol*. 2004;97(1):e17-25.
88. Hiragushi K, Wada J, Eguchi J, Matsuoka T, Yasuhara A, Hashimoto I, et al. The role of adrenomedullin and receptors in glomerular hyperfiltration in streptozotocin-induced diabetic rats. *Kidney Int*. 2004;65(2):540-50.
89. Collaboration NCDRF. Repositioning of the global epicentre of non-optimal cholesterol. *Nature*. 2020;582(7810):73-7.
90. Mathers CD, Loncar D. Projections of global mortality and burden of disease from 2002 to 2030. *PLoS Med*. 2006;3(11):e442.
91. Serhan CN. Pro-resolving lipid mediators are leads for resolution physiology. *Nature*. 2014;510(7503):92-101.
92. Ross R, Harker L. Hyperlipidemia and atherosclerosis. *Science*. 1976;193(4258):1094-100.
93. Kourtzelis I, Mitroulis I, von Renesse J, Hajishengallis G, Chavakis T. From leukocyte recruitment to resolution of inflammation: the cardinal role of integrins. *J Leukoc Biol*. 2017;102(3):677-83.
94. Charo IF, Taub R. Anti-inflammatory therapeutics for the treatment of atherosclerosis. *Nat Rev Drug Discov*. 2011;10(5):365-76.
95. Tabas I, Glass CK. Anti-inflammatory therapy in chronic disease: challenges and opportunities. *Science*. 2013;339(6116):166-72.
96. Head T, Daunert S, Goldschmidt-Clermont PJ. The Aging Risk and Atherosclerosis: A Fresh Look at Arterial Homeostasis. *Front Genet*. 2017;8:216.
97. Barter PJ, Brewer HB, Jr., Chapman MJ, Hennekens CH, Rader DJ, Tall AR. Cholesteryl ester transfer protein: a novel target for raising HDL and inhibiting atherosclerosis. *Arterioscler Thromb Vasc Biol*. 2003;23(2):160-7.
98. Takahashi S, Fukami T, Masuo Y, Brocker CN, Xie C, Krausz KW, et al. Cyp2c70 is responsible for the species difference in bile acid metabolism between mice and humans. *J Lipid Res*. 2016;57(12):2130-7.

99. Xu Y, Li F, Zalzal M, Xu J, Gonzalez FJ, Adorini L, et al. Farnesoid X receptor activation increases reverse cholesterol transport by modulating bile acid composition and cholesterol absorption in mice. *Hepatology*. 2016;64(4):1072-85.
100. Ishibashi S, Brown MS, Goldstein JL, Gerard RD, Hammer RE, Herz J. Hypercholesterolemia in low density lipoprotein receptor knockout mice and its reversal by adenovirus-mediated gene delivery. *J Clin Invest*. 1993;92(2):883-93.
101. Zhang SH, Reddick RL, Piedrahita JA, Maeda N. Spontaneous hypercholesterolemia and arterial lesions in mice lacking apolipoprotein E. *Science*. 1992;258(5081):468-71.
102. Ishibashi S, Goldstein JL, Brown MS, Herz J, Burns DK. Massive xanthomatosis and atherosclerosis in cholesterol-fed low density lipoprotein receptor-negative mice. *J Clin Invest*. 1994;93(5):1885-93.
103. Bjorklund MM, Hollensen AK, Hagensen MK, Dagnaes-Hansen F, Christoffersen C, Mikkelsen JG, et al. Induction of atherosclerosis in mice and hamsters without germline genetic engineering. *Circ Res*. 2014;114(11):1684-9.
104. Roche-Molina M, Sanz-Rosa D, Cruz FM, Garcia-Prieto J, Lopez S, Abia R, et al. Induction of sustained hypercholesterolemia by single adeno-associated virus-mediated gene transfer of mutant hPCSK9. *Arterioscler Thromb Vasc Biol*. 2015;35(1):50-9.
105. Oppi S, Luscher TF, Stein S. Mouse Models for Atherosclerosis Research-Which Is My Line? *Front Cardiovasc Med*. 2019;6:46.
106. Akram ON, Bernier A, Petrides F, Wong G, Lambert G. Beyond LDL cholesterol, a new role for PCSK9. *Arterioscler Thromb Vasc Biol*. 2010;30(7):1279-81.
107. Denis M, Marcinkiewicz J, Zaid A, Gauthier D, Poirier S, Lazure C, et al. Gene inactivation of proprotein convertase subtilisin/kexin type 9 reduces atherosclerosis in mice. *Circulation*. 2012;125(7):894-901.
108. Li J, Tumanut C, Gavigan JA, Huang WJ, Hampton EN, Tumanut R, et al. Secreted PCSK9 promotes LDL receptor degradation independently of proteolytic activity. *Biochem J*. 2007;406(2):203-7.
109. Mullard A. Cholesterol-lowering blockbuster candidates speed into Phase III trials. *Nat Rev Drug Discov*. 2012;11(11):817-9.
110. Cerrone M, Noorman M, Lin X, Chkourko H, Liang FX, van der Nagel R, et al. Sodium current deficit and arrhythmogenesis in a murine model of plakophilin-2 haploinsufficiency. *Cardiovasc Res*. 2012;95(4):460-8.
111. Kaspar BK, Roth DM, Lai NC, Drumm JD, Erickson DA, McKirnan MD, et al. Myocardial gene transfer and long-term expression following intracoronary delivery of adeno-associated virus. *J Gene Med*. 2005;7(3):316-24.

112. Suhy DA, Kao SC, Mao T, Whiteley L, Denise H, Souberbielle B, et al. Safe, long-term hepatic expression of anti-HCV shRNA in a nonhuman primate model. *Mol Ther*. 2012;20(9):1737-49.
113. Emini Veseli B, Perrotta P, De Meyer GRA, Roth L, Van der Donckt C, Martinet W, et al. Animal models of atherosclerosis. *Eur J Pharmacol*. 2017;816:3-13.
114. Andueza A, Kumar S, Kim J, Kang DW, Mumme HL, Perez JI, et al. Endothelial Reprogramming by Disturbed Flow Revealed by Single-Cell RNA and Chromatin Accessibility Study. *Cell Rep*. 2020;33(11):108491.
115. Bell-Pedersen D, Cassone VM, Earnest DJ, Golden SS, Hardin PE, Thomas TL, et al. Circadian rhythms from multiple oscillators: lessons from diverse organisms. *Nat Rev Genet*. 2005;6(7):544-56.
116. de Mairan JJO. *Observation Botanique. Histoire de l'Academie Royale des Science*. 1729:35-6
117. Menet JS, Rodriguez J, Abruzzi KC, Rosbash M. Nascent-Seq reveals novel features of mouse circadian transcriptional regulation. *Elife*. 2012;1:e00011.
118. Panda S, Antoch MP, Miller BH, Su AI, Schook AB, Straume M, et al. Coordinated transcription of key pathways in the mouse by the circadian clock. *Cell*. 2002;109(3):307-20.
119. Zhang R, Lahens NF, Ballance HI, Hughes ME, Hogenesch JB. A circadian gene expression atlas in mammals: implications for biology and medicine. *Proc Natl Acad Sci U S A*. 2014;111(45):16219-24.
120. Mohawk JA, Takahashi JS. Cell autonomy and synchrony of suprachiasmatic nucleus circadian oscillators. *Trends Neurosci*. 2011;34(7):349-58.
121. Bass J, Takahashi JS. Circadian integration of metabolism and energetics. *Science*. 2010;330(6009):1349-54.
122. Scheiermann C, Kunisaki Y, Lucas D, Chow A, Jang JE, Zhang D, et al. Adrenergic nerves govern circadian leukocyte recruitment to tissues. *Immunity*. 2012;37(2):290-301.
123. Curtis AM, Bellet MM, Sassone-Corsi P, O'Neill LA. Circadian clock proteins and immunity. *Immunity*. 2014;40(2):178-86.
124. Buhr ED, Yoo SH, Takahashi JS. Temperature as a universal resetting cue for mammalian circadian oscillators. *Science*. 2010;330(6002):379-85.
125. Dibner C, Schibler U, Albrecht U. The mammalian circadian timing system: organization and coordination of central and peripheral clocks. *Annu Rev Physiol*. 2010;72:517-49.
126. Dickmeis T. Glucocorticoids and the circadian clock. *J Endocrinol*. 2009;200(1):3-22.

127. Bass J, Lazar MA. Circadian time signatures of fitness and disease. *Science*. 2016;354(6315):994-9.
128. Stokkan KA, Yamazaki S, Tei H, Sakaki Y, Menaker M. Entrainment of the circadian clock in the liver by feeding. *Science*. 2001;291(5503):490-3.
129. Hastings MH, Reddy AB, Maywood ES. A clockwork web: circadian timing in brain and periphery, in health and disease. *Nat Rev Neurosci*. 2003;4(8):649-61.
130. Yan J, Wang H, Liu Y, Shao C. Analysis of gene regulatory networks in the mammalian circadian rhythm. *PLoS Comput Biol*. 2008;4(10):e1000193.
131. Lamia KA, Storch KF, Weitz CJ. Physiological significance of a peripheral tissue circadian clock. *Proc Natl Acad Sci U S A*. 2008;105(39):15172-7.
132. Yoo SH, Yamazaki S, Lowrey PL, Shimomura K, Ko CH, Buhr ED, et al. PERIOD2::LUCIFERASE real-time reporting of circadian dynamics reveals persistent circadian oscillations in mouse peripheral tissues. *Proc Natl Acad Sci U S A*. 2004;101(15):5339-46.
133. Dunlap JC. Molecular bases for circadian clocks. *Cell*. 1999;96(2):271-90.
134. Halberg F, Johnson EA, Brown BW, Bittner JJ. Susceptibility rhythm to *E. coli* endotoxin and bioassay. *Proc Soc Exp Biol Med*. 1960;103:142-4.
135. Shackelford PG, Feigin RD. Periodicity of susceptibility to pneumococcal infection: influence of light and adrenocortical secretions. *Science*. 1973;182(4109):285-7.
136. Haspel JA, Chettimada S, Shaik RS, Chu JH, Raby BA, Cernadas M, et al. Circadian rhythm reprogramming during lung inflammation. *Nat Commun*. 2014;5:4753.
137. Ando N, Nakamura Y, Aoki R, Ishimaru K, Ogawa H, Okumura K, et al. Circadian Gene Clock Regulates Psoriasis-Like Skin Inflammation in Mice. *J Invest Dermatol*. 2015;135(12):3001-8.
138. Castanon-Cervantes O, Wu M, Ehlen JC, Paul K, Gamble KL, Johnson RL, et al. Dysregulation of inflammatory responses by chronic circadian disruption. *J Immunol*. 2010;185(10):5796-805.
139. Li WQ, Qureshi AA, Schernhammer ES, Han J. Rotating night-shift work and risk of psoriasis in US women. *J Invest Dermatol*. 2013;133(2):565-7.
140. Nojkov B, Rubenstein JH, Chey WD, Hoogerwerf WA. The impact of rotating shift work on the prevalence of irritable bowel syndrome in nurses. *Am J Gastroenterol*. 2010;105(4):842-7.
141. Pagel R, Bar F, Schroder T, Sunderhauf A, Kunstner A, Ibrahim SM, et al. Circadian rhythm disruption impairs tissue homeostasis and exacerbates chronic inflammation in the intestine. *FASEB J*. 2017;31(11):4707-19.
142. Takeda N, Maemura K. Circadian clock and the onset of cardiovascular events. *Hypertens Res*. 2016;39(6):383-90.

143. Culic V. Daylight saving time transitions and acute myocardial infarction. *Chronobiol Int.* 2013;30(5):662-8.
144. Durrington HJ, Farrow SN, Loudon AS, Ray DW. The circadian clock and asthma. *Thorax.* 2014;69(1):90-2.
145. Olsen NJ, Brooks RH, Furst D. Variability of immunologic and clinical features in patients with rheumatoid arthritis studied over 24 hours. *J Rheumatol.* 1993;20(6):940-3.
146. Perry MG, Kirwan JR, Jessop DS, Hunt LP. Overnight variations in cortisol, interleukin 6, tumour necrosis factor alpha and other cytokines in people with rheumatoid arthritis. *Ann Rheum Dis.* 2009;68(1):63-8.
147. Casanova-Acebes M, Pitaval C, Weiss LA, Nombela-Arrieta C, Chevre R, N AG, et al. Rhythmic modulation of the hematopoietic niche through neutrophil clearance. *Cell.* 2013;153(5):1025-35.
148. Keller M, Mazuch J, Abraham U, Eom GD, Herzog ED, Volk HD, et al. A circadian clock in macrophages controls inflammatory immune responses. *Proc Natl Acad Sci U S A.* 2009;106(50):21407-12.
149. Nguyen KD, Fentress SJ, Qiu Y, Yun K, Cox JS, Chawla A. Circadian gene *Bmal1* regulates diurnal oscillations of Ly6C(hi) inflammatory monocytes. *Science.* 2013;341(6153):1483-8.
150. Silver AC, Arjona A, Walker WE, Fikrig E. The circadian clock controls toll-like receptor 9-mediated innate and adaptive immunity. *Immunity.* 2012;36(2):251-61.
151. Druzd D, Matveeva O, Ince L, Harrison U, He W, Schmal C, et al. Lymphocyte Circadian Clocks Control Lymph Node Trafficking and Adaptive Immune Responses. *Immunity.* 2017;46(1):120-32.
152. Dallmann R, Brown SA, Gachon F. Chronopharmacology: new insights and therapeutic implications. *Annu Rev Pharmacol Toxicol.* 2014;54:339-61.
153. Picelli S, Faridani OR, Bjorklund AK, Winberg G, Sagasser S, Sandberg R. Full-length RNA-seq from single cells using Smart-seq2. *Nat Protoc.* 2014;9(1):171-81.
154. Dobin A, Davis CA, Schlesinger F, Drenkow J, Zaleski C, Jha S, et al. STAR: ultrafast universal RNA-seq aligner. *Bioinformatics.* 2013;29(1):15-21.
155. Butler A, Hoffman P, Smibert P, Papalexi E, Satija R. Integrating single-cell transcriptomic data across different conditions, technologies, and species. *Nat Biotechnol.* 2018;36(5):411-20.
156. Mishra AP, Yedella K, Lakshmi JB, Siva AB. *Wdr13* and streptozotocin-induced diabetes. *Nutr Diabetes.* 2018;8(1):57.

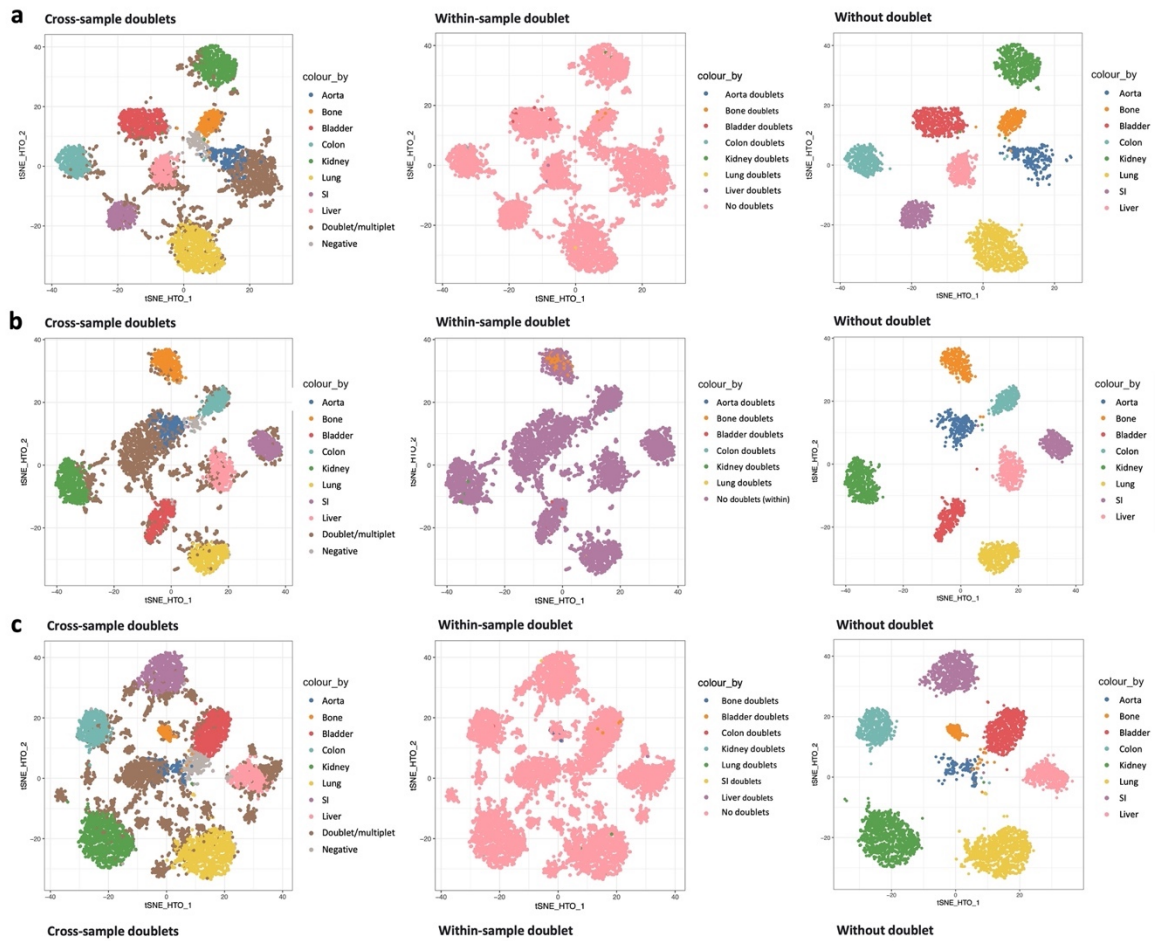
157. Lagace TA, Curtis DE, Garuti R, McNutt MC, Park SW, Prather HB, et al. Secreted PCSK9 decreases the number of LDL receptors in hepatocytes and in livers of parabiotic mice. *J Clin Invest*. 2006;116(11):2995-3005.
158. Amezquita RA, Lun ATL, Becht E, Carey VJ, Carpp LN, Geistlinger L, et al. Orchestrating single-cell analysis with Bioconductor. *Nat Methods*. 2020;17(2):137-45.
159. McCarthy DJ, Campbell KR, Lun AT, Wills QF. Scater: pre-processing, quality control, normalization and visualization of single-cell RNA-seq data in R. *Bioinformatics*. 2017;33(8):1179-86.
160. Kim HJ, Lin Y, Geddes TA, Yang JYH, Yang P. CiteFuse enables multi-modal analysis of CITE-seq data. *Bioinformatics*. 2020;36(14):4137-43.
161. Lun AT, McCarthy DJ, Marioni JC. A step-by-step workflow for low-level analysis of single-cell RNA-seq data with Bioconductor. *F1000Res*. 2016;5:2122.
162. Chen Y, Lun AT, Smyth GK. From reads to genes to pathways: differential expression analysis of RNA-Seq experiments using Rsubread and the edgeR quasi-likelihood pipeline. *F1000Res*. 2016;5:1438.
163. Robinson MD, McCarthy DJ, Smyth GK. edgeR: a Bioconductor package for differential expression analysis of digital gene expression data. *Bioinformatics*. 2010;26(1):139-40.
164. Blighe KR, S.; Lewis, M. EnhancedVolcano: Publication-ready volcano plots with enhanced colouring and labeling. R package version 1.12.0. 2021.
165. Jain V, Bordes S, Bhardwaj A. Physiology, Pulmonary Circulatory System. *StatPearls*. Treasure Island (FL)2021.
166. Dalla Vecchia E, Mortimer N, Palladino VS, Kittel-Schneider S, Lesch KP, Reif A, et al. Cross-species models of attention-deficit/hyperactivity disorder and autism spectrum disorder: lessons from CNTNAP2, ADGRL3, and PARK2. *Psychiatr Genet*. 2019;29(1):1-17.
167. Jackson VA, del Toro D, Carrasquero M, Roversi P, Harlos K, Klein R, et al. Structural basis of latrophilin-FLRT interaction. *Structure*. 2015;23(4):774-81.
168. O'Sullivan ML, Martini F, von Daake S, Comoletti D, Ghosh A. LPHN3, a presynaptic adhesion-GPCR implicated in ADHD, regulates the strength of neocortical layer 2/3 synaptic input to layer 5. *Neural Dev*. 2014;9:7.
169. Kang SS, Ebbert MTW, Baker KE, Cook C, Wang X, Sens JP, et al. Microglial translational profiling reveals a convergent APOE pathway from aging, amyloid, and tau. *J Exp Med*. 2018;215(9):2235-45.
170. Hicks SC, Townes FW, Teng M, Irizarry RA. Missing data and technical variability in single-cell RNA-sequencing experiments. *Biostatistics*. 2018;19(4):562-78.

171. Kronman H, Richter F, Labonte B, Chandra R, Zhao S, Hoffman G, et al. Biology and Bias in Cell Type-Specific RNAseq of Nucleus Accumbens Medium Spiny Neurons. *Sci Rep.* 2019;9(1):8350.
172. Sanz E, Bean JC, Carey DP, Quintana A, McKnight GS. RiboTag: Ribosomal Tagging Strategy to Analyze Cell-Type-Specific mRNA Expression In Vivo. *Curr Protoc Neurosci.* 2019;88(1):e77.
173. Kaur H, Carvalho J, Looso M, Singh P, Chennupati R, Preussner J, et al. Single-cell profiling reveals heterogeneity and functional patterning of GPCR expression in the vascular system. *Nat Commun.* 2017;8:15700.
174. Potente M, Makinen T. Vascular heterogeneity and specialization in development and disease. *Nat Rev Mol Cell Biol.* 2017;18(8):477-94.
175. Amaya R, Pierides A, Tarbell JM. The Interaction between Fluid Wall Shear Stress and Solid Circumferential Strain Affects Endothelial Gene Expression. *PLoS One.* 2015;10(7):e0129952.
176. Wu W, Xiao H, Laguna-Fernandez A, Villarreal G, Jr., Wang KC, Geary GG, et al. Flow-Dependent Regulation of Kruppel-Like Factor 2 Is Mediated by MicroRNA-92a. *Circulation.* 2011;124(5):633-41.
177. Durr E, Yu J, Krasinska KM, Carver LA, Yates JR, Testa JE, et al. Direct proteomic mapping of the lung microvascular endothelial cell surface in vivo and in cell culture. *Nat Biotechnol.* 2004;22(8):985-92.
178. Lacorre DA, Baekkevold ES, Garrido I, Brandtzaeg P, Haraldsen G, Amalric F, et al. Plasticity of endothelial cells: rapid dedifferentiation of freshly isolated high endothelial venule endothelial cells outside the lymphoid tissue microenvironment. *Blood.* 2004;103(11):4164-72.
179. Sun L, Wang R, Hu G, Liu H, Lv K, Duan Y, et al. Single cell RNA sequencing (scRNA-Seq) deciphering pathological alterations in streptozotocin-induced diabetic retinas. *Exp Eye Res.* 2021;210:108718.
180. Jonsson A, Hedin A, Muller M, Skog O, Korsgren O. Transcriptional profiles of human islet and exocrine endothelial cells in subjects with or without impaired glucose metabolism. *Sci Rep.* 2020;10(1):22315.
181. Wilson PC, Wu H, Kirita Y, Uchimura K, Ledru N, Rennke HG, et al. The single-cell transcriptomic landscape of early human diabetic nephropathy. *Proc Natl Acad Sci U S A.* 2019;116(39):19619-25.
182. Beckman JA, Doherty SP, Feldman ZB, Banks ES, Moslehi J, Jaffe IZ, et al. Comparative Transcriptomics of Ex Vivo, Patient-Derived Endothelial Cells Reveals Novel Pathways Associated With Type 2 Diabetes Mellitus. *JACC Basic Transl Sci.* 2019;4(5):567-74.

183. Bell RC, Khurana M, Ryan EA, Finegood DT. Gender differences in the metabolic response to graded numbers of transplanted islets of Langerhans. *Endocrinology*. 1994;135(6):2681-7.
184. Le May C, Chu K, Hu M, Ortega CS, Simpson ER, Korach KS, et al. Estrogens protect pancreatic beta-cells from apoptosis and prevent insulin-deficient diabetes mellitus in mice. *Proc Natl Acad Sci U S A*. 2006;103(24):9232-7.
185. Leiter EH. Multiple low-dose streptozotocin-induced hyperglycemia and insulinitis in C57BL mice: influence of inbred background, sex, and thymus. *Proc Natl Acad Sci U S A*. 1982;79(2):630-4.
186. Deeds MC, Anderson JM, Armstrong AS, Gastineau DA, Hiddinga HJ, Jahangir A, et al. Single dose streptozotocin-induced diabetes: considerations for study design in islet transplantation models. *Lab Anim*. 2011;45(3):131-40.
187. Rossini AA, Williams RM, Appel MC, Like AA. Sex differences in the multiple-dose streptozotocin model of diabetes. *Endocrinology*. 1978;103(4):1518-20.
188. Saadane A, Lessieur EM, Du Y, Liu H, Kern TS. Successful induction of diabetes in mice demonstrates no gender difference in development of early diabetic retinopathy. *PLoS One*. 2020;15(9):e0238727.
189. Aronson D, Rayfield EJ. How hyperglycemia promotes atherosclerosis: molecular mechanisms. *Cardiovasc Diabetol*. 2002;1:1.
190. Calkin AC, Allen TJ. Diabetes mellitus-associated atherosclerosis: mechanisms involved and potential for pharmacological invention. *Am J Cardiovasc Drugs*. 2006;6(1):15-40.
191. Funk SD, Yurdagul A, Jr., Orr AW. Hyperglycemia and endothelial dysfunction in atherosclerosis: lessons from type 1 diabetes. *Int J Vasc Med*. 2012;2012:569654.
192. Hansson GK. Inflammation, atherosclerosis, and coronary artery disease. *N Engl J Med*. 2005;352(16):1685-95.
193. Zhao G, Lu H, Liu Y, Zhao Y, Zhu T, Garcia-Barrio MT, et al. Single-Cell Transcriptomics Reveals Endothelial Plasticity During Diabetic Atherogenesis. *Front Cell Dev Biol*. 2021;9:689469.
194. Depuydt MAC, Prange KHM, Slenders L, Ord T, Elbersen D, Boltjes A, et al. Microanatomy of the Human Atherosclerotic Plaque by Single-Cell Transcriptomics. *Circ Res*. 2020;127(11):1437-55.
195. Gu W, Ni Z, Tan YQ, Deng J, Zhang SJ, Lv ZC, et al. Adventitial Cell Atlas of wt (Wild Type) and ApoE (Apolipoprotein E)-Deficient Mice Defined by Single-Cell RNA Sequencing. *Arterioscler Thromb Vasc Biol*. 2019;39(6):1055-71.

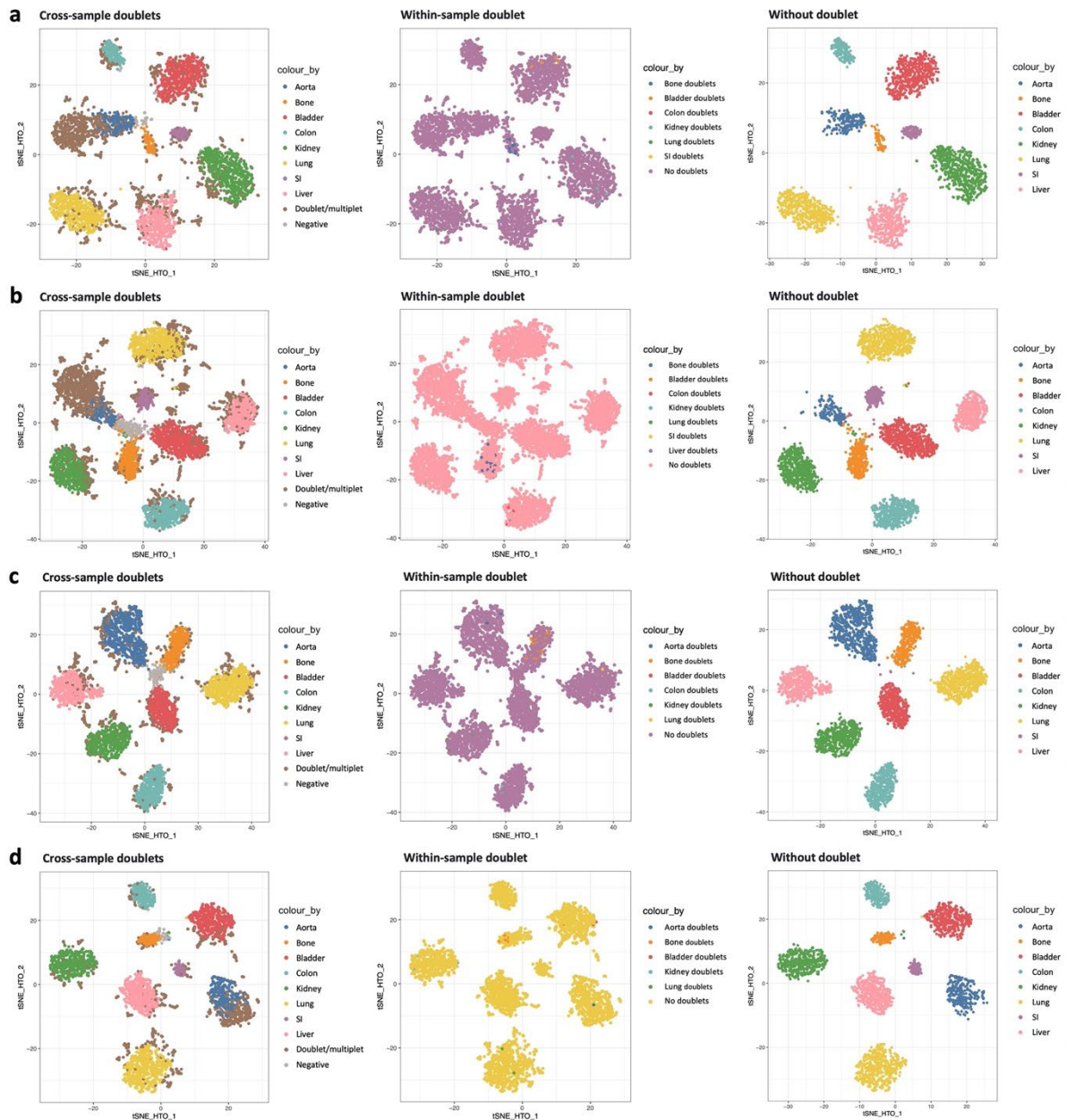
196. Kan H, Zhang K, Mao A, Geng L, Gao M, Feng L, et al. Single-cell transcriptome analysis reveals cellular heterogeneity in the ascending aortas of normal and high-fat diet-fed mice. *Exp Mol Med*. 2021;53(9):1379-89.
197. Endemann G, Stanton LW, Madden KS, Bryant CM, White RT, Protter AA. CD36 is a receptor for oxidized low density lipoprotein. *J Biol Chem*. 1993;268(16):11811-6.
198. Li F, Yan K, Wu L, Zheng Z, Du Y, Liu Z, et al. Single-cell RNA-seq reveals cellular heterogeneity of mouse carotid artery under disturbed flow. *Cell Death Discov*. 2021;7(1):180.
199. Min JK, Park H, Choi HJ, Kim Y, Pyun BJ, Agrawal V, et al. The WNT antagonist Dickkopf2 promotes angiogenesis in rodent and human endothelial cells. *J Clin Invest*. 2011;121(5):1882-93.
200. Holtkamp SJ, Ince LM, Barnoud C, Schmitt MT, Sinturel F, Pilonz V, et al. Circadian clocks guide dendritic cells into skin lymphatics. *Nat Immunol*. 2021;22(11):1375-81.

Supplement



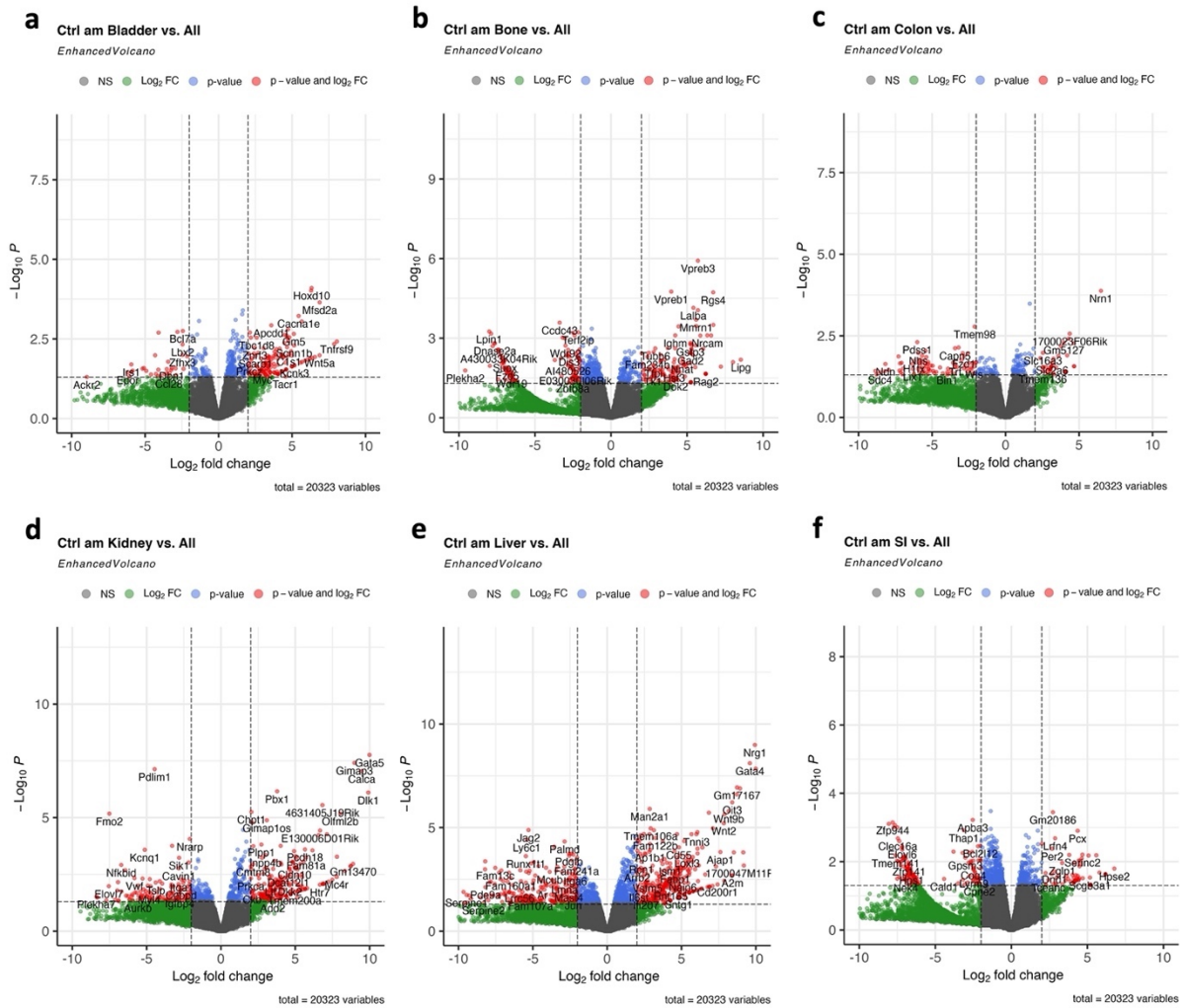
Supplementary Figure 1. Doublet detection of endothelial cells of homeostatic mice and mice experiencing acute inflammation.

Dimension reduction on Feature Barcoding count by using t-SNE. Portraying cross-sample doublets, within-sample doublet, doublet free dataset, and number of cells per treatment/timepoint of mice in homeostasis **(a)** Ctrl pm, after exposure to an acute inflammatory stimulus **(b)** LPS am, and **(c)** LPS pm. Endothelial cells, DAPI – 4',6-Diamidino-2-phenylindol, SI – Small intestine, tSNE – t-distributed stochastic neighbour embedding, VE-Cad – VE-Cadherin.



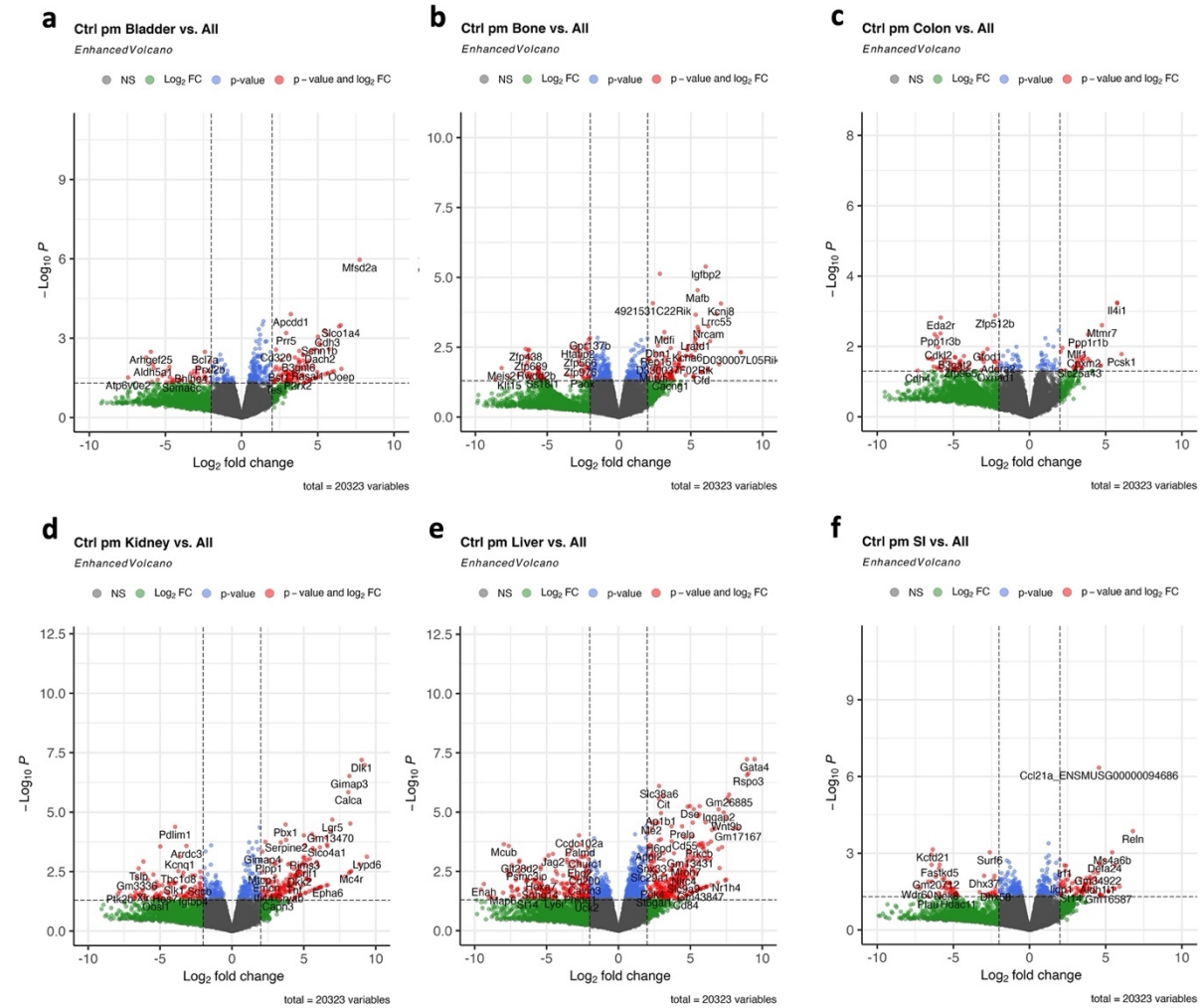
Supplementary Figure 2. Doublet detection of endothelial cells mice experiencing chronic inflammation.

Dimension reduction on Feature Barcoding count by using t-SNE. Portraying cross-sample doublets, within-sample doublet, doublet free dataset, and number of cells per treatment/timepoint of mice exposed to hyperglycemia **(a)** STZ am, and **(b)** STZ pm, or hyperlipidemia **(c)** AAV am, **(d)** AAV pm. AAV – Adeno Associated Virus, Endothelial cells, DAPI – 4',6-Diamidino-2-phenylindol, t-SNE – t-distributed stochastic neighbour embedding, SI – Small intestine, STZ – Streptozotocin, VE-Cad – VE-Cadherin.



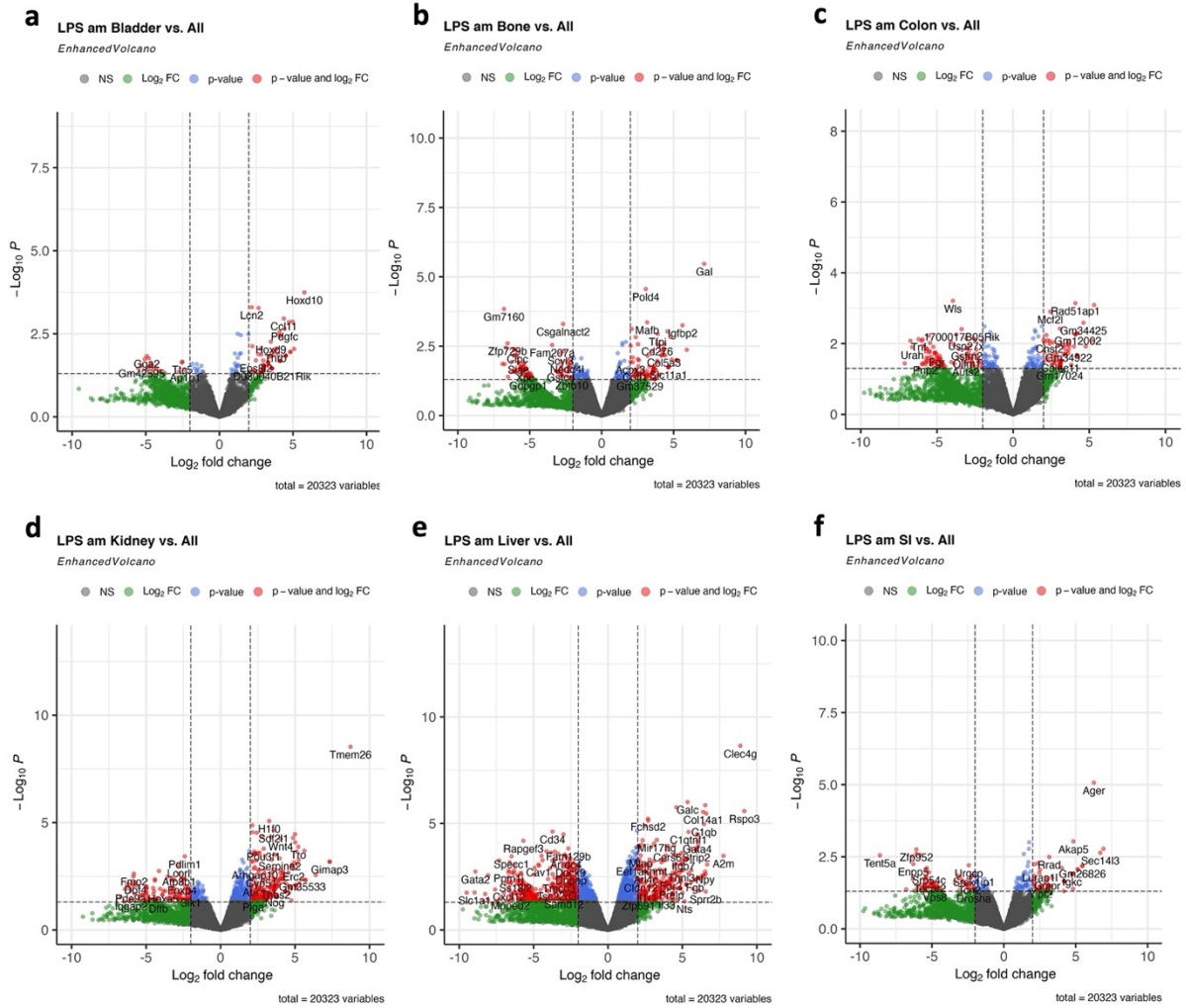
Supplementary Figure 3. Differentially expressed genes of mice in homeostasis sacrificed in the morning.

Volcano plots representing the DE genes of the (a) bladder, (b) bladder, (c) colon, (d) kidney, (e) SI (Ileum), and (f) liver from mice sacrificed when in homeostasis (Ctrl). Organ collection took place in the morning (am). Gene colors: grey – p-value NS and log₂FC > -2 or < 2, green - log₂FC < -2 or > 2, blue - p-value < 0.05, red - p-value < 0.05 and log₂FC < -2 or > 2. FC – Fold Change, LPS – Lipopolysaccharides, NS – Not Significant, SI – Small Intestine (ileum), vs. – versus.



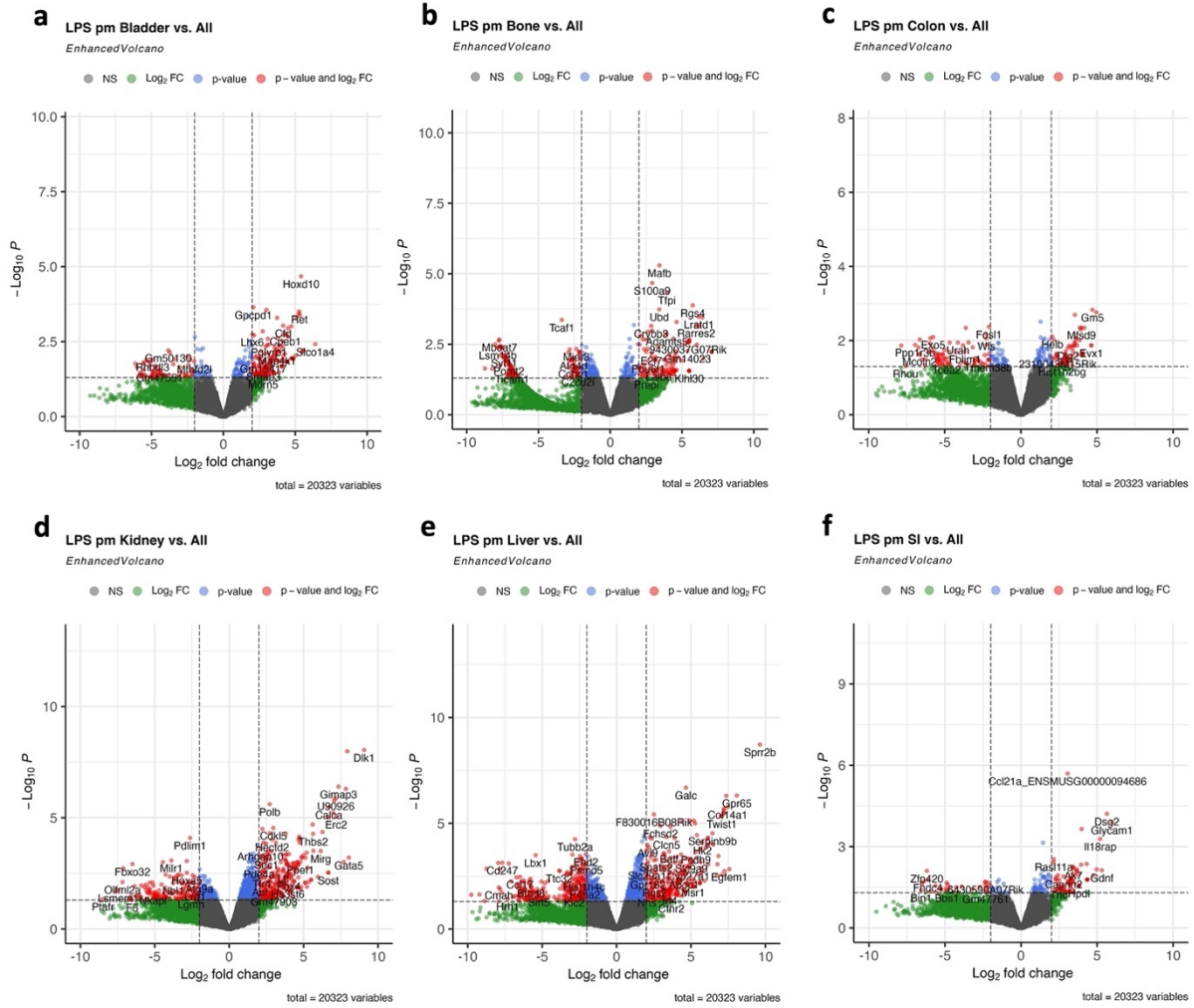
Supplementary Figure 4. Differentially expressed genes of mice in homeostasis, organs were harvested in the evening.

Volcano plots representing the DE genes of the (a) bladder, (b) bladder, (c) colon, (d) kidney, (e) SI (Ileum), and (f) liver from mice sacrificed when in homeostasis (Ctrl). Tissues were collected in the evening (pm). Gene colors: grey – p-value NS and log₂FC > -2 or < 2, green - log₂FC < -2 or > 2, blue - p-value < 0.05, red - p-value < 0.05 and log₂FC < -2 or > 2. FC – Fold Change, LPS – Lipopolysaccharides, NS – Not Significant, SI – Small Intestine (ileum), vs. – versus.



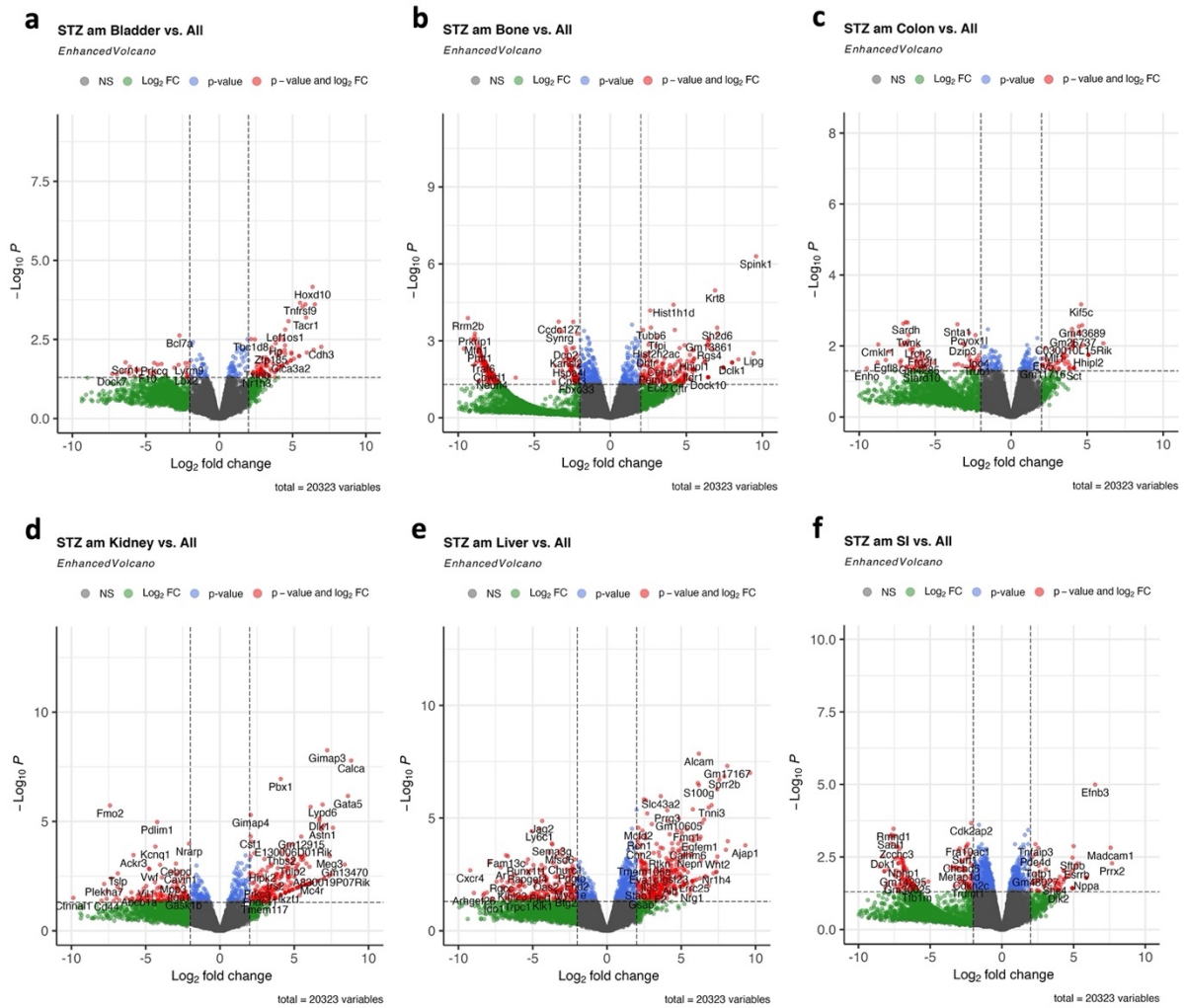
Supplementary Figure 5. Differentially expressed genes of mice exposed to an acute inflammatory stimulus sacrificed in the morning.

Volcano plots representing the DE genes of the (a) bladder, (b) bladder, (c) colon, (d) kidney, (e) SI (Ileum), and (f) liver from mice sacrificed when subjected to acute inflammatory stimulus (LPS). Organ collection took place in the morning (am). Gene colors: grey – p-value NS and log₂FC > -2 or < 2, green - log₂FC < -2 or > 2, blue - p-value < 0.05, red - p-value < 0.05 and log₂FC < -2 or > 2. AAV - Adeno Associated Virus, FC – Fold Change, NS – Not Significant, SI – Small Intestine (ileum), vs. – versus.



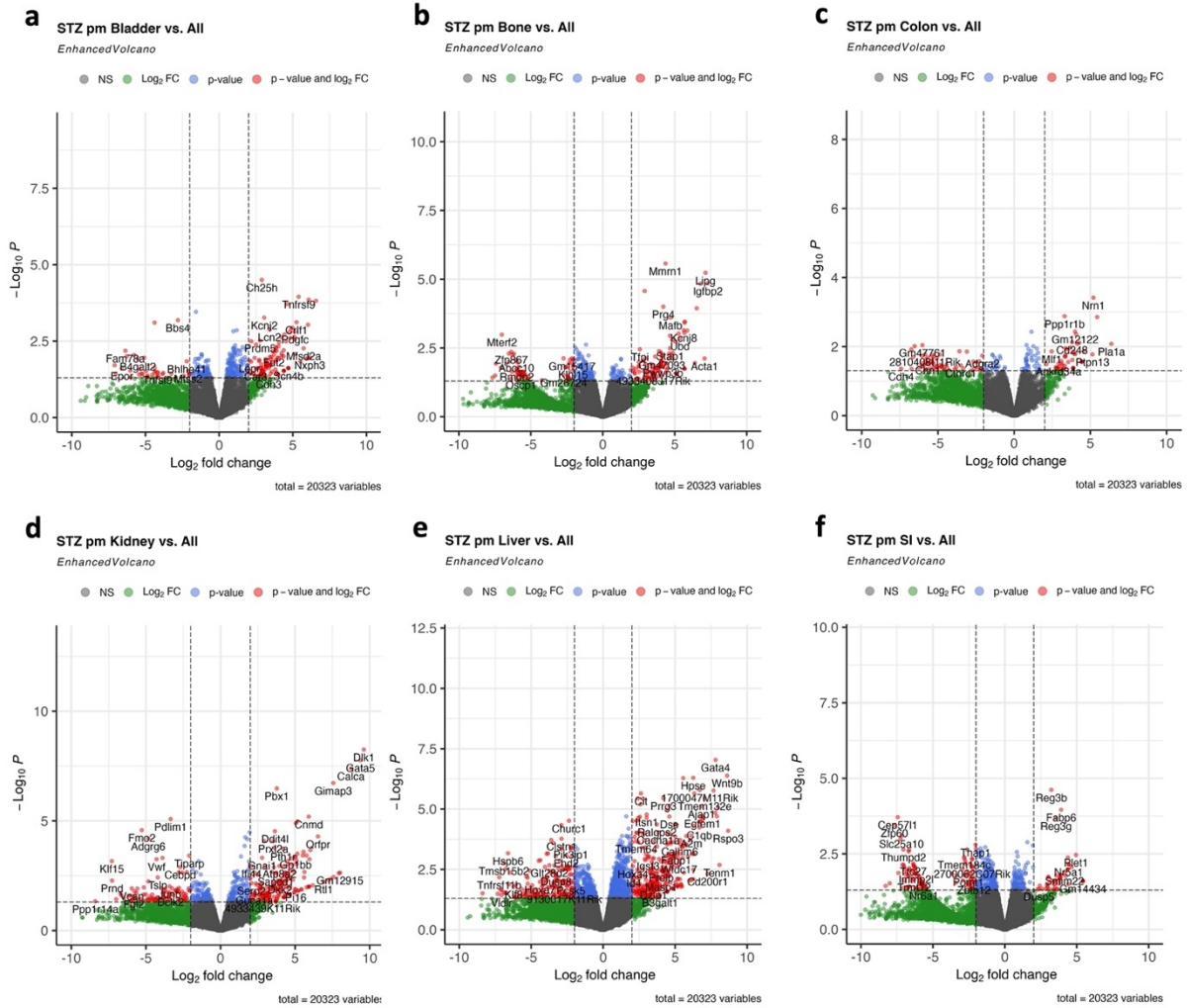
Supplementary Figure 6. Differentially expressed genes of mice exposed to an acute inflammatory stimulus, organs were collected in the evening.

Volcano plots representing the DE genes of the (a) bladder, (b) bladder, (c) colon, (d) kidney, (e) SI (Ileum), and (f) liver from mice sacrificed when subjected to acute inflammatory stimulus (LPS). Organs were collected in the evening (pm). Gene colors: grey – p-value NS and log₂FC > -2 or < 2, green - log₂FC < -2 or > 2, blue - p-value < 0.05, red - p-value < 0.05 and log₂FC < -2 or > 2. AAV - Adeno Associated Virus, FC – Fold Change, NS – Not Significant, SI – Small Intestine (ileum), vs. – versus.



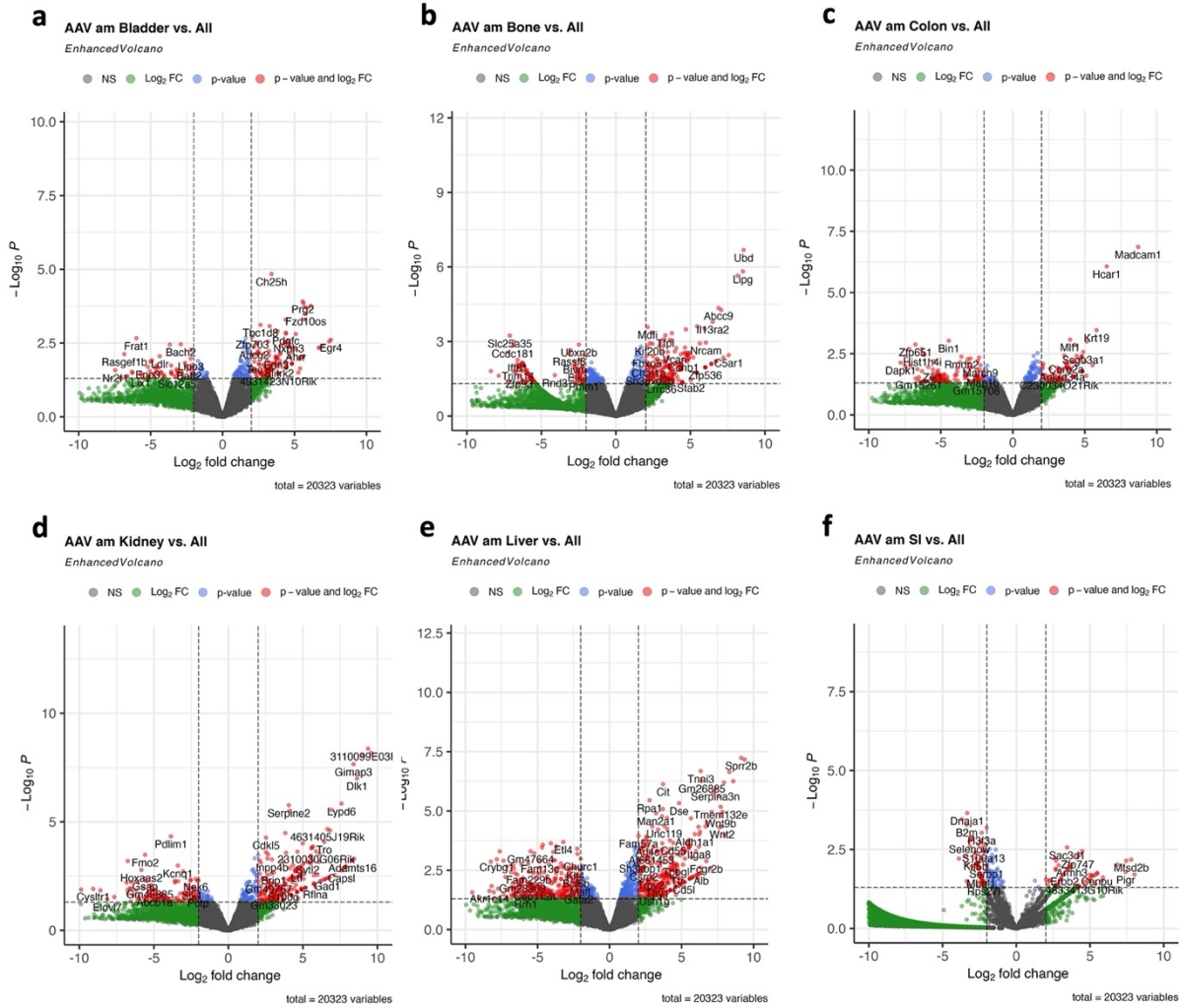
Supplementary Figure 7. Differentially expressed genes of mice exposed to hyperglycemia sacrificed in the morning.

Volcano plots representing the DE genes of the (a) bladder, (b) bladder, (c) colon, (d) kidney, (e) SI (Ileum), and (f) liver from mice sacrificed while subjected to hyperglycemia in a chronic inflammatory model. Tissue collection took place in the morning (am). Gene colors: grey – p-value NS and log₂FC > -2 or < 2, green - log₂FC < -2 or > 2, blue - p-value < 0.05, red - p-value < 0.05 and log₂FC < -2 or > 2. FC – Fold Change, NS – Not Significant, STZ – Streptozotocin, SI – Small Intestine (ileum), vs. – versus.



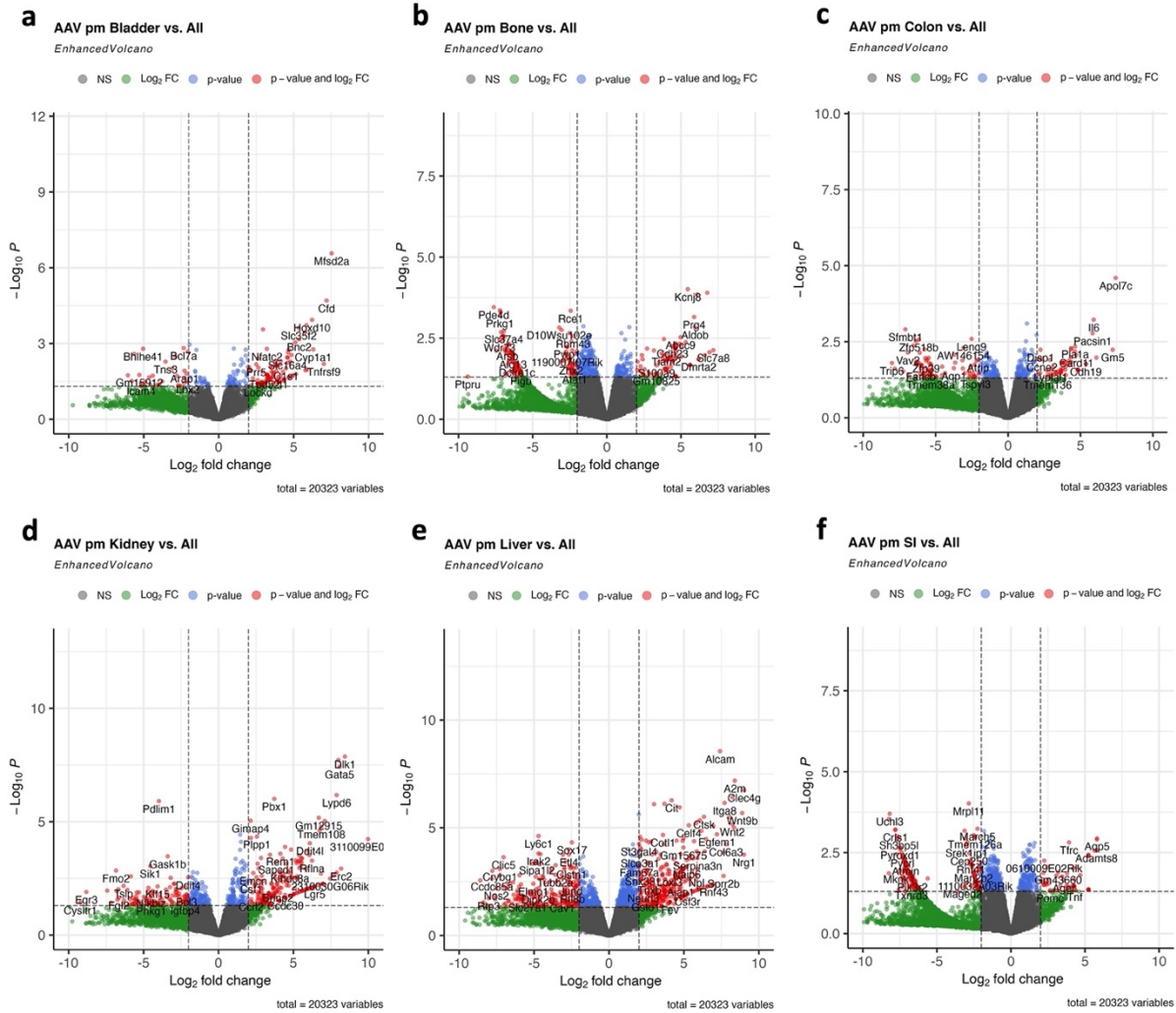
Supplementary Figure 8. Differentially expressed genes of mice exposed to hyperglycemia sacrificed in the evening.

Volcano plots representing the DE genes of the **a**) bladder, **b**) bladder, **c**) colon, **d**) kidney, **e**) SI (Ileum), and **f**) liver from mice sacrificed while subjected to hyperglycemia in a chronic inflammatory model. Organs were collected in the evening (pm). Gene colors: grey – p-value NS and log₂FC > -2 or < 2, green - log₂FC < -2 or > 2, blue - p-value < 0.05, red - p-value < 0.05 and log₂FC < -2 or > 2. FC – Fold Change, NS – Not Significant, STZ – Streptozotocin, SI – Small Intestine (ileum), vs. – versus.



Supplementary Figure 9. Differentially expressed genes of mice exposed to hyperlipidemia sacrificed in the morning.

Volcano plots representing the DE genes of the (a) bladder, (b) bladder, (c) colon, (d) kidney, (e) SI (Ileum), and (f) liver from mice sacrificed while exposed to hyperlipidemia in a chronic inflammatory model (AAV). Tissue collection took place in the morning (am). Gene colors: grey – p-value NS and log₂FC > -2 or < 2, green - log₂FC < -2 or > 2, blue - p-value < 0.05, red - p-value < 0.05 and log₂FC < -2 or > 2. Ctrl – Control, FC – Fold Change, NS – Not Significant, SI – Small Intestine (ileum), vs. – versus.



Supplementary Figure 10. Differentially expressed genes of mice exposed to hyperlipidemia, organs were collected in the evening.

Volcano plots representing the DE genes of the (a) bladder, (b) bladder, (c) colon, (d) kidney, (e) SI (Ileum), and (f) liver from mice sacrificed while exposed to hyperlipidemia in a chronic inflammatory model (AAV). Organs were collected in the evening (pm). Gene colors: grey – p-value NS and log₂FC > -2 or < 2, green - log₂FC < -2 or > 2, blue - p-value < 0.05, red - p-value < 0.05 and log₂FC < -2 or > 2. Ctrl – Control, FC – Fold Change, NS – Not Significant, SI – Small Intestine (ileum), vs. – versus.

Supplementary Table 1. Organ-specific genes and organ-specific genes encoding for surface proteins.

Organ	Specific gene transcripts				Specific gene transcripts encoding for surface protein			
Aorta	Timp4				Fabp4	C1qtnf9		
	Mgl1				Aqp7	Meox2		
Brain	5430407P10 Rik	Ddc	Isyna1	Pglyrp1	Aqp11	Prnp	Slc38a5	Tsc22d3
	9430020K01 Rik	Degs2	Itih5	Prom1	Cxcl12	Sgms1	Slc39a10	Ttyh2
	A930038C07 Rik	Edn3	Itm2a	Ptn	Elovl7	Slc16a1	Slc7a1	
	Abcb1a	Efr3b	Lef1	Sorbs2	Fn1	Slc16a4	Slc7a5	
	Ablim1	Fam63a	Lsr	Spock2	Foxq1	Slc1a1	Slco1a4	
	Apcdd1	Foxf2	Maoa	Tsc22d1	Glul	Slc19a3	Slco1c1	
	Apod	Gpcpd1	Net1	Tspan5	Igf1r	Slc2a1	Slco2b1	
	Apold1	Gpd2	Ocln	Vwa1	Lrp8	Slc22a8	Smox	
	Arl4a	Gsta4	Osbpl1a	Wfdc1	Mal	Slc30a1	Stra6	
	Bsg	Gstm7	Paqr5		Mfsd2a	Slc35f2	Tfrc	
	Ccdc141	Hmgcs2	Pcp4l1		Ndr1	Slc38a3	Tpd52	
Kidney	Plscr2				Rsad2	Socs3		
					Egr1			
Liver	Aass	Degs1	Hmha1	Serpina3f	Alb	F8	Jak1	Ptprb
	Akr1b8	Dnase1l3	Itga9	Serpina3g	Apoa1	Fcgr2b	Lamp2	Renbp
	Ap1b1	Fam124a	Man2b1	Serpina3k	Apoe	Gata4	Lgmn	Snx2
	Arhgdib	Fam167b	Mup20	Slc43a2	Calr	Gc	Lifr	Snx5
	Bace2	Fam174b	Mup3	Slc9a9	Cd55	Gpr182	Maf	Stab1
	Bhmt	Fga	Nqo2	Tmem106a	Clec1b	Hdc	Man2a1	Stab2
	Bmp2	Fgb	Oit3	Wnt2	Clec4g	Hp	Mertk	Tfpi
	C1qtnf1	Fgg	Ralgapa2		Ctsl	Hpx	Mrc1	Trf
	Ccdc80	Gm14023	Sepp1		Cxcl16	Igfbp7	Msr1	
	Cd302	Gm4980	Serpina1c		Dab2	Il1a	Myo7a	
	Darc	Gpr97	Serpina1e		Dpp4	Il6st	Plxnc1	
Lung	1110050K14 Rik	Dpysl2	Hpgd	Pde9a	Ace	Eccscr	Slco2a1	
	Abi3bp	Fmo1	Hs3st1	Phlda3	Acvr1	Emp2	Stmn2	
	Atp2a3	Foxf1a	Mfap2	Prss23	Adrb1	Icam2	Thbd	
	BC028528	Grtp1	Mmrn1	Prx	Adrb2	Lyve1	Timp2	
	Cd97	H2-Aa	Myzap	Rasgef1a	Calcr1	Nsg1	Tmem100	
	Cebpd	H2-Eb1	Nhlrc2	Serpib1a	Cd9	Ramp2	Vwf	
	Clec1a	Hilpda	Pde4b	Tmem221	Cd93	Scn7a		

Supplementary Table 2. Top 10 upregulated and organ-specific genes of endothelial cells isolated from the aorta and lung from mice in homeostasis.

The aorta and lung (a) upregulated genes and (b) organ specific genes genes when comparing the organs from the homeostatic condition to each other. Log2FC > 0, p-value < 0.05. Ctrl – Control, FC – Fold Change.

a		b	
Upregulated		Organ specific	
Aorta Ctrl	Lung Ctrl	Aorta Ctrl	Lung Ctrl
Klk10	Tmem100	Ephx2	Pard6g
Sfrp1	Foxf1	1500015O10Rik	Scn7a
Cyt11	BC028528	Efna5	Inmt
Cdh13	Aard	Scn1b	Tox3
Gkn3	Gpihbp1	Pdlim4	Scgb3a1
Adh1	Mfap2	Isl1	Grp
Cpe	Car4	Arhgap44	Tmeff2
Rbp1	C920021L13Rik	Mall	Zfp641
Htra1	Glp1r	Ccdc3	Nkd2
Ephx2	Lyve1	Plek2	Sftpa1

Supplementary Table 3. Aorta and lung top 10 upregulated and organ-specific genes of endothelial cells isolated from mice exposed to acute inflammation.

The aorta and lung **(a)** upregulated genes and **(b)** organ specific genes when comparing the organs from the acute inflammatory condition to each other. Log2FC > 0, p-value < 0.05. FC – Fold Change, LPS – lipopolysaccharides.

a		b	
Upregulated		Organ specific	
Aorta LPS	Lung LPS	Aorta LPS	Lung LPS
Acta2	Lyve1	Nppa	Fendrr
Cyt11	Fendrr	Gm13054	Cldn18
Cdh13	Ifi213	Tnnt2	Krt7
Nppa	Car2	Sln	S1pr3
Cpe	Adrb2	Serpinf1	Disp2
Sfrp1	Foxf1	Car3	Gm10584
Gm13054	Scgb1a1	Cnn1	Ciita
Pgf	Agpat4	Mb	Dzip3
Ccdc80	Ackr2	Ephx2	Fcgr3
Fabp4	Ifi206	Ccdc3	Tnfrsf11b

Supplementary Table 4. Top 10 upregulated and organ-specific genes of endothelial cells of the homeostatic condition.

The aorta and lung **(a)** upregulated genes and **(b)** organ specific genes representing the homeostatic condition. Log₂FC > 0, p-value < 0.05. FC – Fold Change, LPS – lipopolysaccharides, vs – versus.

a		Upregulated		b		Organ specific	
		Aorta Ctrl vs LPS	Lung Ctrl vs LPS			Aorta Ctrl vs LPS	Lung Ctrl vs LPS
		Pkn3	Hey1			Cldn15	Zfyve21
		Sox18	Sox18			Scx	Coro2b
		Cldn15	Plp			Plekha6	Fdps
		G0s2	Kank3			Pcyox1l	Gpr180
		Adamts10	Tmem223			Kcne3	Aqp11
		Eln	Myzap			Gucy1a1	Sugct
		Chst12	Ypel3			Lefty1	Dbnnd2
		Vamp5	Gm45767			Map3k4	Zfand2b
		Abhd17a	Cavin2			Aldh1a2	Ccdc91
		Nfic	Cbx1			Ankrd29	Fbxo31

Supplementary Table 5. Top 10 upregulated and organ-specific genes of endothelial cells isolated from mice exposed to acute inflammation.

The aorta and lung **(a)** upregulated genes and **(b)** organ specific genes representing the acute inflammatory condition. Log2FC > 0, p-value < 0.05. FC – Fold Change, LPS – lipopolysaccharides, vs – versus.

a		b	
Upregulated		Organ specific	
Aorta LPS vs Ctrl	Lung LPS vs Ctrl	Aorta LPS vs Ctrl	Lung LPS vs Ctrl
Il6	Sphk1	Cxcl9	Cxcl9
Slc1a1	Mx1	Cxcl2	Rasd1
Tnfrsf9	Ifi211	Pgf	Cxcl10
Car13	Lbx1	Cxcl10	Mt2
Sh2d5	Noct	Rsad2	Gm45774
Steap4	Prr7	Akap12	Mt1
Apod	Car13	Lcn2	Lcn2
Ubd	Stx11	Sphk1	Saa3
Spry1	37681	Ccl2	Cxcl2
Lum	Fosl1	Lpl	AA467197

Supplementary Table 6. Top-10 DE genes in homeostatic condition.

Organ were harvested in the morning (am) or evening (pm). Log2FC > 2, p-value < 0.05. Ctrl – Control, DE – Differentially expressed.

DE genes Ctrl am							
Aorta	Bladder	Bone	Colon	Kidney	Ileum	Liver	Lung
Klk10	Hoxd10	Vpreb3	Nrn1	Gm20186	Gata5	Nrg1	Aard
Sfrp1	Pdgfc	Vpreb1	Socs5	Dnajb1	Gimap3	Gata4	Slc6a2
Ecr4	Mfsd2a	Rgs4	1700023F06Rik	Pcx	Calca	Sprr2b	Nhlrc2
Eln	Marc2	Lalba	Ifnlr1	Crybg3	Pbx1	Gm17167	Car14
Parm1	Stt3b	Igfbp2	Gm5127	Lyst	Dlk1	Tfec	Ntrk2
Kcnt2	Cacna1e	Mmrn1	Mtmr7	Lrfn4	4631405J19Rik	Tmem132e	Fibin
Col1a2	Abca3	Kcnj8	Rnf181	Taf1c	Chpt1	Oit3	Grtp1
Smoc1	Slc35f2	Igl1	Gls2	Tiparp	Olfml2b	Man2a1	Prx
Wt1	Apcdd1	Mafb	Figl2	Ythdc2	Gimap1os	Wnt9b	Raver2
Mfap5	Fam184a	Nrcam	Braf	Malt1	Gimap4	Alcam	Glb1l2

DE genes Ctrl pm							
Aorta	Bladder	Bone	Colon	Kidney	Ileum	Liver	Lung
Mfap5	Mfsd2a	Igfbp2	Il4i1	DIK1	Ccl21a	Gata4	Fibin
Ecr4	Apcdd1	2900060B14Rik	Nrn1	Gata5	Reln	Nrg1	Slc6a2
Klk11	Rrp15	Mafb	Mtmr7	Gimap3	Tdp2	Rspo3	Hopx
Ptprj	Nhp2	4921531C22Rik	Cd274	Calca	Ms4a6b	Clec4g	Adgrl3
Sod3	Slco1a4	Kcnj8	Ppp1r1b	Lgr5	Pcf11	Slc38a6	Prx
Cyt11	Hoxd10	Lrrc55	Fut8	3110099E03Rik	Med7	Gm26885	Hilpda
Isl1	Gnl3	Nav3	Socs5	Pbx1	Dnajb1	Cit	Stk4
Vit	Slc35f2	Nrcam	Mif1	Polb	Defa24	1700047M11Rik	Aard
Pkhd11	Prr5	Wnt5b	Timeless	Gm13470	Ddx23	Man2a1	Nhlrc2
Col1a2	Cdh3	Ttn	Etv5	Olfml2b	Ing2	A2m	Stmn1

Supplementary Table 7. Top-10 marker genes in homeostatic condition.

Log2FC > 0 and p-value < 0.05. Log2FC > 0 and FDR < 0.05. Organ were harvested in the morning (am) or evening (pm). Ctrl – Control.

Marker genes Ctrl am							
Aorta	Bladder	Bone	Colon	Kidney	Ileum	Liver	Lung
Cyt11	Scarb1	Mafb	Rgcc	Scgb3a1	Igfbp5	Rspo3	Tmem100
Clu	ApoE	Abcg2	Cd24a	Zfp36	Plpp1	Clec4g	Calcr1
Cpe	Tshz2	Maf	Ly6a		Pbx1	Cd55	Hpgd
Igfbp7	Ctla2a		Plscr2		Plscr2	F8	Cldn5
Ltbp4	Abcb1a		Thbd		Meis2	Cd59a	Sema3c
Eln	Lepr		Pltp		Plat	Gpr182	Pltp
Fn1	Rps21		Rtl8a		Pi16	Maf	Foxf1
Bmx	Bsg		Rbp7		Emcn	Il6st	Tspan7
Cp	Rpl10		Rdx		Srgn	ApoE	BC028528
Gkn3	Rps6		Ly6c1		Dkk2	Man2a1	Ramp2

Marker genes Ctrl pm							
Aorta	Bladder	Bone	Colon	Kidney	Ileum	Liver	Lung
Cyt11	Mgp	Mafb	Rgcc	Igfbp5		Rspo3	Tmem100
Cpe	Cyp1a1	Cav1	Plvap	Plat		Clec4g	Hpgd
Mgp	Tshz2	Bgn	Igfbp7	Pbx1		Gpr182	Foxf1
Clu	Lgals3	Sparcl1	Fos	Plpp1		Cd55	Sema3c
Cfh	Tmsb10	Maf	Mef2c	Emcn		Man2a1	Lyve1
Gkn3	Lepr	Itm2c	Zfp36	Plscr2		Selenop	Acvr11
Ctsh	Abcg2	Abcc9	Esm1	Meis2		Maf	Cldn5
Pam	Net1	Abcg2	Plscr2	Gimap4		Il6st	BC028528
Sfrp1	Prss23	Mrc1	BC028528	Sgk1		Cd59a	Scn7a
Eln	Insr	Plod1	Kctd12b	Pi16		Oit3	Epas1

Supplementary Table 8. Top-10 Organ-specific genes in homeostatic condition.

Organ were harvested in the morning (am) or evening (pm). Ctrl – Control.

Organ-specific genes Ctrl am							
Aorta	Bladder	Bone	Colon	Kidney	Ileum	Liver	Lung
Coch	Tnfrsf9	Lipg	Gm16731	Hpse2	Gm13470	1700047M11Rik	Adgrl3
Comp	Dach2	Pwpp3b	Mtag2	Gm9947	Adamts16	A2m	Gm26878
Isl1	Wnt5a	Bglap2	Gm26574	1700120K04Rik	Erc2	Calhm6	Dpysl5
Hand2os1	Gm30191	Rag2	Cybrd1	Nkx2-1	Gp1bb	Egfem1	Plcb2
Vit	Pcsk1	Sgk2	Vmn2r1	9130024F11Rik	Mc4r	Cd200r1	Gm16152
Naaladl2	Krt23	Pifo	Nppa	Rgs13	Lgr5	Mpzl2	Slc5a12
4930428N03Rik	Tpd5211	4930553M12Rik	Tecl1	Rbm8a2	Galnt14	Nr1h4	Serpina3m
Ugt8a	Gpr37	Il10ra	Asphd1	Gm37027	Epha6	Gprasp2	Hpcal4
Gm48898	Gm34280	Gm33619	Slc5a2	Nr5a1	Mkx	Ankrd55	Gpnmb
Pclo	Shmt1	Bcl11a	Leap2	Cfap61	Gad1	Tenm1	Cldn18

Organ-specific genes Ctrl pm							
Aorta	Bladder	Bone	Colon	Kidney	Ileum	Liver	Lung
Synpo2	Ooep	D030007L05Rik	Pcsk1	Lypd6	Defa22	Nr1h4	Zfp641
4930428N03Rik	Fzd10os	Lipg	Gm45591	Gp1bb	Dtx1	Cd200r1	Ankrd63
Pxylp1	Dnah10	Rgs4	Gm10532	Mc4r	Lyz1	Alb	Gm26878
Ptgds	Nfasc	Kif1a	Gm14209	Adamts16	Gm16587	Cd209b	Serpina3m
Acpp	Dtna	C5ar1	Tm4sf4	Erc2	Gm14851	Sprr2b	Pcdhac2
Krtap5-5	Fzd10	Irx2	Asic3	Astn1	Gm7861	Cfi	Plcb2
Sobp	Nxph3	4933407L21Rik	Clec4a1	Epha6	Alox12e	Rnf43	Gm5547
Zfhx4	Sh3rf2	Cfd	Sgcz	Cldn10	Cd300lf	6030498E09Rik	Tekt5
Pax9	Hs3st4	Gm41414	Lingo1	Dazl	Nek10	Gm19461	Gm35065
Fgf12	Krt23	A830018L16Rik	Pls1	Lrrc10b	Msc	Irf4	Nrxn1

Supplementary Table 9. Top-10 DE genes in acute inflammatory condition.

Organ were harvested in the morning (am) or evening (pm). Log2FC > 2, p-value < 0.05. DE – Differentially expressed, LPS – Lipopolysaccharide.

DE genes LPS am							
Aorta	Bladder	Bone	Colon	Kidney	Ileum	Liver	Lung
Abca13	Hoxd10	Gal	Rad51ap1	Ager	Tmem26	Clec4g	Serpina3m
Inhba	Lcn2	Pold4	Srd5a1	Akap5	Dlk1	Galc	Klh5
Ecr4	Stra6	Mafb	Mcf2l	Egr1	H1f0	Oit3	Lilr4b
Cyt1	Ccl11	Igfbp2	Gm34425	Gadd45g	lkbkb	Sord	Pard6g
Ephx2	Bpifb5	Mmp14	Plvap	Cldn18	Sdf2l1	Rspo3	Dyrk2
Gsn	Vldlr	Klk1	Nptxr	Sec14l3	Polb	Col14a1	Qsox1
Cpe	Pdgfc	Tfpi	Rab13	Ypel5	Plpp1	Khdrbs3	Rap1a
Cxcl5	Mfsd2a	Osbp2	Adgrl4	Rrad	Hs3st6	Fchsd2	Ntrk2
Smoc1	Efhd2	2900060B 14Rik	Gm12002	Zfp36	Oas1g	Myct1	Gmfg
Klk10	Prkg1	Dusp23	Aox1	Rpap3	Hectd2	C1qb	Vsir

DE genes LPS pm							
Aorta	Bladder	Bone	Colon	Kidney	Ileum	Liver	Lung
Sod3	Hoxd10	Mafb	Gm5	Ccl21a	Dlk1	Spr2b	Adgrl3
G0s2	Gpcpd1	S100a9	Nrn1	Dsg2	Tmem26	Galc	Fibin
Klk10	Stra6	Tfpi	Apln	Glycam1	Gimap3	Gpr65	Prss12
Smoc1	Ret	Rgs4	A630072M 18Rik	Gdf15	3110099E 03Rik	Tfec	Nckap5
Ptprj	Bnc2	Ubd	Mfsd9	Il18rap	U90926	Col14a1	Klh5
Cyt1	Slc35f2	Lratd1	Gm34425	Ddx23	Add2	A2m	Slc6a2
Sgcd	Efhd2	Igfbp2	Gm10432	Rasl11a	Polb	Itga8	Ccdc68
Aldh3a1	Pdgfc	Slc24a1	Olfir520	E230013L 22Rik	Calca	Gata4	Cpeb4
Abca13	Nipal1	Ctsl	Helb	Nxph1	Cnmd	Clec4g	Tmcc2
Ttc28	Cfd	Rarres2	Timeless	Mzf1	Erc2	F830016B 08Rik	Aff3

Supplementary Table 10. Top-10 marker genes in acute inflammatory condition.

Organ were harvested in the morning (am) or evening (pm). Log2FC > 0 and FDR < 0.05. LPS – Lipopolysaccharide.

Marker genes LPS am							
Aorta	Bladder	Bone	Colon	Kidney	Ileum	Liver	Lung
Cyt11	Lcn2	Tmsb4x	AW112010	Egr1	Plat	Ccl2	Cd74
Mgp	Cldn5	Mmp14	Stc1	Ccn1	Plpp1	Serpina3g	Cldn5
Clu	Cpeb4		Igfbp3	Igfbp3	Plpp3	Rspo3	Lyve1
Cp	Lgals3		Sparc	Plat	AA467197	Gm12840	St3gal1
Cpe	Abcb1a		Hspg2	Scgb3a1	Igfbp5	Hdc	Fkbp1a
Ptgs2	Prx		Plvap	Gadd45g	Dram1	Serpina3n	H2-Aa
Gm12840	Stra6		Igfbp7	Ier2	Pdgfa	Hk2	Ucp2
Grina	Scn7a		Timeless	Fos	Cmpk2	Olr1	Cpeb4
Cfh			Lamb1	Igfbp7	Sema4c	Zeb2	H2-Eb1
Cst3			Stat1	Zfp36	Pola2	Spr2b	Ccl2

Marker genes LPS pm							
Aorta	Bladder	Bone	Colon	Kidney	Ileum	Liver	Lung
Cyt11	Lcn2		AW112010	Scgb3a1	Plat	Serpina3g	Lyve1
Clu	Lgals3		Lamb1	Igfbp7	Plpp3	Cxcl9	Cldn5
Cp	Clu		Sparcl1	Egr1	Serpine1	Rspo3	Cd74
Cpe	Mustn1		Egr1	Hmgb1	Rsad2	F8	Rapgef5
Gm12840	Bst1		Col15a1	Igfbp4	Meis2	Gm12840	Ucp2
Mgp	Neat1		Clic5	Ppp1r15a	Timp3	Il1r1	Pltp
Pam	Ch25h		Fmo2	Ier2	Plpp1	Serpina3n	Ctla2a
Ptgs2	Rpl39		Plpp3	C1ca3a1	Cd40	Lyve1	Ly6a
Vcam1	Rpl36a		Itga6	Lamb1	Tinagl1	Serpina3f	Cpeb4
Ltbp4	Abcg2		Mgll	Nr4a1	Cmpk2	F830016B08Rik	Rap1a

Supplementary Table 11. Top-10 Organ-specific genes in acute inflammatory condition.

Organ were harvested in the morning (am) or evening (pm). LPS – Lipopolysaccharide.

Organ-specific genes LPS am							
Aorta	Bladder	Bone	Colon	Kidney	Ileum	Liver	Lung
Ereg	Txlnb	D830036C 21Rik	Apol7e	Cldn18	Dlk1	A2m	Ckm
Gpc6	Cyp1a1	Igsf6	Adamts13	Sec14l3	Gimap3	Cd200r1	Postn
Frmd5	Dsg2	2810403G 07Rik	Tfcp2l1	Gm26826	Calca	Sprr2e	Gm5547
Isl1	Gm13652	Ii13ra2	Cstad	Krt7	3110099E 03Rik	H19	Cdca3
Plac9b	Pxmp2	Slc11a1	Gm14391	Myh14	Gata5	1700047M 11Rik	Abhd15
Tbx18	Rerg	Gm32200	Gm11008	Cox8b	Qrfpr	Gm17167	Slc24a4
Al838599	Agtr1a	Lrsam1	Gm43017	Upk3bl	Gm39464	Alb	Lama1
Klk11	Cxcl14	Prrg4	4930404A 12Rik	Igkc	Ptgds	Fgb	Slc5a12
Mapk13	Ap1s3	Gm42743	Ccdc142os	9230112J1 7Rik	Lypd6	Lrrc66	Iqgap3
Naaladl2	B3galt2	Gm15551	Mtmr7	Ptcra	Rnf207	Adamts3	Ano1

Organ-specific genes LPS pm							
Aorta	Bladder	Bone	Colon	Kidney	Ileum	Liver	Lung
Tbx18	Slco1a4	Adgrg5	Evx1	Gdnf	Gata5	Egfem1	Lama1
Gdf6	Cdh3	Grin2a	Cd83	Mfap3l	Qrfpr	Gm42679	Gm16152
Pipox	Prdm6	1700122C 19Rik	Mroh2a	Gm29083	Sost	Gm48159	Gm43465
Gm28722	Pappa	Fcnb	4930519P 11Rik	1700112D 23Rik	Cdh6	Akr1c19	Pamr1
Pramef12os	Rorc	Klhl30	Tbx15	Sez6l	Arhgef10l	Slc9a7	Fcgr3
Stk32b	Pid1	Cfap61	Gm15721	Gm43913	Epha6	Tenm1	Dpysl5
Rbm24	Fxyd7	Cass4	Hottip	Rsf1os1	Meiob	Slc39a12	Gm26878
Plac9b	Pimreg	Gm12522	Gm21119	Tcerg1l	D030045P 18Rik	Sprr2d	Mchr1
Tceal3	Gm48236	Gm10570	4933404K 13Rik	Vpreb3	Gm15558	Cnr1	Glb1l2
Klk9	Nfasc	Wnt16	Fam241b	Cyp2d11	Foxs1	Ppp1r3a	Rorb

Supplementary Table 12. Top-10 DE genes in hyperglycemic condition.

Organ were harvested in the morning (am) or evening (pm). Log2FC > 2, p-value < 0.05. DE – Differentially expressed, STZ – streptozotocin.

DE genes STZ am							
Aorta	Bladder	Bone	Colon	Kidney	Ileum	Liver	Lung
Tbx20	Hoxd10	Spink1	Kif5c	Gimap3	Efnb3	Alcam	Slc6a2
Hand2os1	Tnfrsf9	Krt8	Gm43689	Calca	Tjap1	Gm17167	Aard
Hand2	Cfd	Hist1h1d	Nkain4	Pbx1	Arl5b	Rspo3	Prx
Lum	Ooep	Fam102a	Camk4	Gata5	Srf	Sprr2b	Adgrl3
Dcn	Cyp2e1	Tpm1	Rbpms2	Lypd6	Tnfaip3	Itga8	Hilpda
Cdh11	Tacr1	Tubb6	4930525G 20Rik	Olfml2b	Resf1	Hpse	Fibin
Col3a1	Tmem182	Sh2d6	Gm26737	Gimap4	Gbp2	S100g	Grtp1
Epha7	Lef1os1	Hist1h3d	Kazn	DIK1	Gm43581	Tmem132e	Scn3b
Hapln1	Pif1	Ezh2	Gm5129	Slco4a1	Hivep2	Slc43a2	Raver2
Pkhd11	Tbc1d8	Nrcam	C030010L 15Rik	Rian	Slc23a2	Cit	Nhlrc2

DE genes STZ pm							
Aorta	Bladder	Bone	Colon	Kidney	Ileum	Liver	Lung
Sfrp1	Ch25h	Mmrn1	Nrn1	DIK1	Reg3b	Gata4	Sema3c
Ephx2	Tnfrsf9	Lipg	Ppp1r1b	Gata5	Fabp6	Wnt9b	Adgrl3
Ecr4	Wfdc18	Igfbp2	Pcsk1	Calca	Reg3g	Hpse	Slc6a2
Mfap5	Cfd	Rgs4	Gm12122	Gimap3	Jag1	Tpbg1	Prx
Pkhd11	Slc35f2	Ccl21a	Ttpal	Pbx1	Slc45a4	1700047M 11Rik	Nhlrc2
Smoc1	Kcnj2	Prg4	Shc2	Cnmd	Atxn7	Wnt2	Grtp1
Adh7	Crlf1	D030007L 05Rik	Cd248	Fam81a	Plet1	Cit	Aard
Adra2a	Ooep	Mafb	Pcsk6	Thbs2	Rictor	Itga8	Hilpda
Coch	Cd79a	Aldob	Defa22	Ddit4l	Art5	Prrg3	Hopx
Klk10	Pappa	Kcng2	Pla1a	3110099E 03Rik	Braf	Tmem132e	Car14

Supplementary Table 13. Top-10 marker genes in hyperglycemic condition.

Organ were harvested in the morning (am) or evening (pm). Log2FC > 0 and FDR < 0.05. STZ – streptozotocin.

Marker genes STZ am							
Aorta	Bladder	Bone	Colon	Kidney	Ileum	Liver	Lung
Cst3	Scarb1		Cxcl12	Igfbp5	Scgb3a1	Rspo3	Tmem100
Clu	Tshz2		Thbs1	Pbx1		Clec4g	Calcl
Cyt11	Prnp		Thrsp	Plat		Cd55	Hpgd
Mgp	Insr		Ptpr	Plpp1		Cemip2	Pltp
Cpe	Ifitm3		Pltp	Plscr2		Nr2f2	Acvr1
Foxc1	C130074G19Rik		Plscr2	Meis2		Gpr182	BC028528
Ptgis	Lepr		Igfbp7	Pi16		Wnt2	Tspan7
Irf6	Pltp		Coro2a	Emcn		Man2a1	Sema3c
	Bsg			Cd24a		F8	Ramp2
	Cyp1a1			Rsad2		Cd59a	Foxf1

Marker genes STZ pm							
Aorta	Bladder	Bone	Colon	Kidney	Ileum	Liver	Lung
Cyt11	Cyp1a1	Mafb	Rgcc	Igfbp5	Scgb3a1	Rspo3	Hpgd
Mgp	Lgals3	Abcg2	Plvap	Emcn		Gpr182	Tmem100
Cpe	Tmsb10	Fth1	Esm1	Plpp1		Clec4g	Calcl
Cfh	Net1	Mrc1	Igfbp7	Pbx1		Selenop	Pltp
Ctsh	Hspb1		Mef2c	Meis2		Maf	Cldn5
Clu	Lepr		Mfge8	Plat		Cd55	Foxf1
Tmem158	Rps6		Plscr2	Plscr2		Bmp2	Sema3c
Rbp1	Ptn		AW112010	Gimap4		Nr2f2	Lyve1
Gkn3	Tshz2		Thrsp	Rsad2		Wnt9b	Tspan7
Sfrp1	Clu		Ncoa7	Cd24a		Dnase113	Adgre5

Supplementary Table 14. Top-10 organ-specific genes in hyperglycemic condition.

Organ were harvested in the morning (am) or evening (pm). STZ – streptozotocin.

Organ-specific genes STZ am							
Aorta	Bladder	Bone	Colon	Kidney	Ileum	Liver	Lung
5033428I2 2Rik	Cdh3	Lipg	Pla1a	3110099E 03Rik	Prrx2	Ajap1	Slc24a4
Kcnt2	Col28a1	Eps8l3	Hhpl2	Gm13470	Nppa	Nr1h4	Gm16152
Isl1	Gm30191	Dclk1	Hnf4g	A830019P 07Rik	Gm42518	Ccl2	Dpysl5
Gdf2	Rnf183	Tm4sf4	Ccdc169	Lgr5	Ankk1	Atp1a4	GpnmB
Pde1a	Gm34280	Ptpn6	Sgcz	D030045P 18Rik	Shc2	Mroh7	Tekt5
Gdf6	Slitrk2	Rgs13	Gm47163	Capsl	Gm28722	Ly6f	Lilrb4a
Corin	Clca3a2	Gm13074	Msc	Epha6	Gm28792	Tenm1	Slc5a12
Wnt16	Saa3	Bcl2l14	Gm26574	Frmpd2	Tnfsf18	Lrrc25	Gm35065
Serinc2	Nfasc	Acta1	Gm16534	Mc4r	Gm16587	Fcna	Crym
Fhl2	Cidec	Gm11525	Gm13496	Htr7	Gm38155	Spr2a3	Tex14

Organ-specific genes STZ pm							
Aorta	Bladder	Bone	Colon	Kidney	Ileum	Liver	Lung
Krtap5-5	Nxph3	Acta1	Pla1a	3110099E 03Rik	Gm14434	Gm17167	Slc24a4
Epha3	Fzd10	Gpr88	Ptpn13	Gm12915	Gm42921	Tenm1	Gm26878
Trbc2	Krt23	Ak5	Gm34653	Lgr5	Egr4	Cd200r1	GpnmB
Unc5d	Sh3rf2	Gm13074	4930417H 01Rik	Gm13470	Klrb1c	Mpzl2	Crym
Tbx18	Scn4b	Zfp536	Hsd3b3	Mc4r	Saa1	Rnf43	Serpina3m
Chst10	Cilp	Gm29083	Gm17055	Capsl	Gm16302	Mroh7	Slc5a12
2610316D 01Rik	B230206L 02Rik	Kif1a	Gm47398	Rtl1	Gm3164	Fcna	Plcb2
1110032F0 4Rik	Gm47695	Tnfsf18	9830166K 06Rik	Htr7	Tspyl5	Dab1	Pcdhac2
Abca13	Cacna1h	Rasgrp1	Prrx2	Gm30692	Btnl6	Rgs7	Gm35065
Srl	Slc19a3	Atp6v0d2	Pjvk	Cmtm5	Gal3st2	Adh6a	Tekt5

Supplementary Table 15. Top-10 DE genes in hyperlipidemic condition.

Organ were harvested in the morning (am) or evening (pm). Log2FC > 2, p-value < 0.05. AAV – Adeno associated virus, DE – Differentially expressed.

DE genes AAV am							
Aorta	Bladder	Bone	Colon	Kidney	Ileum	Liver	Lung
Sod3	Ch25h	Ubd	Madcam1	3110099E03Rik	Sac3d1	Sprr2b	Adgrl3
Ecr4	Prg2	Lipg	Hcar1	Gata5	Tmem191c	Rspo3	Slc6a2
Ephx2	Hoxd10	Igfbp2	Krt19	Calca	Wdr24	Tnni3	Hilpda
Dcn	Scnn1b	Abcc9	Mlf1	Gimap3	Zfp747	Serpib9b	Ntrk2
Atp1b1	Rasal1	Kcnj8	Card11	Dlk1	Agpat5	Gm26885	Prx
Scx	Tnfrsf9	Il13ra2	Col13a1	Lypd6	Mfsd2b	Clec4g	Raver2
Aldh3a1	Fzd10os	Wnt5b	Scgb3a1	Serpine2	Snhg12	A2m	Gpx3
Itgbl1	Dusp2	Mdfi	Mgl1	Olfml2b	3110045C21Rik	Cit	Tmeff2
Mfap5	Gm42949	Cxadr	Pcx	Pbx1	1700088E04Rik	Serpina3n	Nckap5
Col1a2	Tbc1d8	Prg4	Zfp287	4631405J19Rik	Armh3	Gjc2	Hopx

DE genes AAV pm							
Aorta	Bladder	Bone	Colon	Kidney	Ileum	Liver	Lung
Mfap5	Mfsd2a	Kcnj8	Apol7c	Dlk1	Aqp5	Alcam	Adgrl3
Ecr4	Cfd	Lipg	Il6	Gimap3	Sftpa1	A2m	Prx
Isl1	Hoxd10	Cxadr	Trmt11	Gata5	Tfr3	Clec4g	Slc6a2
Slc4a4	Pdgfc	Prg4	Pacs1	Lypd6	Prkd1	1700047M11Rik	Ntrk2
Perp	Slc35f2	Aldob	Cd274	Pbx1	Fem1c	Cit	Hilpda
Adra2a	Apcdd1	Ercc1	Fut8	Gm12915	Erf	Rspo3	Tmcc2
Klk10	Adamts18	Tpr	Pla1a	Gimap4	Rcan1	Itga8	Grtp1
Dcn	Bnc2	Abcc9	Gng3	4631405J19Rik	Tmc6	Prrg3	Nckap5
Efemp1	Zdbf2	Mafb	Pou2f3	Tmem108	Adamts8	Man2a1	Car14
Clu	Nfatc2	Ascc2	Mcm6	Olfml2b	4930545L23Rik	Dse	Antxr2

Supplementary Table 16. Top-10 marker genes in hyperlipidemic condition.

Organ were harvested in the morning (am) or evening (pm). Log2FC > 0 and FDR < 0.05. AAV – Adeno associated virus.

Marker genes AAV am							
Aorta	Bladder	Bone	Colon	Kidney	Ileum	Liver	Lung
Cyt11	Lepr	Maf	Rbp7	Igfbp5	Arl4a	Rspo3	Hpgd
Cpe	Tmem252	Abcc9	Nkx2-3	Plat	U2af1	Wnt2	Sema3c
Sfrp1	Cyp1a1	Cdkn1c	Col13a1	Sgk1	Sp100	Clec4g	Foxf1
Cfh	Ctsh	Kcnj8	Thrsp	Tnfaip2	Ldha	F8	Adgre5
Gxylt2	Tbc1d8	Ccdc88c	Mef2c	Slc6a6	Ndufa6	Cd55	Scn7a
Klk10	Dusp2	F8	Thbd	Pi16	Eef1g	Man2a1	Bmpr2
Gata6	Stt3b	Plod1	Depp1	Dkk2	Crip1	Ptprb	Fmo1
Htra1	H2-Q7	Pparg	Rsad2	Meis2	Rpl36	Wnt9b	Hopx
Gkn3	Nuak1	Nav3	Sema7a	Rsad2	Pcbp2	Maf	Hilpda
Ptgis	Scn1b	Jam3	Bhlhe40	Tbxa2r	Rpl4	Fcgr2b	Stmn1

Marker genes AAV pm							
Aorta	Bladder	Bone	Colon	Kidney	Ileum	Liver	Lung
Cyt11	Cyp1a1		Plscr2	Igfbp5		Rspo3	Tmem100
Clu	Mgp		Rbp7	Plat		Cd59a	Hpgd
Mgp	Prss23		Mef2c	Pbx1		Il6st	Sema3c
Cpe	Tmsb10		Jam3	Plpp1		Nr2f2	Foxf1
Gkn3	Tshz2		Col13a1	Meis2		Gpr182	Calcr1
Sfrp1	Abcg2		Ar	Srgn		Stab1	Ramp2
Mt1	Scarb1			Emcn		Selenop	Tspan7
Klk10	Net1			Plscr2		Cd55	Cldn5
Eln	Ccn2			Pi16		Man2a1	Adgre5
Tmem158	Insr			Gimap4		Maf	Scn7a

Supplementary Table 17. Top-10 organ-specific genes in hyperlipidemic condition.

Organ were harvested in the morning (am) or evening (pm). AAV – Adeno associated virus.

Organ-specific genes AAV am							
Aorta	Bladder	Bone	Colon	Kidney	Ileum	Liver	Lung
Isl1	Egr4	C5ar1	Gm13362	Gm13470		Gm17167	Slc24a4
Naaladl2	Gpr183	Kif1a	Ckmt1	Adamts16		Spr2a3	Dpysl5
Dlx5	Gm30191	Lratd1	Upk3bl	Lgr5		Alb	Gpnmb
Vwc2	Sh3rf2	4930431P03Rik	Agrp	Astn1		Rubcnl	Tekt5
Tbx18	Fzd10	S100a5	D730003K21Rik	Cnmd		Atp1a4	Xpnpep2
Pax9	Bpifb5	Camp	Igha	Erc2		Rhox5	Plcb2
1110032F04Rik	Krt23	H2-DMb2	Gm48857	Gm12915		Rbfaos	Hpcal4
Agr2	Glycam1	Zfp536	Lrrc63	Capsl		Gm10612	Glb1l3
Pxylp1	Cacna1h	4930583K01Rik	Cdh19	D030045P18Rik		E030013I19Rik	Serp1b1b
Atp6v0d2	Aldh1b1	Tnni2	Mptx1	Mc4r		Irf4	2810030D12Rik

Organ-specific genes AAV pm							
Aorta	Bladder	Bone	Colon	Kidney	Ileum	Liver	Lung
Lum	Tnfrsf9	Slc7a8	Gm5	3110099E03Rik	Inava	Gata4	Raver2
Mapk13	Ooep	D030007L05Rik	Upk3bl	Erc2	Lhx9	Nrg1	Zfp641
Vit	Retn	Igfbp2	Cdh19	Calca	Nectin4	Spr2b	Rprml
Crispld2	H19	Dmrta2	Al463229	Mc4r	Nr5a1	Rnf43	Slc24a4
Clec3b	Alox12e	Gm3739	Vmn2r1	2310030G06Rik	Tuft1	Serp1b9b	Gm16152
Klk13	Spdya	Rasgrp1	Cd276	Add2	Shh	AC168977.2	Dpysl5
Tnnt2	Fam110b	Fcho1	Pif1	D030045P18Rik	Aym1	Cd200r1	Prdm8
Rgma	Scnn1b	Gm36670	Gm47398	Cnmd	Gm30270	Rgs7	Hpcal4
Vwc2	Rnf183	Raet1d	Gm47163	Astn1	Gm10069	Greb1l	Serp1a3m
Tbx18	Gm8579	A630072L19Rik	Dph1	Lgr5	Gm43913	Irf4	Gm26878

Supplementary Table 18. Number of marker genes of mice in homeostasis and exposed to acute and chronic inflammation.

Number of marker genes in the dataset from mice sacrificed at am or pm while in homeostasis (Ctrl), subjected to an acute inflammatory condition (LPS), or chronic inflammatory conditions (hyperlipidemia (AAV), or hyperglycemia (STZ)). FDR < 0.05. AAV - Adeno associated virus, Ctrl – Control, FC – Fold Change, LPS – lipopolysaccharides, STZ – Streptozotocin.

	Ctrl am				Ctrl pm				LPS am				LPS pm			
Log2FC	2	1	0.5	0	2	1	0.5	0	2	1	0.5	0	2	1	0.5	0
Aorta	0	1	14	51	6	28	94	275	4	17	52	127	1	12	26	44
Bone	0	0	3	3	0	1	6	21	0	1	1	2	0	0	0	0
Bladder	0	3	51	169	0	3	17	142	0	1	2	8	1	2	17	54
Colon	0	0	10	13	0	0	14	49	0	2	11	22	0	5	25	59
Kidney	7	22	77	283	5	14	42	237	0	5	27	127	3	21	82	248
Lung	11	51	122	376	4	41	109	399	3	14	64	208	3	33	115	377
Ileum	0	2	2	2	0	7	22	47	0	1	20	29	0	1	11	36
Liver	5	39	124	407	3	23	84	350	0	21	67	181	2	23	60	208

	STZ am				STZ pm				AAV am				AAV pm			
Log2FC	2	1	0.5	0	2	1	0.5	0	2	1	0.5	0	2	1	0.5	0
Aorta	0	4	5	8	3	11	49	79	2	14	47	332	3	16	45	136
Bone	0	0	0	0	0	0	2	4	0	0	2	10	0	0	0	0
Bladder	0	3	7	20	0	1	15	76	0	0	5	69	1	3	15	44
Colon	1	2	7	8	0	1	8	17	0	4	15	49	0	0	5	6
Kidney	7	30	74	183	5	16	46	204	2	10	32	205	5	17	61	214
Lung	15	64	141	311	7	47	131	419	5	27	69	307	9	51	127	288
Ileum	0	0	1	1	0	0	1	1	1	4	10	15	0	0	0	0
Liver	4	37	111	284	1	26	96	443	3	17	59	334	7	49	120	377

Acknowledgments

In the last years during this PhD thesis, I grew as a scientist, but also as a person. This progress I owe to several people, to who I would like to express my gratitude.

I would like to thank Univ.-Prof. Dr. Dr. med Oliver Söhnlein, my supervisor, for his extensive support in the past years. He gave me the opportunity to work on this fascinating project, which I was able to present on meetings and conferences. Thank you for the chance to work in this wonderful scientific environment and for your supervision and guidance during my project. Your enthusiasm is contagious.

To my daily supervisor, Dr. Joana Viola, thank you for your scientific and personal guidance. On a scientific level you taught me to write with a critical sense and made sure I set up my experiments step by step. You were able to reflect my personality and pointed out my weaknesses and strengths, which made me able to grow as a person. Thank you for your support!

Furthermore, I am grateful for my thesis advisory committee members Prof. Christoph Reichel and Prof. Aphrodite Kapurniotu, who helped me to successfully accomplish my PhD project.

Of course, I want to thank AG Söhnlein, the Kellerkinder: PC for your help in the lab, irrespective of the time of the day. You always cheered me up and I was very happy to be your desk neighbor. Ariana and Carla for sharing your drive and brighting up the basement. Laura and Celia (Mona Lisa) without you two this would have not been so much fun. Renske and Bartolo it was a pleasure to learn from you and you were great company (in and outside of the lab). Janine and Pati, for your patience, and the tips and tricks you taught me in the laboratory. And not to forget, a special thanks for your friendship over the past years. Carlos, Quinte, and Kristof for your scientific advice and overcoming our fears of heights in the climbing hall. Rapha for always making time to talk about my project and your willingness to help. Almudena, Giovanna, and Max for a great working atmosphere. Hasan, Timo, and Olga for your support in the lab. Thank you all for being great colleagues and friends.

A big thanks to the IPEK family. Emiel for supporting and believing in me. For continuing to work with me also during the first steps of my postdoc. Your trust and appreciation mean so much to me! Mariaevly for your cheerfulness and your hospitality, it was great to spend Christmas lunch with you. To all other IPEK colleagues, a big thanks for the warm welcome at the institute and your willingness to help.

I would like to thank the secretaries Frau Stöger, Frau Damaris Bindl and Frau Iliriana Vatovci, and Herr Putz for the excellent support related to office matters and for the nice conversations.

The Central Laboratory Animal Husbandry (ZVH) of the University Clinic made an important contribution to the animal experimental which are part of my doctoral thesis. Many thanks to the entire ZVH team for the support in the animal facility.

I would like to thank collaborators. Prof. Kupatt and Tarik for the possibility to work with the endothelial specific AAVs. Prof. Chris Reutelingsperger and Dr. Gerry Nicolaes for your trust to run your mouse studies. Prof. Erik Biessen for hosting me in your lab in Maastricht. Lena, thank you for measuring all my samples, even on short notice. Markus for introducing me to bioinformatics and analyzing the *Tabula Muris* dataset. Simon for your willingness to explain the course of the experiments and preparing the libraries for the sequencing of the small bulk. Monica for sharing your motivation and give us the ability to work with your compounds.

I am proud to be part of the amazing EVOluTION network, through which I was able to meet great scientist and make friends for life. A special thanks to Silvia, Jan, and Chiara I really enjoy the balance we have found between science and fun. Silvia, from our first meeting we knew this was the start of a long-lasting friendship. I admire your knowledge and motivation. I am very happy that I have met you! Jan, you showed us how to create a healthy work-life balance. I am always happy to spend time with you and have a good conversation (with a beer). Chiara, my roommate throughout the whole program. I am very impressed by your (scientific) drive and want to thank you for your company and support.

I was very happy to be a member of the IRTG914 and IRTG1123 graduate schools. I want to thank both schools for the interesting lectures, courses, activities, get-togethers, and financial support. A special thanks to you Verena Kochan for the best guidance through the bureaucracy of obtaining a PhD and my fellow students for being always very helpful and friendly.

Not only your colleagues make your PhD time, friend play also a very important role. Julia and Andrea, I met you one month after arriving to Munich and you have made my time in Munich unforgettable! Thank you for being there for me and providing me with the right amount of distraction from work! Jelmer and Lena thank you for leaving the Netherlands and join me in Munich. Even though we did not know each other that well back home I am very happy we took our friendship to another level after travelling 700 km South. My flat mates, Dimi, Ralf,

Marta, and Mira for giving me a warm welcome, a place that felt like home, and being there when I arrived home after a 24-hour experiment.

Mijn ouders, Henk en Wilma verdienen een groot dankjulliewel! Bedankt dat jullie altijd in mij geloven. Jullie zijn er altijd voor mij door zowel de ups als de downs van mijn proefschrift. Soms beschouwde ik dit als vanzelfsprekend, maar ik weet nu beter. Jelte en Fenna ook jullie wil ik heel graag bedanken. Zonder jou zou ik niet zijn wie ik nu ben. Ik weet niet eens hoe ik jullie daarvoor kan bedanken! Heel veel liefs voor jullie alle vier!

Mariano you just joined this rollercoaster, but I am very happy you joined the ride ♥.

Affidavit

Sanne Lidewij Maas
Pauwelsstraße 30
52074 Aachen
Germany

I hereby declare, that the submitted thesis entitled

Organ-specific ‘ZIP-codes’

Endothelial heterogeneity in steady state and inflammation

is my own work. I have only used the sources indicated and have not made unauthorized use of services of a third party. Where the work of others has been quoted or reproduced, the source is always given.

I further declare that the submitted thesis or parts thereof have not been presented as part of an examination degree to any other university.

6.12.2021, Aachen

Date, Place

Sanne Lidewij Maas

Signature doctoral student

Confirmation of Congruency

Sanne Lidewij Maas
Pauwelsstraße 30
52074 Aachen
Germany

I hereby declare that the electronic version of the submitted thesis, entitled

Organ-specific ‘ZIP-codes’

Endothelial heterogeneity in steady state and inflammation

is congruent with the printed version both in content and format.

6.12.2021, Aachen

Date, Place

Sanne Lidewij Maas

Signature doctoral student

List of scientific publications

Original articles

1. Maciuszek M, Ortega-Gomez A, **Maas SL**, *et al.* (2021). Design, synthesis, and biological evaluation of novel pyrrolidinone small-molecule Formyl peptide receptor 2 agonists. European Journal of Medicinal Chemistry
2. Tullemans BEM, Karel MFK, Léopold V, (and 11 others including **Maas SL**). (2021). Comparison of inhibitory effects of irreversible and reversible Btk inhibitors on platelet function. eJHaem.
3. Maciuszek M, Ortega-Gomez A, **Maas SL**, *et al.* (2021). Synthesis and evaluation of novel cyclopentane urea FPR2 agonists and their potential application in the treatment of cardiovascular inflammation. European Journal of Medicinal Chemistry
4. Schumski A, Ortega-Gómez A, Wichapong K, (and 23 others including **Maas SL**). (2021). Endotoxemia Accelerates Atherosclerosis via Electrostatic Charge-Mediated Monocyte Adhesion. Circulation
5. Ferraro B, Leoni G, Hinkel R, (and 18 others including **Maas SL**). (2019). Pro-Angiogenic Macrophage Phenotype to Promote Myocardial Repair. J Am Coll Cardiol.
6. Paulin N, Viola JR, **Maas SL**, *et al.* (2018). Double-Strand DNA Sensing Aim2 Inflammasome Regulates Atherosclerotic Plaque Vulnerability. Circulation
7. Viola JR, Lemnitzer P, Paulin N, (and 9 others including **Maas SL**). (2018). Deletion of MFGE8 Inhibits Neointima Formation upon Arterial Damage. Thromb Haemost.
8. van der Vorst EPC, **Maas SL**, Ortega-Gomez A, *et al.* (2017). Functional ex-vivo Imaging of Arterial Cellular Recruitment and Lipid Extravasation. Bio Protoc.

Reviews

1. Marquez, AB, van der Vorst, EPC, & **Maas, SL**. (2021). Key Chemokine Pathways in Atherosclerosis and Their Therapeutic Potential. Journal of Clinical Medicine
2. **Maas SL**, Soehnlein O, Viola JR. (2018). Organ-Specific Mechanisms of Transendothelial Neutrophil Migration in the Lung, Liver, Kidney, and Aorta. Front Immunol.

